Experimental and numerical modelling of tsunami waves generated by landslides
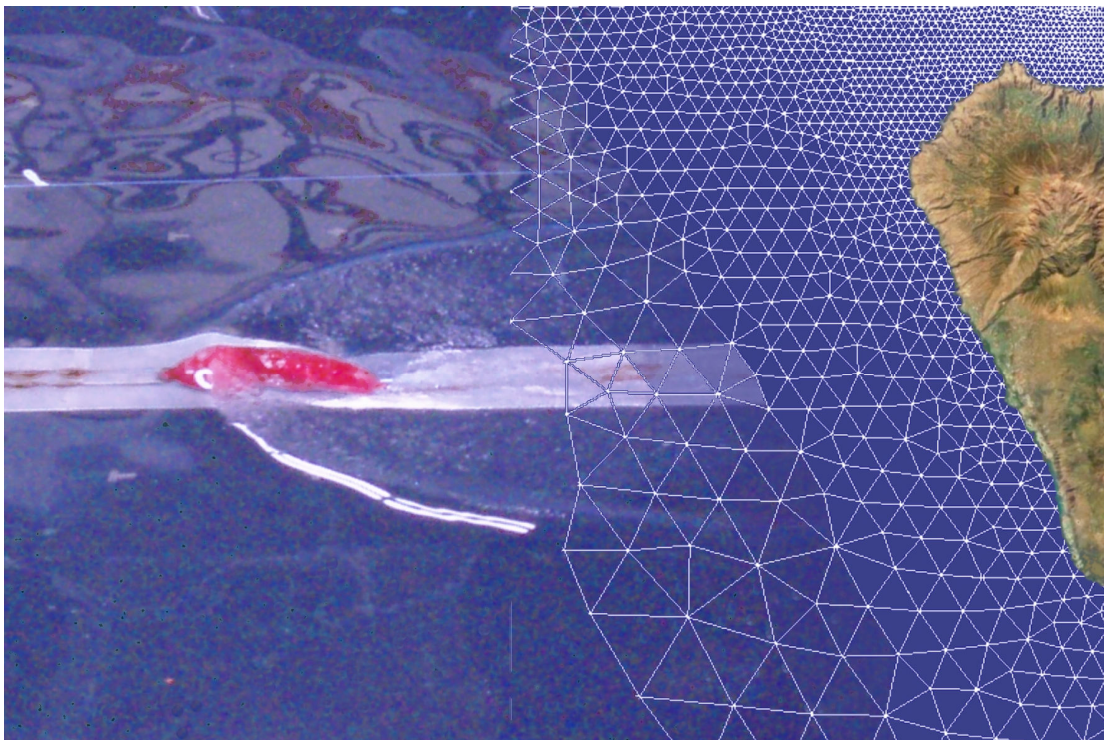
J.C.C. van Nieuwkoop
Msc Thesis

Delft, November 2007

i. Preface

This thesis concludes the Master of Science program at the Faculty of Civil Engineering and Geosciences at Delft University of Technology, The Netherlands.

The thesis is a continuation of the research that has been done on La Palma and its potential to generate a landslide induced tsunami. In 2006 Van Berlo investigated the slope stability of the Cumbre Vieja volcano in La Palma for her Master thesis in Engineering Geology. J.D. Nieuwenhuis, professor in soil mechanics and waterworks, has investigated the potential flank collapse by means of analytical stability analyses. With the results of their investigations the group of Environmental Fluid mechanics, under the authority of Prof. dr.ir. G.S. Stelling and practical execution by ir. R.J. Labeur, has computed a first picture of the wave-effects that could arise from a flank collapse of La Palma.

In this Master thesis further research will be done on the landslide induced tsunami waves that could result from a mass failure on the Cumbre Vieja in La Palma. The work has been supervised by Prof. dr.ir. G.S. Stelling, ir. R.J. Labeur and Prof. J.D. Nieuwenhuis, Dr.ir. W.S.J. Uijttewaal and Dr.ir. S. van Baars.

I would like to thank the members of the graduation committee for their comments and suggestions. Especially Robert Jan Labeur for giving frequent feedback and for his assistance with the numerical model Finlab and Wim Uijttewaal for his support with the experimental model. I would also like to thank the staff members of the Fluid Mechanics laboratory for helping me with the realization of the experiment.

Special thanks go out to Robert, my friends and my family. You all have been very supportive.

Delft, November 2007

J.C.C. van Nieuwkoop

ii.   Summary

In Ward and Day (2001) it is conjectured that discusses that a collapse of La Palma's western flank could trigger a tsunami that affects the USA with 25 meter high waves. Their assumptions concerning critical slope instability of La Palma's western flank and their method of tsunami modelling faced criticism. The slope instability of the western flank has been investigated by Van Berlo (2006). In this Master thesis the landslide generated tsunami waves will be investigated. The objective of this study therefore is *to understand and quantify the generation of a landslide induced tsunami in case of a flank collapse of the Cumbre Vieja volcano in La Palma*. To fulfil the objective a numerical model has been made which can compute the three-dimensional tsunami generation. Experimental model tests are carried out to learn more about the tsunami generation process and to provide a dataset to verify the numerical model.

The physical scale model is based on the dimensions of the La Palma landslide, with a scale of 1:8500. The experiments are carried out in the wave basin of DUT with a semi-elliptical landslide model. The landslide velocity and the initial position of the landslide model are varied and information of the surface elevation is measured with six wave meters. In addition, a stereo camera setting is tested in order to obtain three-dimensional information of the generated waves. When the landslide model moves into the water, it pushes away the fluid generating a leading positive wave crest. The first crest amplitude increases initially, peaks and decreases when the landslide model gradually enters into deeper water. The accelerating fluid and turbulent wake above and behind the landslide model create a region of low pressure, which results in a water surface depression. The trough is forced to propagate at the same speed as the landslide until the landslide enters deeper water and the influence of the landslide on the water surface declines.

It is observed that when the initial position of the landslide is sub-aerial, higher waves are generated than when the initial position is submerged and with increasing submergence the wave height decreases. Moreover, when the landslide velocity is increased, an increase in the wave amplitude is measured.

For the two-dimensional numerical model the experimental setting of Sue (2007) in a wave flume is used. The results of the numerical runs are verified with Sue's experimental results and a good resemblance between the models is found.
With the two-dimensional model also other model configurations are tested. The influence of various parameters on the tsunami generation is determined. It is found that the landslide height, the slope in the experiment and the landslide velocity influence the wave amplitude. The landslide length influences the wave length of the first wave.

The three-dimensional numerical model is based on the experimental model of this study. The dataset, where a landslide velocity of 0.7 m/s and an initial position of 4.2 meter are used, is taken for the verification of the numerical model. The resemblance is reasonably good for the leading wave. However, the high frequency waves which are generated at the trailing end of the landslide are underestimated in the numerical model. Further improvements in the numerical model concerning the mesh size and the landslide shape are required to get a better correspondence for these waves.

Finally, a numerical model is set up to compute the landslide induced wave generation in case of a flank collapse in La Palma. The model is a simplification of the real situation, although the bathymetry of the western side of La Palma is used. Unfortunately, no results were obtained from the La Palma model yet.

From the experimental results, it can be concluded that the tsunami wave which is generated, is much lower than was stated by Ward and Day (2001). The tsunami is mainly a threat for La Palma and the surrounding Canary Islands. At a distance of 40 kilometres from the La Palma coast a wave of approximately 5 meters is left with a wave length of maximal 30 kilometres in the direction of landslide motion. However, it must be noted that no bathymetry data were used in the experiment.

iii.   Table of contents

iv.   Abbreviation and definitions

Collapse scar	The surface of a amphitheatre shaped topographical gap that is left after a collapse
Coseismic dislocation	The pattern of vertical or horizontal ground movement due to an earthquake. Strong vertical ground movement usually triggers tsunamis.
Debris avalanche	A mass of rock debris that moves downslope as a fast-moving giant avalanche that, depending on its size, can travel for tens or even hundreds of kilometres. Characteristically composed of all sizes of fragments, from mud to large sized blocks.
Debris flow	Debris flow is like a debris avalanche, but of slower velocity and is often referred to as mudflow. Debris flow consists primarily of geological material mixed with water.
Dip angle	The angle between a fault and a horizontal plane.
Fault	Faults are planar rock fractures, which show evidence of relative movement.
Hotspot	Hotspots are located on top of mantle plumes, where the convection of Earth's mantle creates a column of hot material that rises until it reaches the crust. A mantle plume is an upwelling of abnormally hot rock within the Earth's mantle.
Intra-plate volcano	Intra-plate volcanoes develop over the moving plate above a hotspot.
Inviscid fluid	An inviscid fluid is a fluid, which has no resistance to shear stress.
Landslide	Thin, translational failure, travelling over long distances.
Pelagic sediment	Microscopic plankton shells and fine flakes of clay that settle out and accumulate on the deep-ocean floor.
Plastic flow	Resistance to flow due to shear resistance.
PNG	Papua New Guinea.
Retrogressive slide	A retrogressive slide releases gradual or stepwise the mass of the slide. It starts with the bottom end and releases progressively upslope from the bottom end.
Rift	A rift is a place where the Earth's crust and lithosphere are being pulled apart. The axis of the rift area commonly contains volcanic rocks and active volcanism is a part of many active rift systems.
Run-up	Wave run-up is the maximum vertical extent of wave up-rush on a beach or a structure above a reference level.

SMF	Submarine Mass Failure; refers to all submerged rock slides, reef failures and many forms of sediment failure, creeping or initial.
Slump	Thick, rotational mass failure, occurring with minimal displacement.
Tsunami	A tsunami is a series of waves created when a body of water, such as an ocean, is rapidly displaced on a massive scale. The term tsunami comes from the Japanese language meaning harbour and wave.
Tsunamigenic	Tsunamigenic is referring to sources that can generate a tsunami.
Turbidity current	A turbidity current or density current is a current of rapidly moving, sediment-laden water moving down a slope through air, water, or another fluid. The current moves because it has a higher density and turbidity than the surrounding fluid through which it flows.
Volcanoclastic sediment	Sediment due to the sedimentation in the sea or in a lake of volcanic products (i.e. ashes).

v.   Symbol list

α	Direction	(°)
a	Acceleration	(m/s²)
a_0	Slide initial acceleration $\left(= \ddot{S}(0) \right)$	(m/s²)
A_w^*	Dimensionless surface area	(-)
β	Shear resistance	(N/m²)
B	Width	(m)
b	Length of the landslide	(m)
c	Wave celerity	(m/s)
C_d	Global (Bulk) hydrodynamic drag coefficient	(-)
C_m	Hydrodynamic added mass coefficient	(-)
C_n	Basal Coulomb friction coefficient	(-)
ΔM_l	Added mass	(kg)
Δt	Time interval or time step	(s)
Δx	Step size in x-direction	(m)
Δy	Step size in y-direction	(m)
Δz	Step size in z-direction	(m)
d_i	Initial submergence	(m)
η	Wave amplitude	(m)
η_0	Maximum wave amplitude	(m)
η_{2D}, η_{3D}	2-dimensional wave amplitude resp. 3-dimensional wave amplitude	(m)
η^+, η^-	Wave crest resp. wave trough height	(m)
E_b	Elasticity modulus of water	(kg/ms²)
E_p	Potential wave energy	(kgm²/s²)
E_k	Kinetic wave energy	(kgm²/s²)
F	Factor of safety	(-)
Fr	Froude number	(-)

θ	Slope angle	(°)
γ	Relative density	(-)
g	Gravitational constant	(m/s^2)
H	Wave height	(m)
Ha_0	Hammack number	(-)
h	Depth	(m)
h_s	Height of the centre of gravity of a landslide	(m)
L	Basin length	(m)
L_r	Length of the landslide in case of a retrogressive slide	(m)
λ	Wave length	(m)
λ_0	Deep water wave length	(m)
μ	Viscosity of water	(kg/ms)
M, m	Mass of the slide	(kg)
N	Number of slide in case of a retrogressive slide	(-)
ρ	Density of the landslide	(kg/m^3)
ρ_l	Landslide bulk density	(kg/m^3)
ρ_s	Slide material density	(kg/m^3)
ρ_w	Water density	(kg/m^3)
R	Radius of the circular arc of the failure plane	(m)
R_u	Run-up	(m)
r	Radial distance	(m)
σ	Surface tension between air and water at 20°	(kg/s^2)
S	Centre of mass motion parallel to a plane or in case of a slump: centre of mass translation parallel to the slope	(m)
S_0	Characteristic distance of slide motion	(m)
$\dot{S}$	Slide velocity	(m/s)
$\ddot{S}$	Slide acceleration	(m/s^2)
t	Time (t_{start}, t_{end}: start time resp. end time)	(s)
t_c	Characteristic time of bed displacement	(s)

t_s^*	Dimensionless time of landslide underwater motion	(-)
t_s	Time of landslide underwater motion	(s)
t_0	Characteristic time of slide motion	(s)
T	Thickness of the slide	(m)
T	Wave period	(s)
T_0	Wave period for deep water waves	(s)
T_{max}, T_1	Wave period of H_{max}, resp. wave period of H_1	(s)
u	Landslide velocity	(m/s)
u_{cr}	Landslide velocity when rate dependent friction becomes important	(m/s)
u_i	Landslide velocity during the impact	(m/s)
u_{max}	Maximum velocity of the slump/ slide	(m/s)
u_t	Terminal velocity of the slide for large times	(m/s)
U	Ursell number	(-)
v	Viscosity of the water	(m^2/s)
V	Velocity	(m/s)
V_s	Landslide volume	(m^3)
V_w^*	Dimensionless volume	(-)
w	Width of the slide	(m)
W	Width of the basin	(m)
ψ	Internal friction angle	(°)
ς_0	Local bed displacement	(m)
x	Distance coordinate	(m)
y	Distance coordinate	(m)
z	Distance coordinate	(m)

PART I: Introduction

1.   Introduction

After the tsunami in 2004 in the Indian Ocean, the public awareness of tsunamis has intensified. Horrifying documentaries about 25 meters high waves hitting the USA coast flooded the television stations and scared many people. The basis for these extreme scenarios came from a publication made three years earlier.

In 2001, Ward and Day make the daring assumption that a collapse of La Palma's western flank will effectively take place during a future eruption. They modelled the wave effects of this landslide and concluded that the East coast of the USA will be hit by a tsunami of 10 to 25 meters high.

Ward and Day's publication has caused a lot of commotion. In the scientific world both their assumption of the critical slope-instability of La Palma and their method of tsunami modelling has been subject to harsh criticism.

The slope-instability of La Palma's western flank has been investigated at Delft University of Technology (e.g., Van Berlo 2006) and it was concluded that it is very unlikely that the flank will collapse in the current configuration. The flank could only be brought close to failure in the worst case scenario. However for overall flank failure at least a thoroughly weakened rock- and soil mass and steeper flanks than in the current configuration are necessary. Furthermore in the case the flank collapses, it is more probable that a landslide volume of circa 7 km^3 moves into the sea, instead of 500 km^3 which was assumed by Ward and Day (Nieuwenhuis 2005).

Using the worst case scenario assumptions made by Nieuwenhuis (2005), the Environmental Fluid Mechanics department of Delft University of Technology made some preliminary tsunami calculations with rough input parameters. They came to the conclusion that even if the worst case scenario occurs, the waves arriving on the coast of the USA will be probably in the order of 1 meter instead of 25 meters.

1.1.   Problem description

For the worst case scenario of a landslide in La Palma, the induced tsunami has been computed by the Environmental Fluid Mechanics department of Delft University of Technology. However, in order to do these computations several assumptions and simplifications were used, especially concerning the generation of the tsunami. Moreover, the bathymetry used for these calculations near La Palma had a strongly schematized grid. Both these simplifications lead to uncertainties concerning the results of the model.

Therefore a study concerning the generation of a landslide tsunami is necessary to gain more insight into the actual danger of a La Palma type landslide.

An additional argument to continue the research on landslide tsunamis is that this research field is relatively new. Extensive studies have been carried out on tsunamis generated by earthquakes and they can be considered well understood. However, the generation mechanism of landslide induced tsunamis and the near field behaviour is far more complex than the generation mechanism of earthquake induced tsunamis and has to be modelled differently.

For this reason a study concerning the generation of a landslide tsunami would also be interesting for the development of a model that can describe the generation process of a landslide tsunami.

1.2.   Objective

The objective of this study is to understand and quantify the generation of a landslide induced tsunami in the case of a flank collapse of the Cumbre Vieja volcano in La Palma with help of the finite element model Finlab. The far field propagation of the tsunami will not be considered.

1.3.   Approach

To fulfil the objective of this study an extensive literature study will be done: (1) to gain insight into the important processes of landslide induced tsunamis, (2) to learn more about the geological background of the Canaries and especially La Palma and (3) to get an overview of the models that have been made in the past concerning the generation and propagation of landslide induced tsunamis.

Subsequently, the landslide that could take place in the worst case scenario, defined by Van Berlo (2006), will be schematized. Its dimensions and material will be determined and the slope profile, on which the landslide will slide, will be defined. In addition, the sliding process will be examined and a schematization of the velocity profile of the landslide will be made. These schematizations provide the model input for the landslide-tsunami generation process.

The numerical model for the tsunami generation will be made in the finite element model Finlab. The modelling process will be split up in several parts. First a simple two dimensional (in the vertical) model with simplified geometry will be made. This model will be verified with experiment results obtained from Sue (2007).

After the 2DV-model has been verified, it will extended to a three dimensional model. To verify this model, physical model tests in a wave basin will be carried out.

Finally, bathymetry data of the La Palma case is added to the three dimensional model.

With the three dimensional model and the La Palma model the generation of a landslide induced tsunami will be quantified.

1.4.   Structure of report

Part I, encompasses the literature study. The literature study provides information on (1) tsunamis, in particular landslide induced tsunamis and (2) numerical and physical scale models. Subsequently, in part II the Canary Islands and in particular the situation in La Palma will be described. Part III, presents the physical scale model set-up and results. Part IV shows the numerical set-up and results. Finally, in part V, the conclusions and recommendations will be discussed.

A list of abbreviations and definitions and a list of symbols can be found in iv and v, preceding this chapter.

2. Landslide induced tsunami

2.1. Tsunamis

After the tsunami of 2004, in the Indian Ocean, most of the world knows the meaning of the word 'tsunami'. However, what most people do not know is that tsunamis happen several times a year over the whole world and most of them are far less devastating than the Indian Ocean tsunami. According to the NGDC tsunami event database, most tsunamis have a maximum wave height of only several decimetres.

Tsunamis can originate from several different sources. In figure 1 possible triggering mechanisms of a tsunami, defined by the NGDC tsunami event database, are shown. Most tsunamis originate from earthquakes.
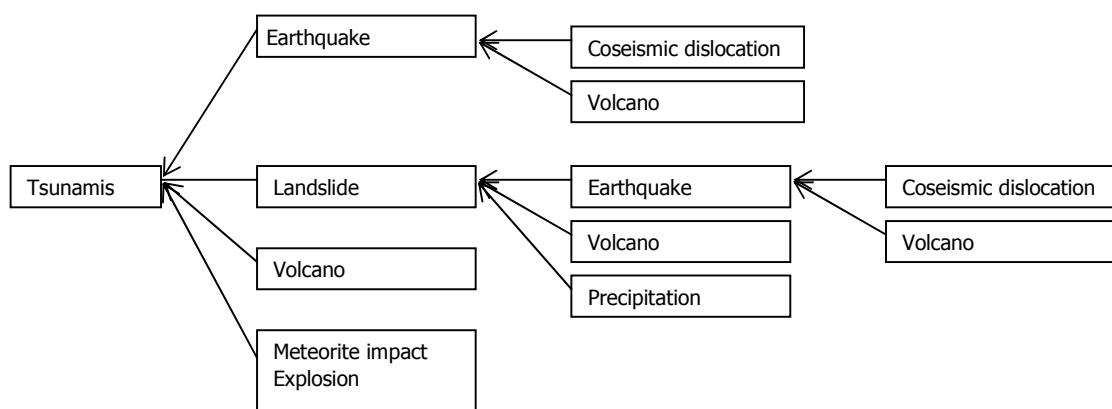
Figure 1: Possible tsunami triggering sources

The generation and propagation of tsunamis resulting from earthquakes have been studied for the last 50 years and are now relatively well understood. In contrast, the importance of tsunamis generated by landslides has only become recognized during the last fifteen years. It became apparent that a landslide source could explain the unusual run-up distributions and propagation characteristics of certain tsunamis. Before that time it was assumed that almost all tsunamis were caused by earthquakes.

If one compares a landslide induced tsunami with an earthquake induced tsunami, one finds that landslide induced tsunamis often have relatively small source areas, compared to the areas affected by large earthquakes. A small source area leads to the generation of shorter waves. In general short waves are more prone to coastal amplification, increasing the local effect and to radial damping, decreasing the far-field effect of the tsunami. Furthermore, the source area of a landslide induced tsunami resembles a point source, while tsunamis generated by earthquakes have a more elongated source. Thus, earthquake induced tsunamis propagate perpendicular to the source fault and have little radial spreading, whereas tsunamis generated by landslides propagate radial and therefore have much radial spreading, see figure 2.

Therefore landslide induced tsunamis have a limited far field effect in contrast to earthquake induced tsunamis.

$$c = \sqrt{gh}$$

h = ca. 1000-4000 m

Earthquake induced tsunami
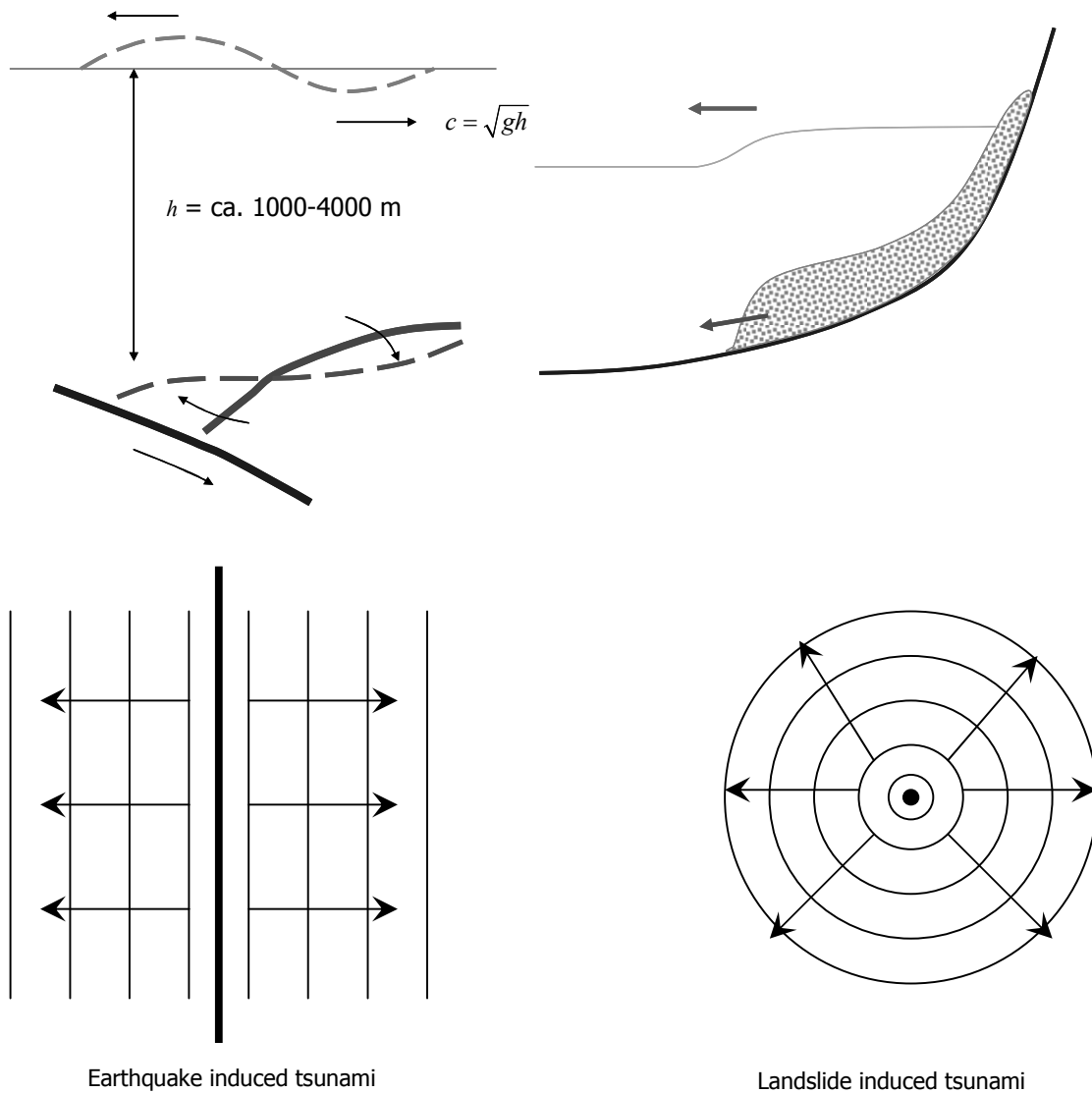
Landslide induced tsunami

Figure 2: Tsunami sources

Landslide tsunamis generated in shallow waters are more harmful than when generated in deep water, since more energy can be converted from the slide to the water. Moreover, shallower water normally means less distance to the coast and a shorter distance available for radial damping. In contrast, tsunamis generated by earthquakes are more critical when the seabed displacement occurs in deeper waters, as the initial wave, which in this case depends much less on the water depth, will become shorter and more dangerously amplified when propagating from deeper to shallower waters.
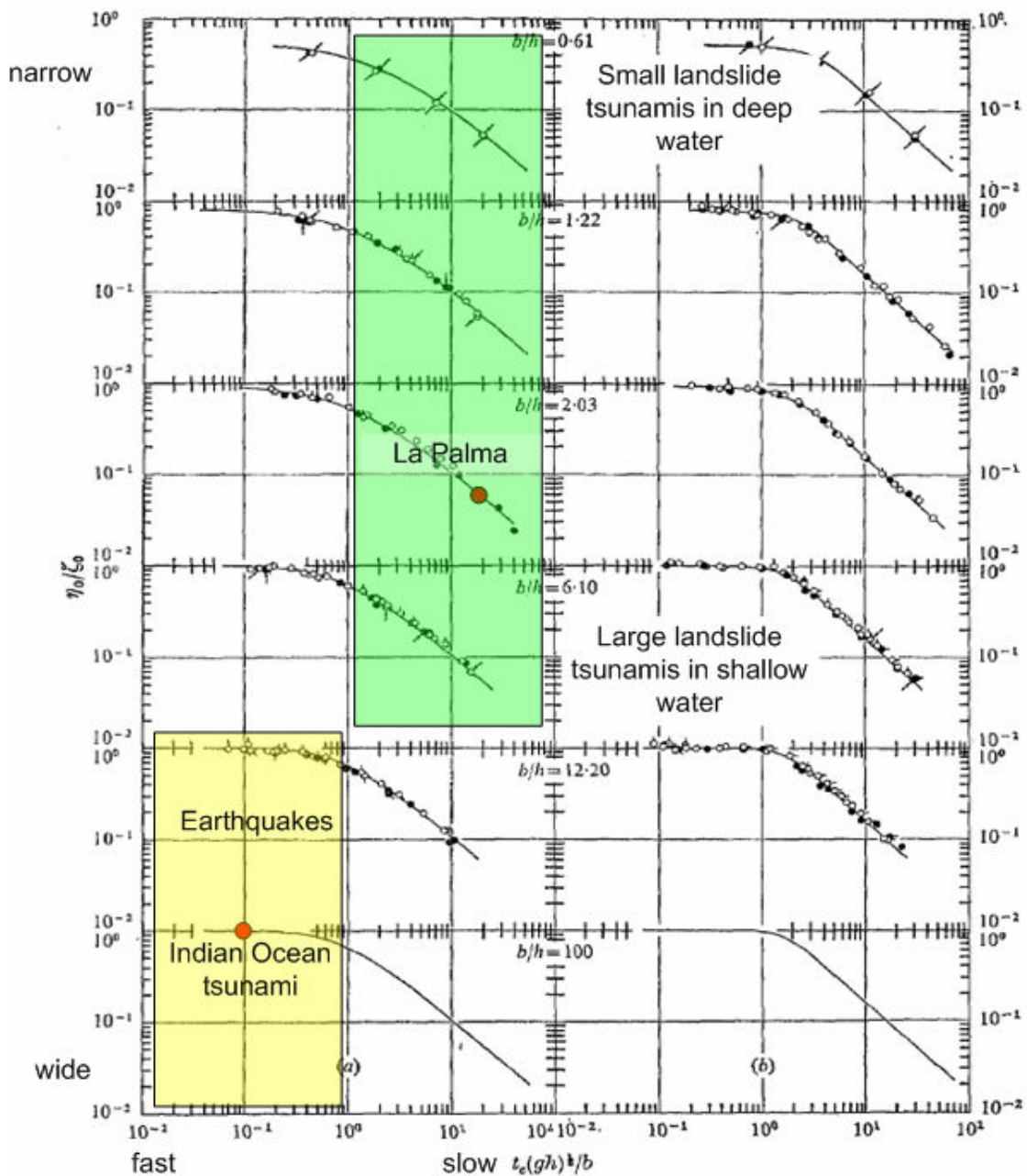
Figure 3: Hammack graphs (source Hammack, 1973)

A good impression of the differences between earthquake and landslide tsunamis can be obtained from the Hammack graphs. J.L. Hammack investigated in 1973 the waves generated by a deformation in a two-dimensional fluid domain. He summarized his experimental and theoretical results based on the linear theory in graphs, see figure 3.

The graph shows the ratio of the maximum wave amplitude η_0 to the local bed displacement ζ_0 as a function of the time/size ratio $t_c(gh)^{\frac{1}{2}}/b$ for $x/h=0$. b is the length of the displacement, h is the water depth and t_c is presented as the characteristic time of bed displacement.

Therefore, $t_c(gh)^{\frac{1}{2}}/b$, which is also called the Hammack number, is the ratio of the timescale of wave generation to the duration of propagation out of the generation region. It means that when $t_c(gh)^{\frac{1}{2}}/b$ is large, which is the case for most landslide induced tsunamis; the tsunami leaves the generation region more rapidly than the duration of landslide motion.

Data are presented separately for each of the five length scales; b/h and for both exponential and half-sine bed motions. Although Hammack did experiments with vertical bed motion instead of horizontal bed motion, the Hammack graph shows also certain relevance for landslide tsunamis.

From the graphs, it can be derived that most earthquake tsunamis have another timescale and length scale than landslide tsunamis. In figure 3 typical timescales and length scales are indicated for earthquake tsunamis in yellow and for landslide tsunamis in green. For small length scales the generated waves are not hydrostatic. For most landslide generated tsunami this means that the generated waves cannot be considered hydrostatic.

For the numerical modelling of landslide tsunamis this means that a different approach is needed than for the modelling of earthquake tsunamis. As said before, landslides produce shorter tsunami waves than earthquake tsunamis. These waves are non-hydrostatic and therefore, in contrast to earthquake tsunamis, vertical velocities cannot be neglected. In addition to this, the dynamic pressure of the waves varies with the water depth. Therefore, when modelling landslide tsunamis, a full three-dimensional flow model is needed. For modelling earthquake tsunamis however, a two-dimensional flow model (in horizontal direction) will suffice.

Furthermore, when $t_c(gh)^{\frac{1}{2}}/b$ is large, which is the case for most landslide induced tsunamis, the timing of the landslide movement becomes important for the generation of waves. Therefore, a good model is needed to estimate the velocity profile of the landslide.

2.2.   Landslides

In the previous section, landslides were considered as one tsunami generation source. However, not all the landslides are the same and therefore not all the landslides produce a tsunami or the same tsunami.

According to Masson et al. (2006), there exist several types of mass failures. Figure 4 shows the different types of mass failures by categorizing the characteristics of the failure.
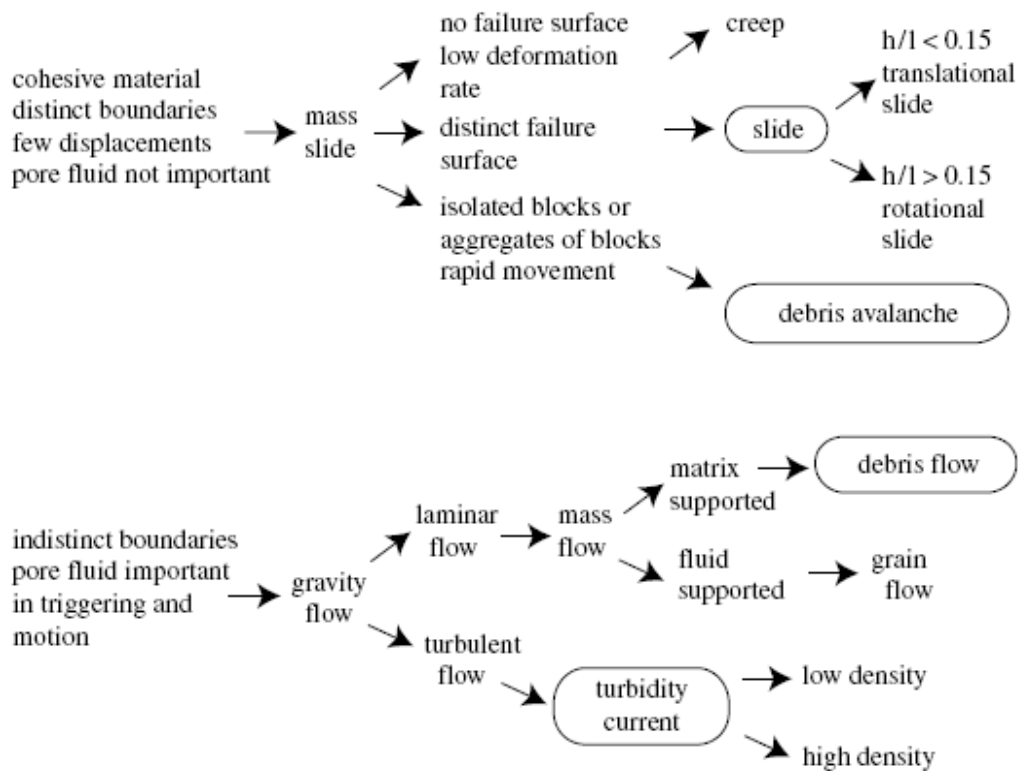
Figure 4: Mass failure categories (source Masson et al. 2006)

Most models of tsunami generation treat landslides as single rapidly moving blocks. As it can be seen from figure 4 the assumption of block movement is not always permitted, as there is a huge difference between the behaviour of a mass slide and gravity flow. Mass slides could be schematized as a block; gravity flow could be schematized as an inviscid or plastic flow.
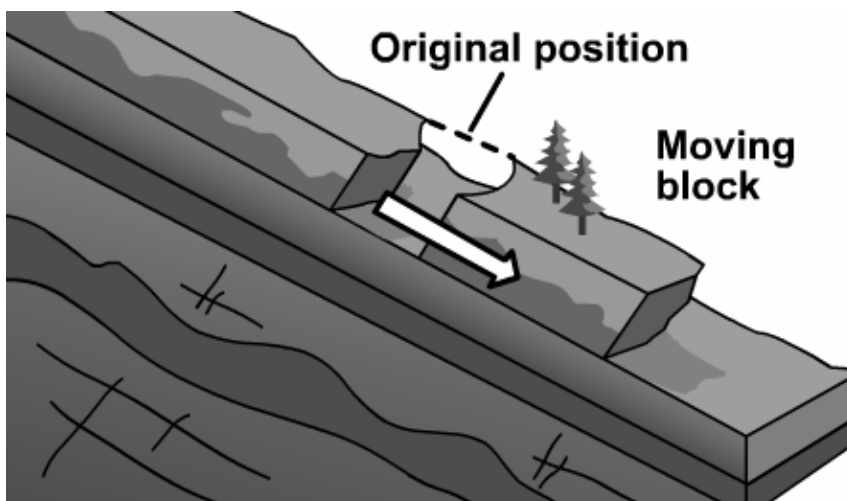

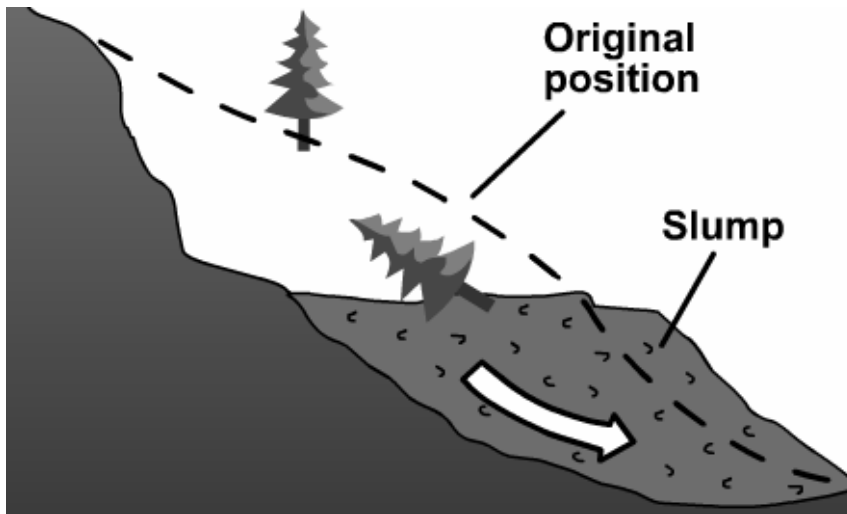Figure 5: Translational slide (source image www.knowledgenetwork.ca/slide)

Figure 6: Rotational slide (source image www.knowledgenetwork.ca/slide)

Looking closer to mass slides, it can be concluded that a mass slide can have different shapes and therefore different behaviours. Translational slides, see figure 5, have a long acceleration phase and a large displacement. Submerged translational slides typically have low basal Coulomb friction once the motion is initiated, which yield a terminal velocity that is essentially limited by hydrodynamic drag, both form and skin friction, and the length of the slope. By the time the slide comes to rest, considerable deformation may have occurred or a turbidity current may have been formed.

On the other hand, rotational slides, also called slumps, have a small displacement and a short acceleration phase. A cohesive slump can experience a significant basal friction and thus hydrodynamic drag will have little influence. Figure 6 shows a slump.
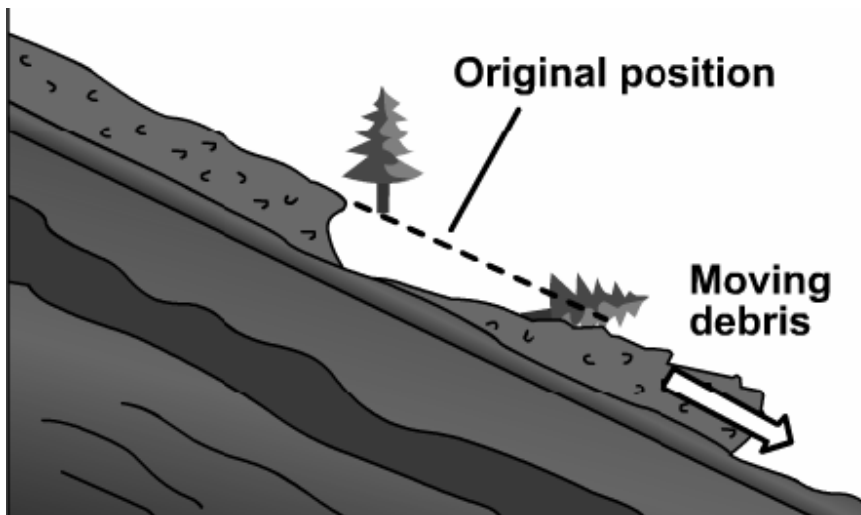

Figure 7: Debris flow (source image www.knowledgenetwork.ca/slide)

Furthermore, a possibility exists that the landslide is not one big slide, but shows multiple stages of sliding. This is called a retrogressive slide, see figure 8. An example of a retrogressive landslide is the Storegga landslide.

The retrogressive landslide, of total length L_r, can be modelled as a train of N fixed block slides released at different times. A retrogressive landslide with short time lags may lead to both shorter wave components originating from the individual blocks and a longer total wave length from superposition compared to rigid submarine landslides. A consequence of the stacked failure is that the potential tsunami hazard may be lower than for a block movement.
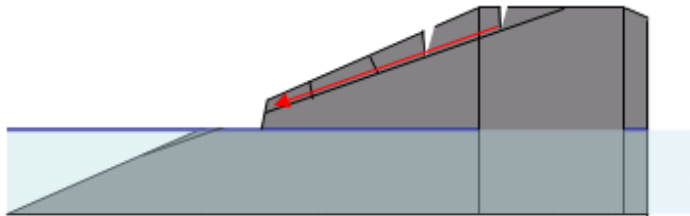

Figure 8: Retrogressive slide (source Van Berlo, 2006)

It can be concluded that the nature of the mass failure has a large influence on the tsunami potential. For landslide modelling it is therefore necessary to make a good prediction of the nature of mass failure.

2.3.   Landslide tsunamis

When the nature of the mass failure is known, it is important to get insight into the parameters of the landslide which determine the wave height, as models of landslide generated tsunamis are dependent on these parameters.

Important parameters are:
- Sliding process, velocity profile
- Shape, depending on the nature of mass failure
- Material, and its chemical composition, grain size, density, porosity
- Slide angle
- Water depth in the area
- Initial position of the landslide: sub-aerial height above the sea or in case of a submarine mass failure, the initial submergence

The velocity of the landslide and the water depth determine the Froude number. Landslides are normally clearly sub critical, i.e. the Froude number (the ratio of slide speed to the speed of wave propagation) is much less than one. This implies that the tsunami will run away from the wave generating slide, limiting the build-up of the wave.
According to Harbitz et al. (2006) the best indicator of tsunamigenic potential is the product of volume and initial acceleration. An abrupt deceleration might also contribute to larger surface elevations.
The slide length affects both the wavelength and the maximum surface elevation, while the wavelength is also determined by the travel time or run-out distance of the slide.
The material of which the landslide consists, determines the weight of the landslide. According to Sue (2007) heavier landslides produce larger waves.

The slide angle of the slope defines the gravity driving force that moves the landslide. The driving force on the landslide on a steep slope is relatively large, which means that the landslide moves

faster and transmits more energy to the water. On the other hand, the time that the landslide is moving in shallow water is shorter than in case of a gentle slope. Therefore a landslide on a gentle slope can generate larger waves.

The initial position of the landslide has influence on the generation of tsunami waves. When the landslide is initially submerged, a trough is created behind the landslide and a crest is created ahead of the landslide. Therefore the first wave which reaches the adjacent coast is a trough, see figure 9. In the meantime, in case of a sub-aerial landslide a crest is created first and will therefore reach the adjacent coast first.
Furthermore, sub-aerial landslide produces a larger tsunami wave than a comparable submerged landslide, as the sub-aerial landslide has a longer path in shallow water.
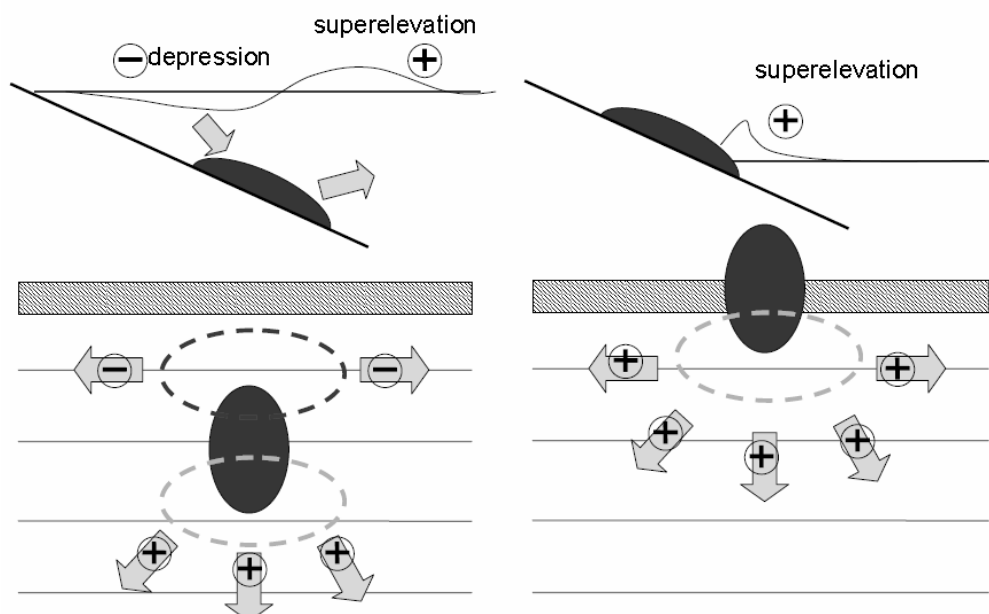

Figure 9: Submerged and sub-aerial landslide (source Belotti 2006)

Several formulae exist, describing the first waves during tsunami generation. Grilli & Watts (2005) converted results from numerical simulations into empirical curve fits predicting characteristic tsunami amplitudes as functions of non-dimensional governing parameters. The empirical formulas are only valid in the vicinity of the tsunami sources and for submerged slides. Formulas, describing the water elevations, exist also for sub-aerial slides. Unfortunately, most of these formulas are based on tsunamis into lakes or reservoirs. Therefore the applicability to predict wave elevations at deep water can be questioned.
An overview of the existing formulas is given in appendix C.

The type of waves that can be expected in the near-field can be determined with calculations on the basis of Hammack 1973. On basis of the Hammack-number, which has already been explained in section 2.1, it can be seen what kind of waves are being generated.
If $Ha_0 >> 1$, which implies for most of the waves generated by landslides, linear water waves are generated that leave the generation region more rapidly than the duration of landslide motion.

A similar analysis can be done with the Ursell-parameter regarding the far-field effects. The Ursell-parameter is the ratio of non-linearity to dispersive effects and may be used to classify waves propagating in constant depth.

Ursell parameter: $U \equiv \dfrac{H\lambda^2}{h^3}$

Where H is the wave height, λ is the dominant wave length and h is the water depth. If $U < 25$, the waves can be well approximated with linear wave theory. For a wave height between $20 - 40$ meter, a wave length of 7000 meter and a water depth of 2000 meter, the Ursell number is smaller than 1. This means that landslide generated tsunamis, when propagating in an ocean, can be described with linear wave theory and are weakly dispersive.

2.4.   Landslide tsunamis in history

The tsunamis in history with the largest waves are landslide tsunamis, which were generated in shallow water areas like bays and lakes, like the Lituya Bay tsunami and the Tafjord tsunami. Furthermore some large tsunamis were generated by huge landslides of several hundred km³. Table 1 shows a record of some landslide tsunamis that occurred in the past. In this table Δt is the time between two retrogressive landslides, θ is the slope angle, b, w and T are respectively the landslide length, width and height and L_r is the total length of a retrogressive slide. Furthermore, η is the wave amplitude of the tsunami wave, T_0 is the wave period of this wave and λ_0 is its deep water wave length.

Table 1: Tsunamis in history

Place	failure type	volume (km^3)	geometry	velocity (m/s)	accelera-tion (m/s^2)	near-field waves (m)	far-field waves (m)	Reference
Tafjord	Rockslide	0.001 – 0.0015	θ = 35 - 45°	50	-	45 m in bay	-	Harbitz et al. (1993)
Izmit Bay (Turkey, 1999)	Slides and one slump triggered by an earthquake	-	w , b , T vary per slide θ = 5°	2.4	0.053	5 – 8 m in bay	-	Watts et al. (2005) Tinti et al. (2005)
Skagway (Alaska, 1994)	Various landslides (retro-gressive)	0.003 – 0.01	w , b , T vary per slide θ = 9 - 24°	31 - 35	0.46 – 1.20	3- 11 m in bay	-	Watts et al. (2005)
Lituya Bay	Rockslide	0.03	-	-	-	30 m in bay	-	Harbitz et al. (1993)
Papua New Guinea (1998)	Earthquake & Underwater slump	4 - 6	$w = b =$ 4,5 km $T = 1200$ m θ = 12°	11.4	0.34	11.2 m	20 km coast affected	Watts et al. (2005) Lynett et al. (2003)
Ritter Island (PNG, 1888)	Lateral collapse with SMF	5	w = 1,5 km T = 780 m	40	-	η = 15 m T_0 = 3 – 4 min.	8 (distance several 100 km)	NGDC Tsunami event database
Grand Banks (Canada, 1929)	Earthquake & SMF & turbidity current	100 - 150	-	15 – 30	-	9 – 15 m or 3 – 7.5 m	Trans-Atlantic tsunami	Fine et al. (2005)
Unimak (Alaska, 1946)	Earthquake & SMF	-	w = 25 km b = 40 km T =400 m θ = 4.3°	199	0.22	32 m λ_0 = 113 km	Trans Pacific tsunami	Watts et al. (2005) Harbitz et al. (2006)
Storegga (Norway, 8200 years ago)	Retro-gressive slide, with Δt = 15 – 20 s	2400	L_r = 1000 km T = 240 m	25 – 30	-	10 – 12 m in shallow water	North sea tsunami	Masson et al. (2006) Bondevik (2005)
Nuuanu (Hawaii)	-	5000	-	-	-	-	-	Masson et al. (2006)

3.   Generation and propagation models

Different models exist for the different stages. Section 3.1 shows which empirical and numerical models have been used in the past. Section 3.2 gives a description of the physical scale models which have been carried out already to simulate the generation of tsunamis.

3.1.   Empirical and numerical models

Landslide induced tsunamis experience three different stages, see figure 10.

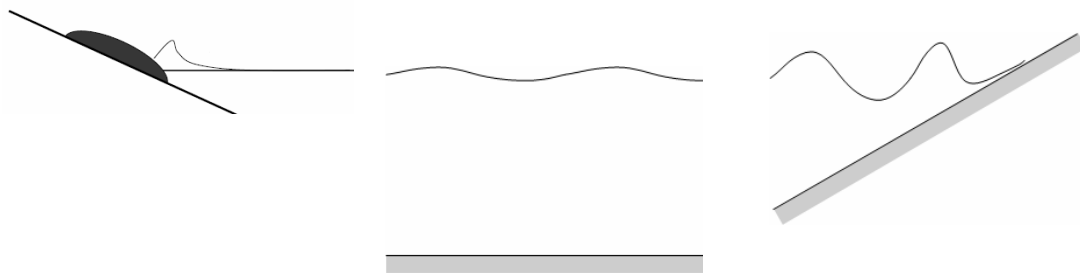Generation near a coast   Propagation in deep water   Interaction with a coast

Figure 10: Schematization

The first crest and through during the generation phase of a landslide induced tsunami can be estimated with the empirical formulas described appendix B. Furthermore the generation and propagation of tsunami waves can be calculated with numerical models. An overview of numerical models found in literature is given in table 2. Most of these models compute one of the stages in detail, whereas the remaining stages are simplified or not modelled at all. This is mainly because a generation model and an interaction model need a fine model grid, while a propagation model, which describes larger areas, has a coarse grid. Moreover, different processes are important in the three stages. To describe all the stages, three different models would be necessary. First a tsunami generation model would be needed, which is a model for tsunami generation due to a specified landslide shape and motion. A second model is a tsunami propagation model to compute the far-field effects of the landslide induced tsunami. The last model is a model, which computes the tsunami run-up when it encounters coasts.

Table 2: Models for water waves generated by landslides (main source Grilli & Watts 2005)

Model		Reference	Comment
Linear shallow water equations (LSW)	2D	Iwasaki (1987, 1997) Harbitz (1992)	In Iwasaki (1987, 1997), the initial wave form of the tsunami due to the landslide is calculated by an analytical method and introduced in the model as an initial condition.
Linearized potential flow equations	2D	Verriere & Lenoir (1992)	
Volume of fluid solution (VOF) of Navier-Stokes (NS) equations	2D	Heinrich (1992) Assier-Rzadkiewicz et al. (1997)	Landslides are modelled as granular or viscous flows.
Non-linear shallow water wave (NSW) equations with a two-phase model	2D	Jiang & LeBlond (1992, 1993, 1994) Imamura & Gica (1996) Fine et al. (1998)	The shallow water wave model is valid when λ/h >10 at the source and λ/h >40 during propagation with T > 15 minutes Landslides are modelled as immiscible fluid flows comprising a second layer.
Non-linear shallow water wave (NSW) equations	2D	Thomson et al. (2001) Titov & Gonzales (2001)	The shallow water wave model is valid when λ/h > 10 at the source and λ/h > 40 during propagation with T > 15 minutes
Green's function representation of LSW, generated over constant depth by an SMF moving with uniform velocity	2D	Tinti & Bortolocci (2000) Tinti et al. (2001) Todorovska et al. (2002) Ward (2001)	
Fully non-linear , dispersive long wave (Boussinesq) (BM) equation	2D	Lynett & Liu (2003) Wei et al. (1995)	Dispersive, non-linear, depth-integrated, inaccurate when tsunami generation occurs in deeper water, cannot model waves close to breaking, inaccurate for simulating very shallow and thick landslides
Fully non-linear potential flow model (FNPF)	2D	Grilli & Watts (2005)	For fully non-linear and dispersive effects without constrictions on wave amplitude, wavelength and submergence depth. Assumption of inviscid, irrational flow is justified for modelling non-breaking wave propagation
Smoothed particle hydrodynamics method (SPH)	2D	Fontaine (2000)	
Smoothed particle hydrodynamics method (SPH)	3D	Gomez-Geisteira (2004) Dalrymple (2004)	
Navier Stokes model	3D	Mader (2004) Gisler et al. (2006)	

3.2. Physical scale models

An overview of interesting physical scale experiments of landslide tsunamis is given appendix B. 2D as well as 3D experiments have been done in the past. The most important results of the experiments will be given in the following sections.

3.2.1. Wave generation

Wiegel (1955) concludes from his landslide experiments that the first wave that is generated is a crest, followed by a trough with a wave amplitude three times the wave amplitude of the first crest. A second wave crest follows the first trough and has approximately the same amplitude. Also Sue et al. (2007) observe a first crest and a first trough and then a second crest followed by smaller wave amplitudes, with short wave lengths. The first crest amplitude continues to increase initially, peaks and then gradually decreases as the wave enters deep water and its wave length increases. The first trough and the second crest exhibit the same behaviour. The first crest forms ahead of the landslide centre of mass and the first trough forms behind it. The motion of the landslide generates the first crest as it pushes water ahead of it, forming a high pressure area. The crest is not attached to the landslide and propagates freely once generated. The accelerating fluid and the turbulent wake above and behind the sliding block creates a region of low pressure; the trough. The first trough propagates at the same speed as the landslide until the landslide decelerates. Dispersion effects further back in the wave train are also present. There is a continual generation of waves at the trailing end of the wave train.

Furthermore, Sue et al. notice that when the landslide block abruptly stops at the end of the slope, waves are generated with amplitudes larger than those initially generated by the accelerating landslide. This indicates that landslide deceleration can have significant effect on the magnitudes of the observed wave run-up.

Enet et al. (2003) conclude from their 3D experiments that cylindrical waves propagate away from the landslide, in the direction of its motion, see figure 11. A main crest develops, leading a train of smaller waves. There is less wave propagation towards the sides of the main crest, but the train of smaller waves following radiates cylindrically.
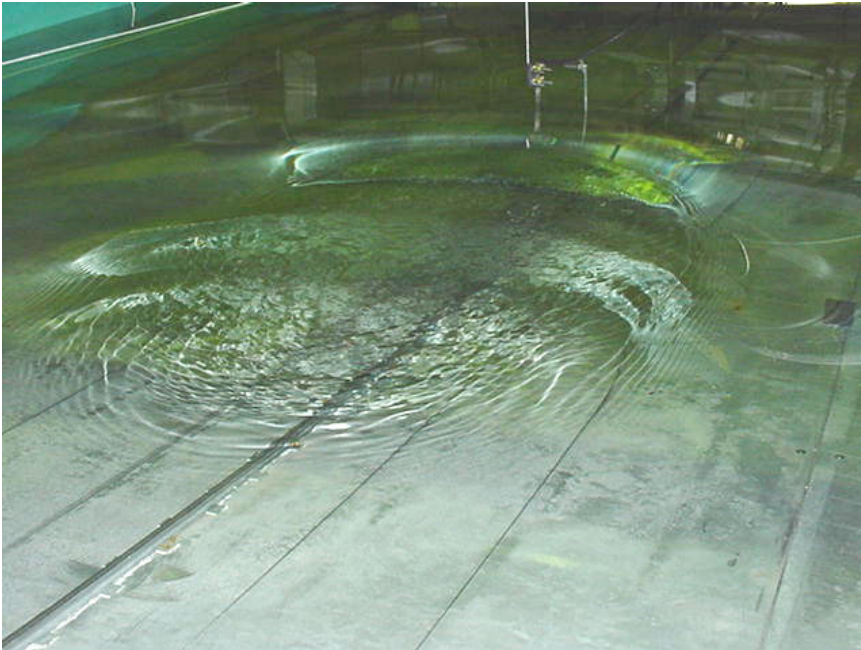
Figure 11: Three dimensional experiment (source Enet et al. 2003)

3.2.2.   Energy conversion

Wiegel (1955) reports that 1-2% of the potential energy of the landslide is converted into wave energy. On the contrary Sue et al. (2007) state that the conversion can be 1.1 – 5.9 % depending on the shape, size and initial submergence etc. of the block.

According to Watts (1997) the conversion of kinetic block energy to wave energy is 3-7 %. Sue et al. (2007) give an amount of 2.8 – 13.8 % for this conversion.
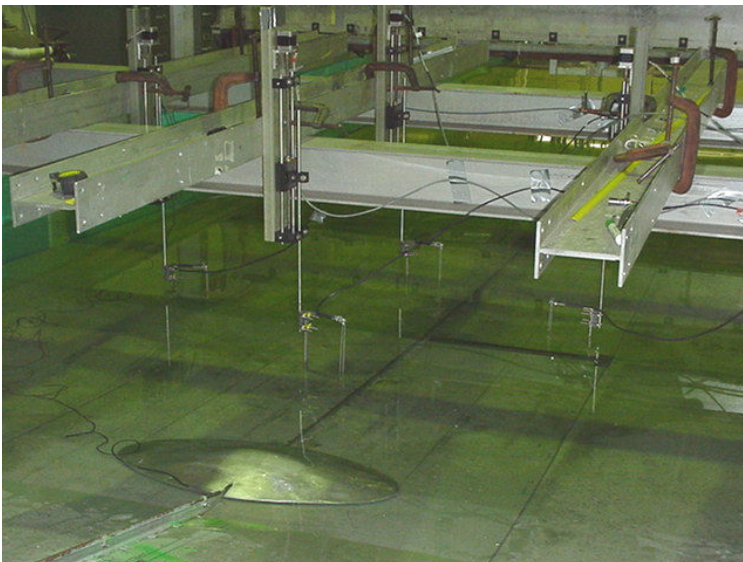

Figure 12: Experimental set-up (source Enet et al. 2003)

PART II: La Palma

4. Location

4.1. Canary Islands

The Canary Islands is a group of seven major volcanic islands that extend for almost 500 km east to west about 100 km off the coast of northwest Africa, see figure 1.

Figure 1: Canary Islands

Nieuwenhuis (2005) describes the origin of the Canary Islands. Volcanic activity of the island group spans 20 million years and it is assumed that the island group has originated over a hotspot. The so-called intra-plate volcanoes developed over the moving plate above the hotspot and traveled with the Africa plate eventually away from the hotspot. Due to the eastward displacement of the Africa plate the most recent and most active volcanism is on the youngest Western islands La Palma and El Hierro.
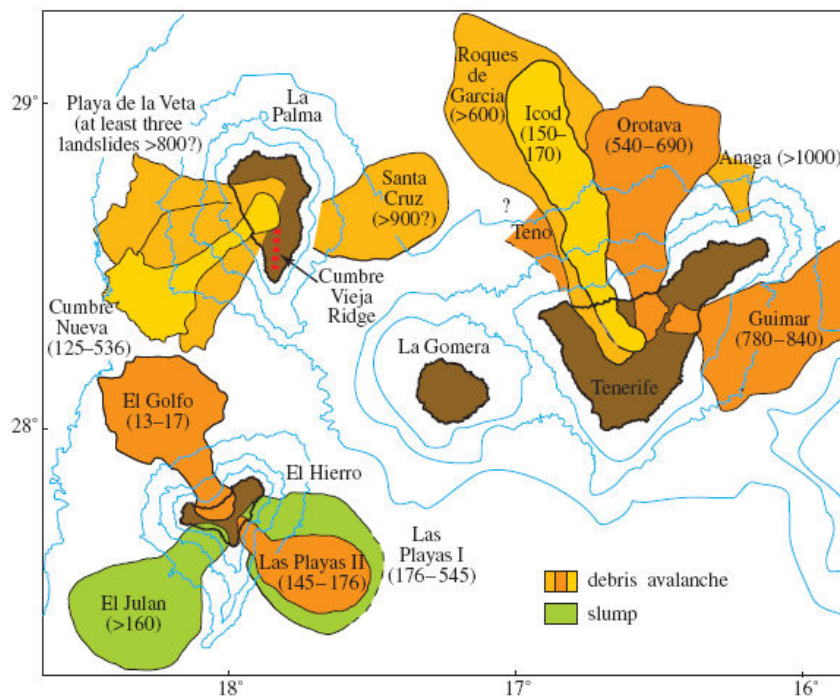
Figure 2: Location and ages of large landslides in the western Canary Islands (source Masson et al. 2006) Note: the ages are indicated in kiloyears (kyr). One kiloyear is 1000 normal years.

According to Masson et al. (2006) the volcanoes of the Canaries produce on average, one landslide somewhere in the Canary Islands every 100.000 years, although this figure masks an irregular distribution through time. Most of the landslides are debris avalanches, with slumps only recognized on the youngest island, El Hierro, perhaps suggesting that this landslide style is a feature of early island development. Glide planes at the base of the landslide are typically up to 10° on the upper slope, decreasing to less than 5° on the lower slope.

Masson et al. (2006) indicate that landslides can also initiate turbidity currents that are capable of flowing considerable distances downslope. Detailed sedimentological analysis of two turbidites derived from Canary Islands landslides has revealed that their source landslides probably occurred in several retrogressive stages over a period of hours or days. Assessing the sedimentary record of deposits derived from these landslides is therefore critical when assessing their tsunamigenic potential, since a series of smaller landslides spread over several hours will have a much smaller tsunami-building potential than a single large, instantaneous landslide.

In table 1 a characteristic landslide at the Canaries is shown.

Table 1: Characteristic landslide in the Canaries (source Masson et al. 2006)

name (location)	failure type	sediment type	water depth (m)	area (km^2)
El Golfo avalanche (Canaries)	Debris avalanche	volcanic rock, volcaniclastic and pelagic sediment	1000 m above sea level to 3900 m below	1500

length (km)	thickness of deposit (m)	volume (km^3)	slope (°)	reference
65	up to 200	150–180	10–1	Masson (1996)

4.2. La Palma

Nieuwenhuis (2005) describes the island La Palma and its volcanoes. La Palma has several volcanoes: Caldera de Taburiente in the north, Cumbre Nueva in the centre and the Cumbre Vieja in the south. The youngest volcano is the Cumbre Vieja (in contradiction to its name), which is 1900 m high. The volcanoes are still active. Eruptions of the Cumbre Vieja volcano occurred in 1971 and 1949. La Palma has witnessed a giant slide, about 560.000 years ago, through the collapse of the Cumbre Nueva volcano. This slide involved a volume of 200 km^3 from the Central-Western part of the island.

In 1999 a discussion about the stability of this western flank of the volcano started. Carracedo et al. (1999) expect that the island is moving again towards a giant lateral flank collapse. They base this hypothesis on qualitative observations; rift reorganization, underlying of the old collapse scar unit of the paleoslide below the western flank and opening of faults during the 1949 eruption, being the most important information supporting their ideas.

In 2001, Day and Ward continue to work on La Palma. They make the daring assumption that a collapse of La Palma's western flank will effectively take place during a future eruption and they model the wave effects that this landslide would trigger. Their conclusion is that in this scenario, the East coast of the USA will be hit by a tsunami of 10 to 25 meters high waves.
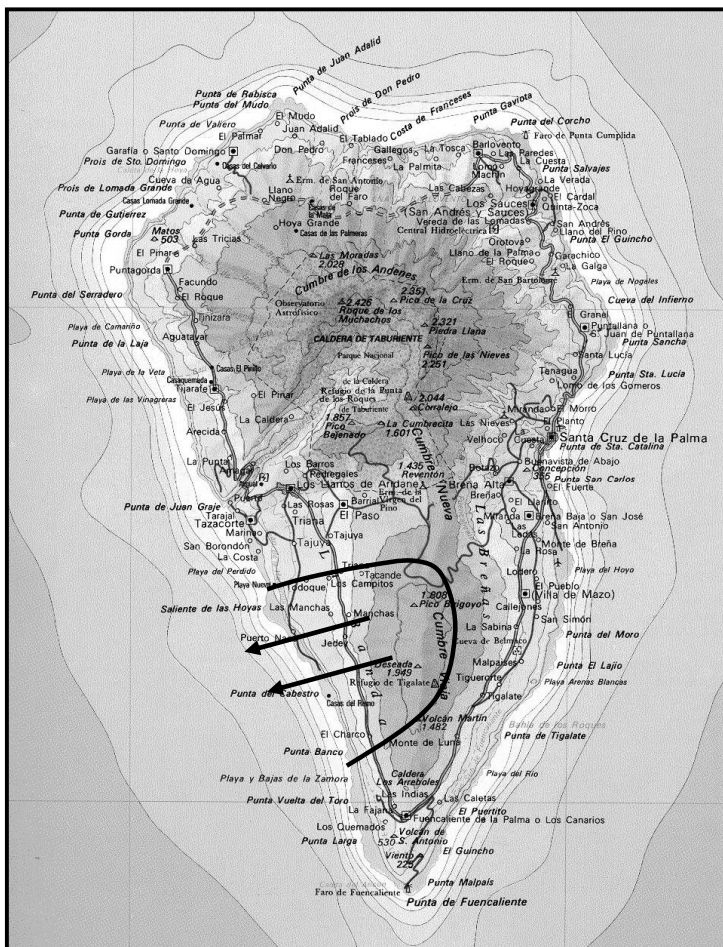

Figure 3: Approximate extent of the possible Cumbre Vieja slide based on the theory of Ward (source Van Berlo 2006)

Following the results of Day and Ward, several researchers decide to model the La Palma landslide tsunami. Table 2 shows the most important parameters for the landslide schematizations that where used in the different modelling attempts.

Table 2: Landslide schematization of the Cumbre Vieja landslide from literature

Reference	failure type	volume (km³)	area to cover (km²)	geometry (k-m)	velocity (m/s)	accelera-tion (m/s²)	near-field waves	far-field waves (m)
Ward & Day (2001)[1]	Wedge shaped block	500	3500	b =25 w =15 T = 1.4	100	0.83	900 m	10 − 25
Mader (2001)[2]	One single block	500	-	-	100	-	η = 650 m λ =30-40 km T =3-4 min.	< 3 m
Gisler (2006)[3]	Inviscid fluid or plastic flow, wedge shaped	308-473	-	-	130-190	-	450 m	1
Delft UT[4]	Block	7 (6-7)	-	b =7 w =0.8 T = 0.5	30 (3-30)	not known	8 m	1

[1] It was assumed that slides likely raft on a highly pressurized layer of mud that reduces basal friction and permits rapid acceleration. Furthermore the slide block travels as a unit for 15 km out to the slope break before it begins to tear apart.
[2] Result of an experimental model of Fritz (2001) ETH. The numerical modelling was done with SWAN.
[3] The results were achieved in several 2D and 3D calculations using SAGE for solving the full Navier-Stokes equations.
[4] A slope of 8° was assumed.

Van Berlo (2006) concluded that it is very unlikely that the flank will collapse in the current configuration. The flank could only be brought close to failure when at least the rock- and soil mass are thoroughly weakened and steeper flanks than in the current configuration are present. Furthermore in the case the flank collapses, it is more probable that a landslide volume of circa 7 km³ moves into the sea, instead of 500 km³ which was assumed by Ward and Day (2001). Table 2 shows the landslide geometry advised by Nieuwenhuis (2005). In appendix A, a summary can be found of the research that has been conducted by the Engineering Geology department.

On account of the worst case scenario assumptions made by Nieuwenhuis (2005), the Environmental Fluid Mechanics department of Delft University of Technology has made some preliminary tsunami calculations with rough input parameters. They came to the conclusion that even if the worst case scenario occurs, the waves arriving on the coast of the USA will be probably in the order of 1 meter instead of 25 meters.

5. Landslide dimensions and velocity profile

5.1. Landslide

Van Berlo (2006) has calculated the stability of three different cross-sections of the west flank of the Cumbre Vieja volcano; the northern, middle and southern section as indicated in figure 4. Van Berlo indicates that the northern section is most prone to mass failure. This is the area where the slide plane of a paleo landslide is found beneath the new volcanic material of the Cumbre Vieja volcano. Additionally, a fault scarp of the 1949 eruption is present in this area. These two factors result in a larger probability that under combined effects of volcanism and gravity a mass failure from the Cumbre Vieja would occur in that area. For these reasons, the northern section will be considered for the determination of the dimensions of the landslide. In figure 4 the area with the former paleo slide plane is shown. Two different southern limits for this paleo slide are given; one is called the conservative side and one limit was denoted by Day (1999). Figure 4 also displays the place and the length of the 1949 fault scarp. The length of the fault scarp is approximately 2 kilometres. In figure 5 the possible area of the landslide is shown.
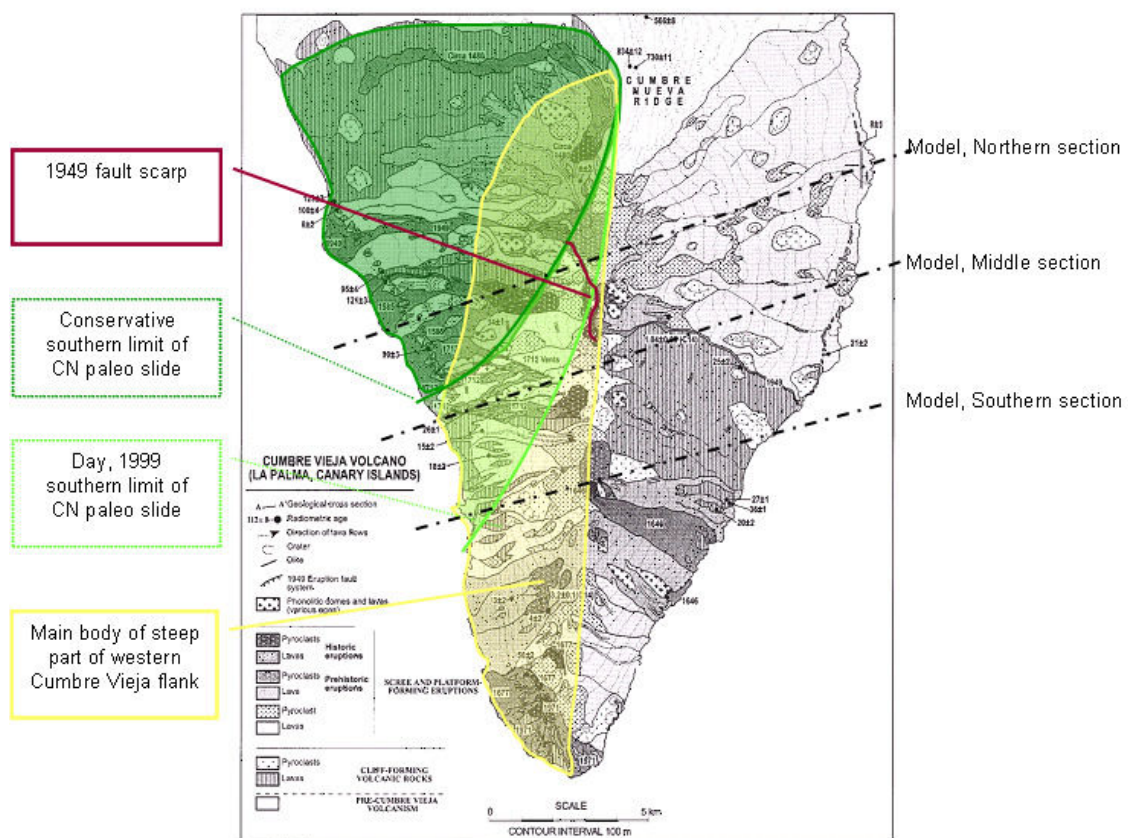

Figure 4: Southern end of La Palma; possible landslide locations (source Van Berlo, 2006)
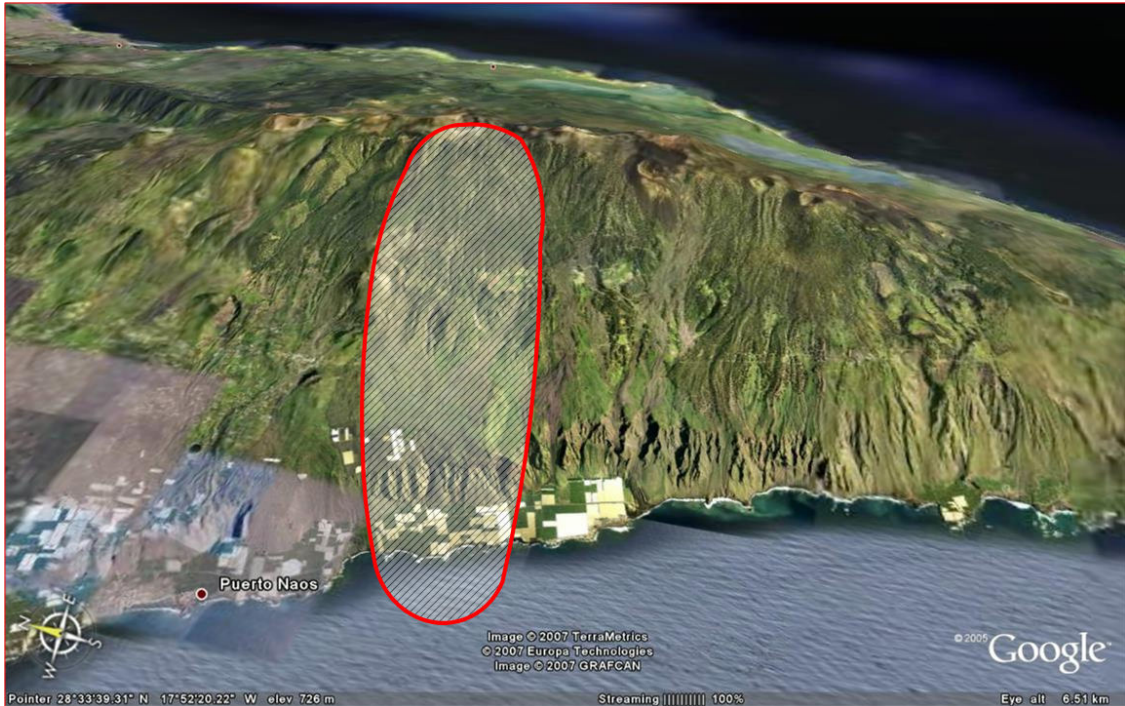
Figure 5: Possible landslide location at the northern section (source image Google earth)

The main dimensions and characteristics of the Cumbre Vieja landslide can be estimated from figure 6. Additionally, the materials of which the landslide consists can be determined from the figure and thereby the density of the landslide. In table 3 a range of landslide dimensions can be found.
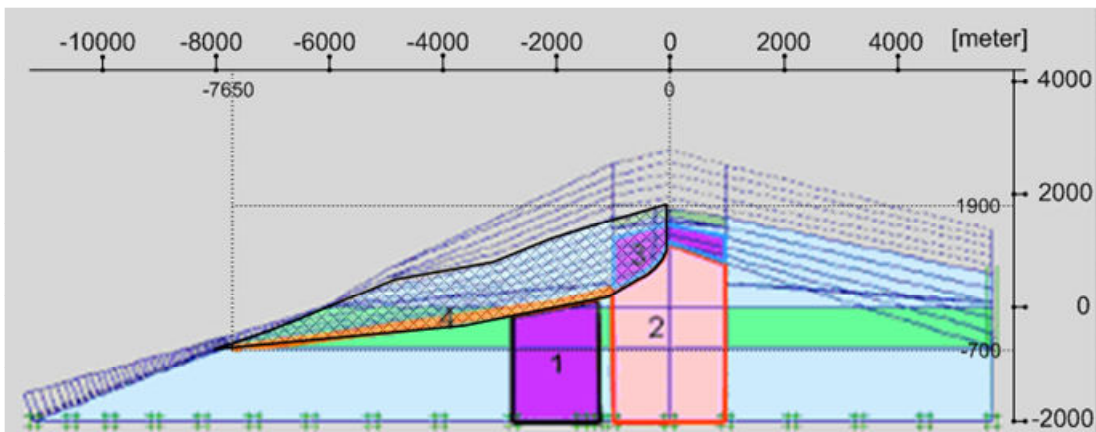

Figure 6: Cross-section of the northern section (source image Van Berlo, 2006)

Van Berlo (2006) calculated that the slide of the northern section could have a dip angle between 5.6 to 9°. As it is known that the dip angle of the paleo slide was 8° [Van Berlo 2006], 8° will be taken as the main slide angle of the landslide. With goniometry, Van Berlo (2006) calculated that the probable slide movement is in the direction 250° to the north, see figure 7.
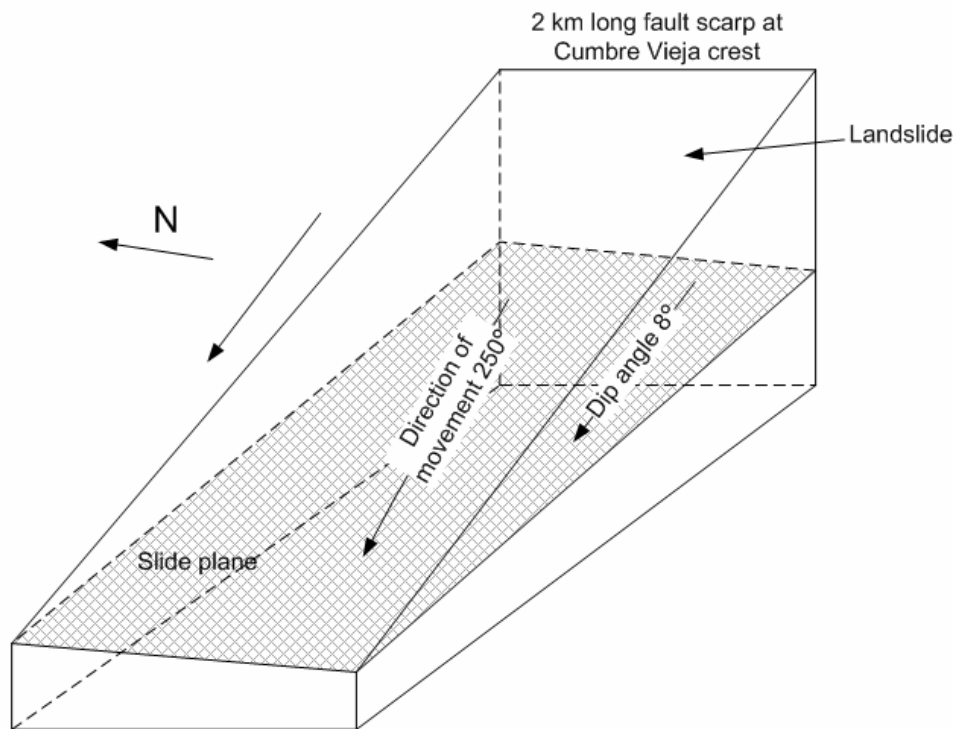
Figure 7: Schematization of the slide plane and the slide direction

Table 3: Parameter ranges of the landslide

Parameter range			
width	w	$500 - 2500$	m
length	b	$6000 - 8000$	m
thickness	T	$700 - 1000$	m
volume (block)	V_s	1 - 12	km³
material		Lava & Breccia Basalt	
density	ρ_s	$1600 - 2600$	kg/m³
dip angle	θ	$5.6 - 9$	°
dip direction		250	°
height of centre of gravity	h_s	500 - 700	m
height above sea level		1950	m
height beneath sea level		-700	m

5.2.   Schematization landslide

In the previous section, a range of dimensions and characteristics of the landslide have been defined. In order to make a model of the landslide, the landslide has to be schematized. For the schematization some practical aspects relating to the physical and numerical model have to be taken into account. For the physical model it is important that the landslide shape is feasible for the practical execution of the experiment. On the other hand, the numerical model must be able
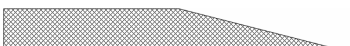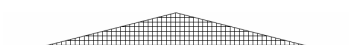
to present the landslide schematization correctly. It is possible that a landslide shape is not feasible, because the numerical model has difficulties with sudden changes in the geometry.
In reality the possible landslide that could occur on the west flank of the Cumbre Vieja would behave like a debris avalanche. The porous basaltic lava and lava and breccia of which the landslide consists, will fracture into pieces as it slides downwards. The slide will move between two east-west slide walls and will possibly experience extra friction.
Unfortunately, it is not possible to simulate this complex sliding process in the experiment. In the experiments found in literature two different options are used to schematize the landslide shape and movement; a solid non-deformable landslide model and a granular deformable landslide model.
For several reasons a solid non-deformable slide has been chosen for the model. Firstly, in most of the available experiment results from literature, a solid non-deformable slide was used. Moreover, the simplification of the deformable porous slide to a solid non-deformable slide is made to make the sliding process easier executable and understandable. For example during the experiments the velocity of the landslide can be controlled more easily when the slide is solid and this improves the repeatability of the experiment. Also the correlation between the water waves and the landslide parameters becomes more transparent. A last argument to use a solid non-deformable slide is that literature has shown [Watts, 2003] that when the focus is on the maximum waves that are being generated by the slide rather than on all the waves that are generated, a solid slide suffices.
The problem that remains is which shape the solid body should get. The shape that would resemble the landslide shape most is a prismatic semi-elliptical shape or a wedge-with a rectangular behind. For the numerical model the easiest shape is a rounded shape. In table 4, possible landslide schematizations are shown.

Table 4: Landslide shapes

Shape	
Round blocks like an elliptical, cosine or Gauss shape	
Rectangular block	
Rectangular wedge combination	
Wedge	

The shape depends on the ability to fabricate the shape for the experiment and the ability to use the landslide geometry in the numerical model. In figure 8, two different shape examples are shown. The first shape is suitable for a 3D-numerical-model and the second shape is suitable for a 2D-numerical-model.
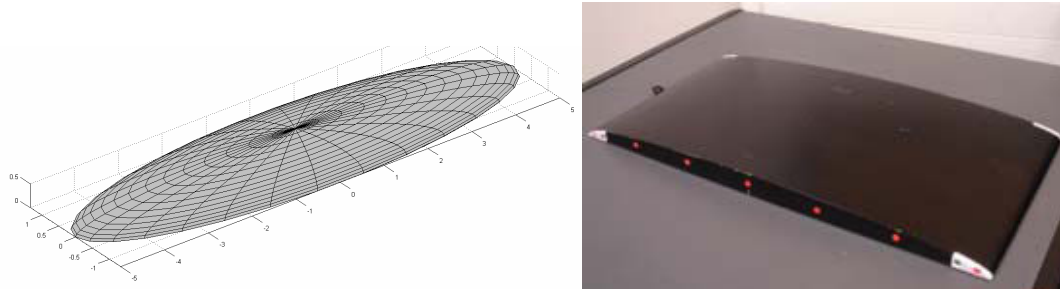
Figure 8: Semi-elliptical and prismatic semi-elliptical shape (image on the right hand: Sue, 2007)

Sue (2007) demonstrated with his semi-analytical model that the two-dimensional shape of the landslide makes little difference for the wave generation, as long as the surface of the shapes is the same. He used landslide shapes varying from a sawtooth model to a semi-elliptical shape. Thus it can be concluded that the exact landslide shape is of minor importance and it suffices to choose a landslide shape that has some resemblance with the experimental model shape and which has no abrupt geometric changes.

Therefore a semi-elliptical shape will be used, as it has a rounded shape and can be described mathematically. The volume formula for the semi-elliptical shape reads:

Formula prismatic semi-elliptical shape: $V_s = \frac{1}{6} \cdot \pi \cdot b \cdot w \cdot T$ Eq. 1

b	= Length of landslide (m)	w	= Width of landslide (m)
T	= Thickness of landslide (m)	V_s	= Landslide volume (m³)

Next step is to define the length, width and thickness of the landslide. In his calculations to determine the landslide volume, Nieuwenhuis (2005) indicates that a volume of 7.85 km²/km seems to be probable for a possible landslide from the Cumbre Vieja flank. His resulting landslide volume becomes 6 to 6.5 km³ with the assumption that the slide width is 700 to 800 meters.

For practical execution of the experiment, the width-length ratio of the landslide is important. A small ratio could make it difficult to simulate the sliding process in the model. Therefore the maximum width of 2.5 kilometres will be chosen as landslide width.

An additional argument for a smaller width-length ratio is that it will be easier to compare the experiment with experiments from literature. In literature most experiments have a width-length ratio larger than 0.3. With a landslide length of 6 kilometres, the ratio for this experiment would become 0.4 instead of 0.1, with a width of 800 meters.

The landslide is between 700 and 1000 meters high. In order to get a landslide volume that is comparable to the volume of Nieuwenhuis (2005) a landslide height of 1000 meters will be chosen. This results, when regarding a semi-elliptical shape, in a landslide volume of 7 km³.

In table 5, the landslide dimensions are summarized.

Table 5: Summary landslide dimensions for the semi-elliptical landslide shape

Parameter		Landslide model	
width	w	2500	m
length	b	6000	m
thickness	T	900	m
volume (block)	V_s	$7 \cdot 10^9$	m³

5.3. Slide plane

In figure 9 the cross-section of the northern section is shown, with a direction of 250° to the north and to a depth of 4200 meters. From this cross-section the different slopes and distances to a depth of 4200 meters can be defined. This information can be found in table 6.
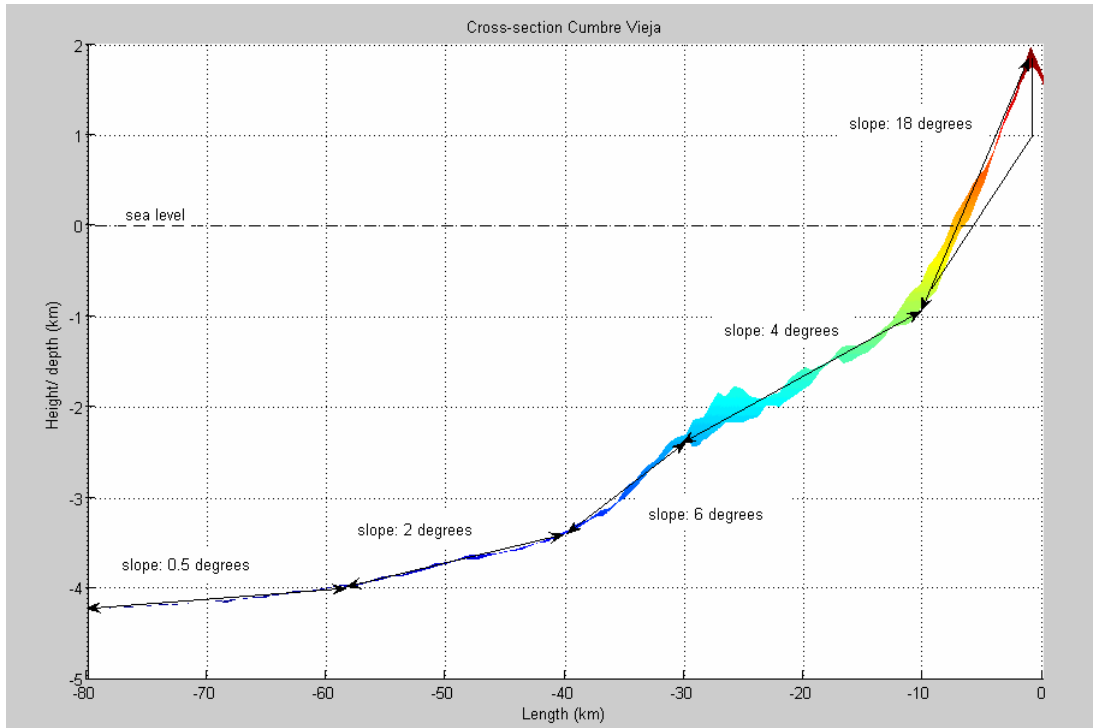

Figure 9: Cross-section of the northern section to a depth of 4200 m (Bathymetry data from the Oceanographic institute in Southampton)

Table 6: Cross-section slopes

Distance	Height/ Depth (m)	Δx (km)	Δh (m)	$\Delta h / \Delta x$	Slope (°)
1 – 10 km	1950 : -950	9	2900	0.32	18
10 – 30 km	-950 : -2400	20	1450	0.07	4
30 – 40 km	-2400 : -3400	10	1000	0.1	6
40 – 58 km	-3400 : -4000	18	600	0.03	2
58 – 80 km	-4000 : -4200	22	200	0.01	0.5

5.4.   Velocity profile La Palma landslide

The La Palma landslide starts its movement at a sub-aerial initial position and from this position it slides down to the adjacent sea bottom. According to Prof. Nieuwenhuis (2005), the highest velocity that is possible in the La Palma case, regarding the geological environment, is a velocity of 30 m/s. This velocity is reached when the landslide moves into the sea. This velocity was derived by a formula which includes rate dependent friction, see eq. 1.

$$\frac{du}{dt} = g \sin \theta \left\{ 1 - F \left(1 + \beta \log \frac{u}{u_{cr}} \right) \right\}$$ Eq. 2

Where β is the shear resistance increase for every tenfold increase in velocity and u_{cr} is the velocity when rate dependent friction becomes important. F is the factor of safety. Nieuwenhuis (2005) assumed a β of 2% and a u_{cr} of 2 m/s and integrated eq. 1 numerically in crude steps of 5 m/s for the landslide velocity. Nieuwenhuis recommends to carry out a more sophisticated analysis in the future.

In appendix D, a model can be found that describes the submarine centre of mass motion of a landslide. The model is based on the first law of Newton and derived by Grilli & Watts (2005) for a submerged landslide. The solution for a sub-aerial landslide was derived by changing the initial conditions and boundary conditions. The model gives an indication of the landslide movement that could occur for La Palma. However, the obtained velocity profile is complicated and given the many unknown input parameters regarding the geological situation, it would not be sensible to use the centre of mass motion model for the numerical and physical scale models, unless further research on this subject is done.

For this study it is chosen to schematize the velocity profile, to keep the numerical model and the physical scale model simple and transparent. For the physical scale model a constant velocity will be used. In the numerical model, different velocity profiles will be used: a constant velocity for the verification with the physical scale model and velocity profiles in other cases. Concerning the velocity quantitatively, velocities will be used that will not exceed 30 m/s when computing the La Palma case.

PART III: Physical scale model

6.   Physical scale model

In this chapter the set-up of the physical scale experiments will be discussed. The configuration of the experiment is based on landslide tsunami experiments described in literature and the La Palma case. In contrary to most physical scale models in the past, the experiment will be carried out in a 3D wave basin instead of a 2D wave flume. Additionally, the landslide will move from a sub-aerial initial position as well as a submerged initial position.

The scaling of the experiment is done with the dimensions of La Palma and its possible landslide. However, it should be noticed that the experiment set-up is not exactly the same as the scaled La Palma case. The experimental set-up is strongly schematized and adapted to the existing conditions of the wave basin. This is not a problem for validating the numerical model, as the schematized set-up makes the modelling process easier and better comparable.

6.1.   Objective

The primary objective of the physical scale experiments is to provide results with which the numerical model of the landslide wave generation can be verified. A secondary objective is to gain insight into the landslide tsunami generation process.

6.2.   Model dimensions

6.2.1.   Wave basin

The physical scale experiments of the generation of a landslide tsunami will be done in the large wave basin in the laboratory for Fluid Mechanics at the Faculty of Civil Engineering and Geosciences of Delft University of Technology. The basin has an effective length of 28 m and an effective width of 15 m. The height of the wave basin is 0.6 m and the maximum water depth is roughly 0.4 m. A 1:20 concrete slope is present on one side of the wave basin, see figure 1.
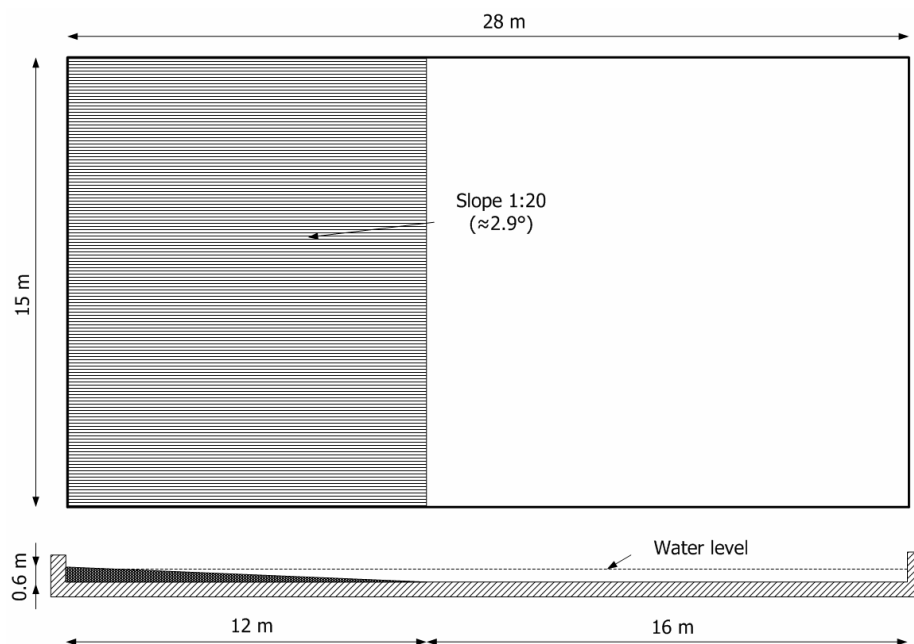

Figure 1: Wave basin, Delft University of Technology

6.2.2. Scaling

For the determination of the values of the model parameters, the prototype parameters need to be scaled. Before the parameters are scaled, a dimensional analysis is carried out in order to group the different parameters into dimensionless parameters. For this scaling analysis reference is made to the books of Hughes (1993) and Chanson (2004).

<u>Dimensional analysis</u>
The independent physical parameters are grouped into dimensionless parameters to reduce the number of parameters. A physical variable of the generated wave field can be expressed as a function of the involved parameters:

$$Z = f(b, w, T, h, u, \alpha, \rho_s, \rho_w, \mu, g, r, \theta, t, \sigma, E_b)$$

|					
b	=	Landslide length (m)	μ	=	Viscosity of water (m^2/s)
w	=	Landslide width (m)	g	=	Gravitational constant (m/s^2)
T	=	Landslide thickness (m)	r	=	Radial distance to a measurement point (m), see fig. 2
h	=	Water depth (m)	α	=	Direction (°), see fig. 2
u	=	Landslide velocity (m/s)	t_s	=	Time of landslide motion (s)
θ	=	Slope angle(°)	σ	=	Surface tension (kg/s^2)
ρ_s	=	Density landslide (kg/m^3)	E_b	=	Elasticity modulus of water (kg/ms^2)
ρ_w	=	Density water(kg/m^3)			
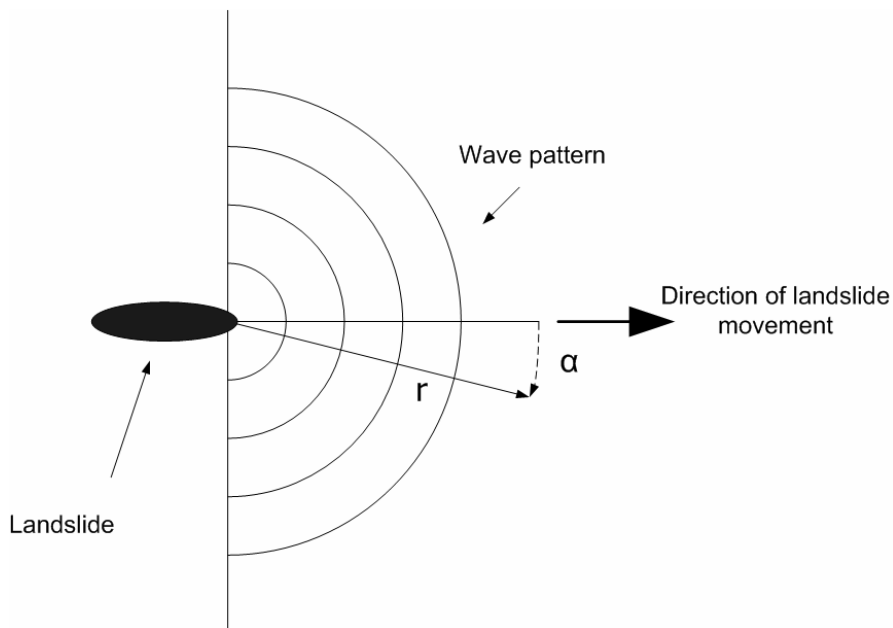
Figure 2: Explanation of radial distance and angle of direction

The parameters and the dimensions of these can be grouped into three categories: mass (M), length (L) and time (T). The dimensionless parameters that originate in this way can be found in table 1.

Table 1: Dimensionless parameters

Dimensionless wave height	$\dfrac{\eta}{h}$	Dimensionless relative density	$\dfrac{\rho_s}{\rho_w}$
Dimensionless wave period	$T\sqrt{\dfrac{g}{h}}$	Time	$t\sqrt{\dfrac{g}{h}}$
Dimensionless volume	$\dfrac{bwT}{h^3}$	Froude number	$\dfrac{u}{\sqrt{gh}}$
Slope	$\sin\theta$	Reynolds number	$\dfrac{\rho u h}{\mu}$
Direction	$\cos\alpha$	Weber (surface tension) number	$\dfrac{u}{\sqrt{\dfrac{\sigma}{\rho_w h}}}$
Dimensionless distance	$\dfrac{r}{h}$	Cauchy (compressibility) number	$\dfrac{u}{\sqrt{\dfrac{E_b}{\rho_w}}}$

The Froude, Reynolds, Weber and Cauchy parameters have contrasting demands for scaling and therefore the most dominant mechanism has to be found. The most dominant mechanism in free-surface flow is the gravity effect and therefore a Froude-scaling has to be used. As the other mechanisms are not scaled properly, scale effects are introduced.

Scale
The maximum water depth of the wave basin is roughly 0.4 m. The minimum water depth to neglect surface tension effects is also 0.4 m. The water depth and the landslide dimensions determine the scale ratio between prototype and model. Several scales can be used, depending on the reference water depth in the prototype. For a reference water depth of 4000 meter, a scale ratio of 10,000 is necessary, while for a reference depth of 2000 meters only a scale ratio of 5000 is needed. However, with a small scale ratio, the landslide dimensions in the laboratory would become very large. In order to be able to handle the landslide model, its length should be smaller than 1 m.
For the experiment a reference depth of 3400 meter is chosen. This is the point in the prototype where the mean slope of 5° merges into a very gentle slope of less than 2°, see part II. A depth of 3400 meter results in a scale ratio of **8500** for a water depth of 0.4 m in the laboratory. The landslide length would be roughly 0.7 meter, which is acceptable.

The landslide parameters with a 1:8500 scaling ratio will be as follows:

Table 2: Scaled landslide parameters

Parameter		Prototype	Model (1:8500)	
depth	h	3400	0.4	m
width	w	2500	0.3	m
length	b	6000	0.7	m
thickness	T	900	0.1	m
volume (block)	V_s	7E9	11E-3	m³
density	ρ_s	2300	2240	kg/m³
mass	m	1.6E13	25	kg
landslide velocity	u_{max}	30	0.33	m/s

Scale effects

Scale effects might occur due to the fact that the Reynolds, Weber and Cauchy similarity have become distorted in the model. The Cauchy number of both the prototype and the model is small enough to become insignificant. However, the Reynolds number of the model should be higher than about 4000 to neglect the effects of viscosity. For a configuration with small landslide velocities the Reynolds number of the waves is in the order of 4000. Therefore some extra damping in the physical scale model could be expected and this leads to a slightly smaller wave height and a slower spreading of the waves. Additionally, capillary wave action, the Weber number, could begin to play a role when the water depth in the model is small and the waves are short. Capillary waves have a wave height in the order of millimetres and a wave length in the order of centimetres. In comparison, the expected maximum wave height in the model has the order of centimetres and the expected wave length is approximately the landslide length. According to Müller (1995) this difference is enough to neglect capillary wave action for the maximum wave. Furthermore, the water depth in the basin will be roughly 0.4 meters, which is large enough to neglect the surface tension effects when the demands on the wave length are satisfied.

6.3.   Experimental set-up

6.3.1.   Landslide model

The landslide model is made of a wooden skeleton, which is ballasted with stainless steel weights. The upper layer of the landslide model is covered with cement to make the landslide model waterproof. This results in a landslide mass of 25 kilograms and thus a landslide density of approximately 2300 kg/m^3. Figures 3a,b,c show the landslide and its dimensions. Four wheels have been fixed to the bottom of the landslide shape to make the motion easier; see figure 3c. The landslide model has a semi-elliptical shape.
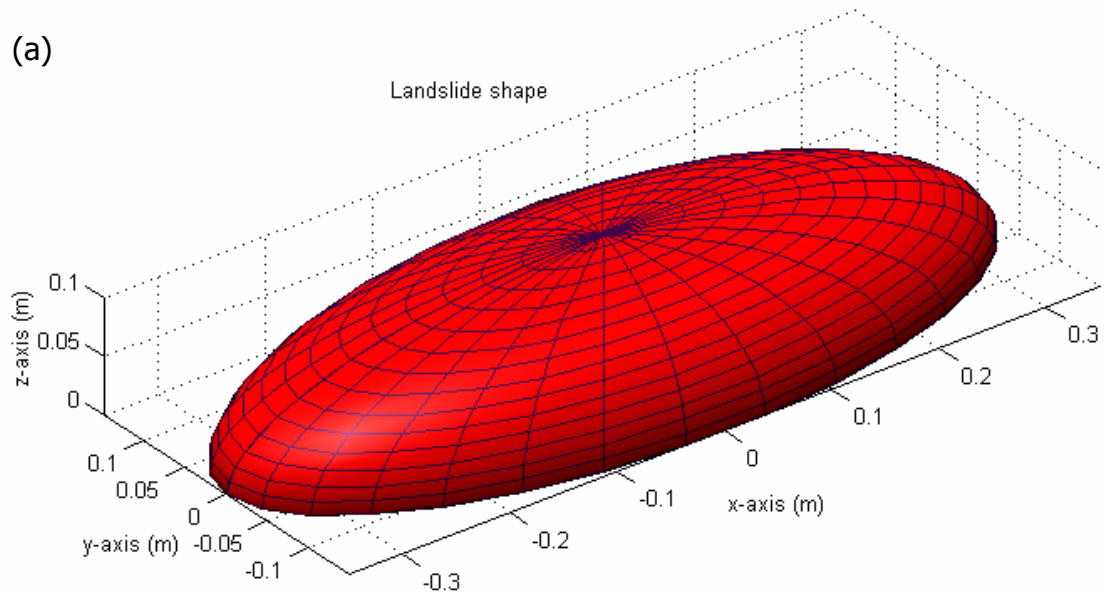
Figure 3a,b,c: The landslide model with its dimensions.

6.3.2.   Basin

The 1:20 slope, which is already present in the wave basin, is used for this experiment. In figure 4 the cross-section of the slope with a water level of 0.4 meters is shown.

As indicated in figures 4 and 5, the upper end of the steel sheet along which the landslide model moves, is used as reference point r = 0 m and α = 0°. From this point the initial positions of the landslide and the positions of the wave gauges will be deduced. The water level is zero meter at r = 0.8 m.
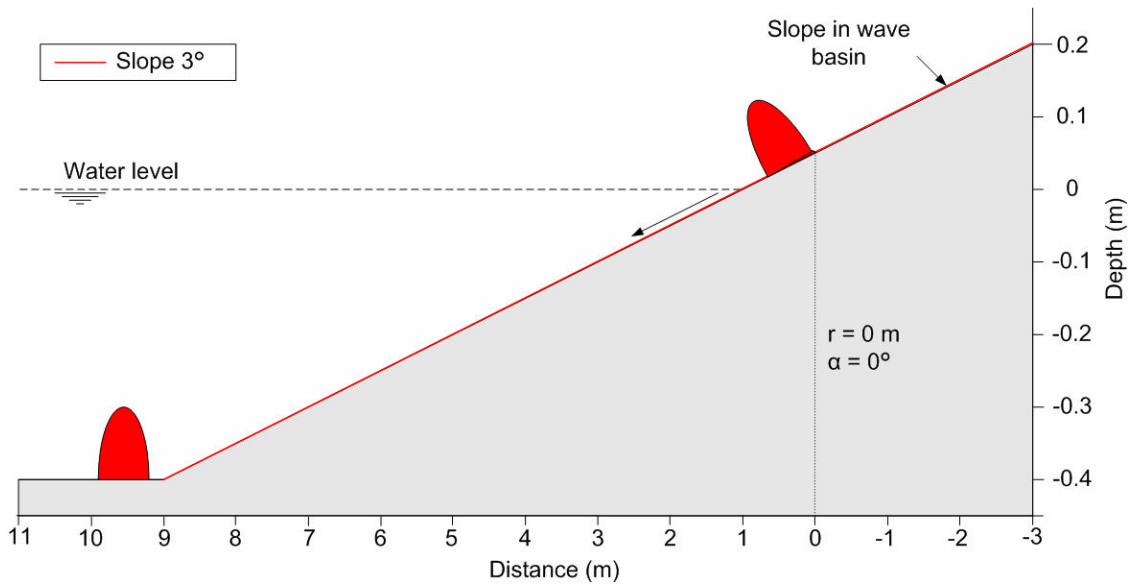

Figure 4: Model cross-section. Note: the relative distortion of the vertical axis.
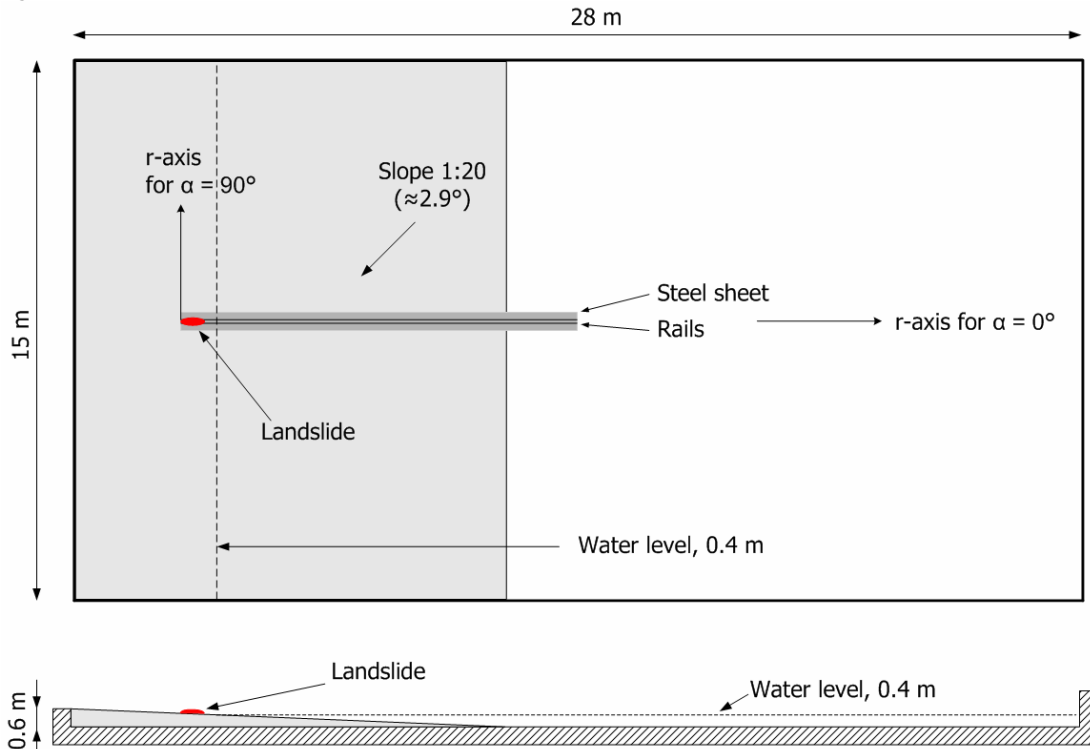

Figure 5: Experimental set-up

A 10 meter long steel sheet is placed in the middle of the basin, see figure 6a. On this sheet two rails are attached, which constrain the landslide model in its motion. The landslide model therefore moves exactly on a specified path.

The landslide motion is controlled by a motor. A flywheel is attached to the motor, which guides a steel wire. This steel wire is able to pull the landslide model forward and backward at various velocities.
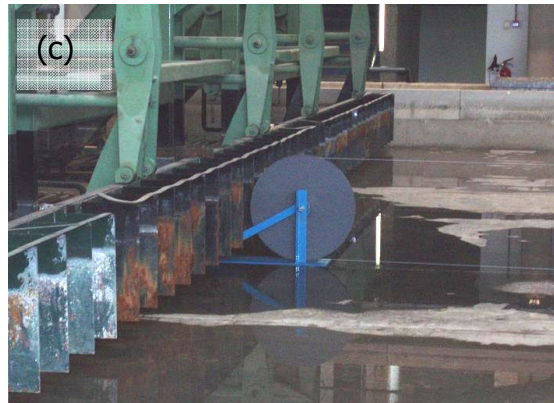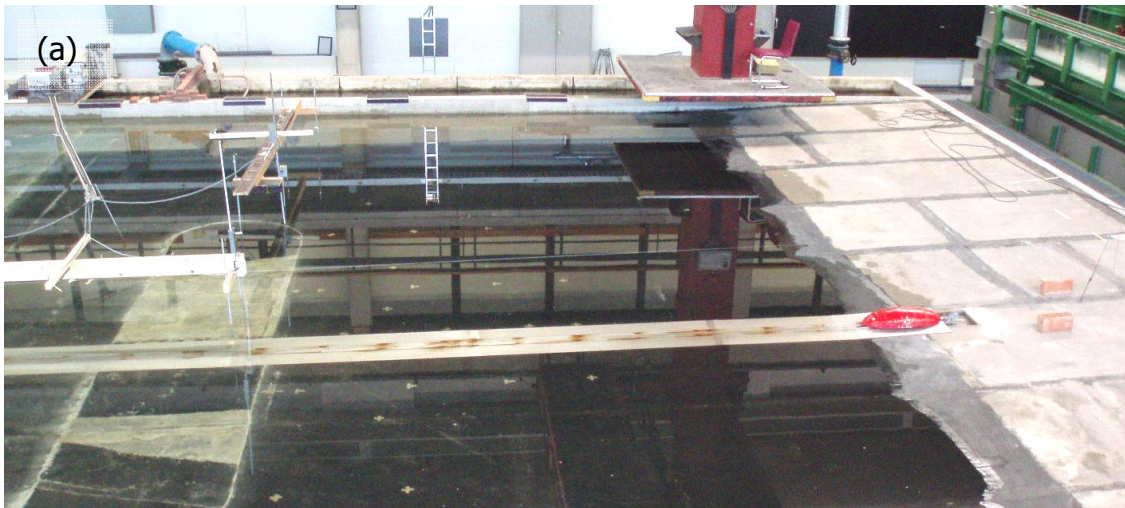

Figure 6a,b,c: Experimental set-up. a: the basin, b: the motor with the flywheel and a steel wire, c: a pulley on the other side of basin.

6.4.   Measurements

6.4.1.   Instruments

Important parameters in the experiment are:
Wave characteristics:
- Wave pattern, wave celerity, frequency and wave length
- First peak height, first trough height and their period

Landslide motion:
- Velocity and displacement of the landslide in time
- The duration of landslide motion

Experiment parameters:
- Slope
- Landslide characteristics; length, width, thickness and density
- Initial water depth

Some of the experimental parameters can be measured beforehand and have already been discussed in the previous section. Table 3 shows how the rest of the parameters will be measured during the experiment.

Table 3: Measurements during the experiments

Measurement	Instrument	In time	Spatial	Derive/calculate
Surface elevation	Wave gauge	Continuous, 100 Hz	At certain places	First peak height First trough height
	Video imaging[1]	Continuous	Continuous in certain area	Wave period Wave pattern Wave celerity Frequencies Wave length
Initial water depth	Ruler	-	-	
Start and end time and landslide displacement	Stopwatch and markings on the steel wire	-	-	Velocity

[1]The video imaging will not be treated in this report.

The surface elevation is measured with six wave gauges, see figure 7. Two different wave gauges are used; three acoustic wave gauges and three resistance wave meters. All the signals are sampled at a frequency of 100 Hz.
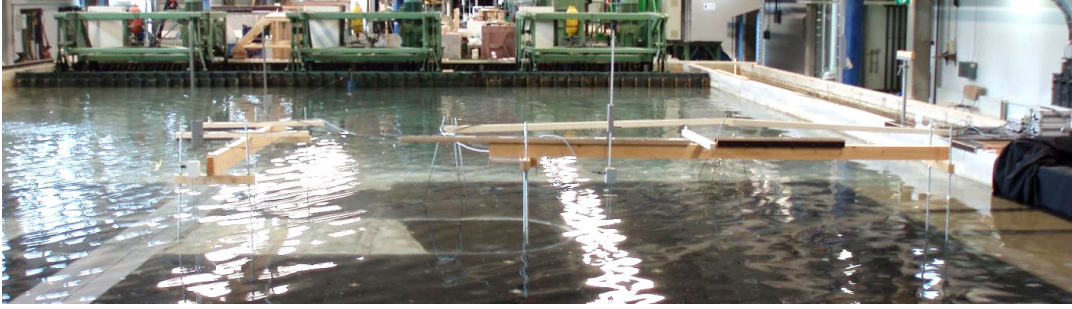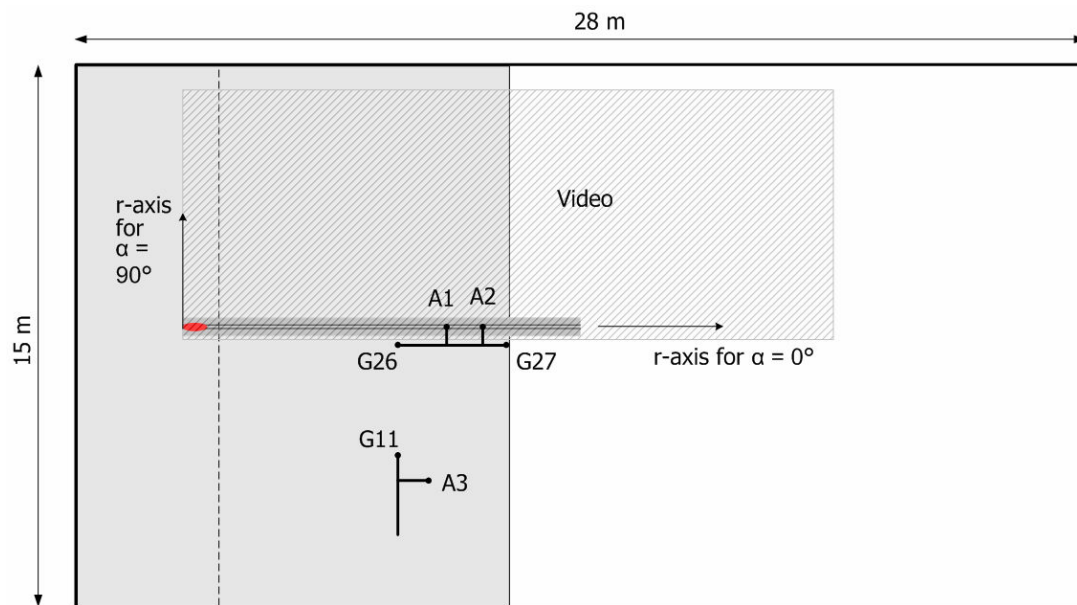
Figure 7: Wave gauges.

Figure 8: Measurement set-up with wave gauges and video imaging

Four wave gauges are placed as close as possible to the axis of landslide motion. The acoustic wave gauges can be placed directly above the axis, and the capacitance wave gauges are placed at a minimal distance from the axis.

Two additional wave gauges are placed on one side of the axis of landslide motion, in order to be able to measure the three-dimensional spreading of the waves. The exact locations of the wave gauges are listed in table 4 and shown in figure 8. G26, G27 and G11 are acoustic wave gauges, A1, A2 and A3 are capacitance wave gauges.

Table 4: Location wave gauges

Wave gauge number	r (m)	α (°)	r/h	x (m)	y (m)
G26	5.92	4.9	14.8	5.90	0.51
G27	8.95	3.3	22.4	8.93	0.52
G11	6.96	30.4	17.4	6.00	3.52
A1	7.33	0	18.3	7.33	0
A2	8.33	0	20.8	8.33	0
A3	8.04	31.7	20.1	6.84	4.22

6.4.2. Scenarios

By varying parameters it can be determined which parameters have a large influence on the wave characteristics. Another reason to vary the parameters is to get some overlap with existing experiments.

Unfortunately, there is not enough time to vary all the important parameters. Moreover, it is expensive and time consuming to change the landslide dimensions and the slope is already present in the wave basin. Therefore it is decided to vary only the landslide velocity and the initial position of the landslide. Sub-aerial as well as submerged initial positions will be examined. Note: the initial position of the landslide is specified as the location where the rear site of the landslide model is situated.

Three sets of experiments will be carried out. The first set, set 0, is to test the configuration and its different possibilities. Sub-aerial as well as submerged initial positions are tried and the velocities of the landslide model are varied. After this set of experiments, a definitive experimental program is composed. In set 1 and set 2, the landslide velocities and the initial position respectively have been varied. The experiments of these sets are repeated several times to check for repeatability. For each experiment the starting time and end time of the landslide motion is measured.

Table 5: Set 1, different velocities (low velocity range)

Set 1	Experiment	Velocity (m/s)	Froude
Sub-aerial Initial position at r = 0 m	1. (1,2,3,4)	0.1	0.05
	2.	0.2	0.1
	3.	0.3	0.15
	4.	0.4	0.2
	5.	0.5	0.25
	6.	0.6	0.3
	7.	0.7	0.35

Table 6: Set 2, different submergences (low velocity range)

Set 2	Experiment	Initial position relative to r = 0 m	Velocity (m/s)	r/h	Froude
Submerged	1. (1,2,3,4)	3	0.46	7.5	0.23
	2.	4	0.46	10	0.23
	3.	5	0.46	12.5	0.23
	4.	6	0.46	15	0.23
	5.	3	0.7	7.5	0.35
	6.	4	0.7	10	0.35
	7.	5	0.7	12.5	0.35
	8.	6	0.7	15	0.35

After set 1 and set 2 have been measured, a larger flywheel is placed in the setting. With the larger flywheel, larger landslide velocities can be achieved (thus, higher Froude numbers) and therefore higher waves can be generated. Basically, set 1 and set 2 are repeated with different velocities, see table 7 and 8. In set 3 an overlap with set 1 is created for two velocities. Naturally, the results of the overlapping tests should be the same.

Table 7: Set 3, different velocities (higher velocity range)

Set 3	Experiment	Velocity (m/s)	Froude
Sub-aerial Initial position at r = 0 m	1. (1,2)	0.6	0.3
	2.	0.7	0.35
	3.	0.8	0.4
	4.	0.9	0.45
	5.	1.0	0.5
	6.	1.1	0.56
	7.	1.2	0.61
	8.	1.3	0.66
	9.	1.33	0.67

Table 8: Set 4, different submergences (higher velocity range)

Set 4	Experiment	Initial position relative to r = 0 m	Velocity (m/s)	r/h	Froude
Submerged	1. (1,2)	4	1.0	10	0.5
	2.	5	1.0	12.5	0.5
	3.	4	1.3	10	0.66
	4.	5	1.3	12.5	0.66

6.4.3.   Test procedure

The procedure of each test is as follows: First the landslide is placed at the selected initial position along the slope. After a couple of minutes, when the natural oscillations of the water surface have reduced to some extent, the electrical signal from the wave gauges to the computers is switched on. At the same time a stopwatch is turned on at the start of the measurement. Subsequently the landslide is released and also this time, the time of release, is saved in the stopwatch. When the landslide moves past the position r = 8 meters, the landslide model is stopped and the time, the end time of motion, is clocked. Finally the electrical signal of the wave gauges is switched off and the landslide is pulled back to the next initial position.

6.5. Experimental parameters compared to literature

6.5.1. Experimental set-up

In the previous section the set-up for the experiment at DUT has been discussed. As already been described in Part I, several experiments on landslide tsunamis have been carried out in the past. In appendix A an overview can be found of the parameter ranges of some of these experiments. The most relevant experiments have been chosen from this overview to compare them with the DUT experiment. In table 9 the dimensionless parameter values for these experiments are given and are compared with the Delft UT experiment.

Table 9: Dimensionless parameters in experiments

	Sue et al. (2006)	Enet et al. (2003)	Liu et al. (2005)	Walder et al. (2003)	Belotti et al. (2007)	Panizzo et al. (2005)	**Delft UT**
	2D	3D	3D	2D	3D	3D	**3D**
	Sub-merged	Sub-merged	Both	Sub-aerial	Sub-aerial	Sub-aerial	**Both**
$\frac{bwT}{h^3}\,(=V_w{*})$	0.039	0.004	0.019	0.199 - 23.126	0.026 – 0.074	0.022 - 0.7	**0.33**
$\frac{wT}{h^2}\,(=A_w{*})$	0.034	0.017	0.050	0.275 - 2.941	0.030 – 0.056	0.042 - 0.675	**0.19**
$\frac{T}{b}$	0.052	0.2	0.5	0.08 – 0.54	0.06	0.22 – 0.44	**0.14**
$\frac{w}{b}$	0.5	1.75	0.71	0.37 - 1.60	0.5	0.73 – 1.46	**0.43**
$\frac{u}{\sqrt{gh}}$	0.702	0.440	-	0.8855 - 4.9482	0.141 – 0.577	0.999 - 2.221	**0.025 – 0.66**
$\frac{\rho_s}{\rho_w}$	0.63 - 4.02	2.700	1.4 - 3.5	-	1.83	2.200	**2.24**
$t_s\sqrt{\frac{g}{h}}\,(=t_s{*})$	8.781	4.482	-	-	-	0.39 - 5.112	**25 – 125[1]**
$\sin\theta$	0.259	0.259	0.423	0.19 - 0.33	0.31	0.259 - 0.588	**0.05**
$\cos\alpha$	1	-	-	-	-	0 - 1	**0 - 1**
$\frac{r}{h}$	0 - 33.7	-	-	-	-	1.312 - 15.125	**0 – 25**

[1] According to the formulas of Panizzo et al. (2005)

The sub-aerial experiments of Panizzo resemble the Delft UT experiment most. However, these experiments were carried out with a rectangular block instead of an elliptic shape.
Generally, the landslide dimensions in relation to the water depth are larger in the Delft UT experiment. On the other hand the slope angle is very small compared to the other experiments and therefore the time of motion on the slope is large.

6.5.2. Expected wave characteristics

Empirical formulas to calculate wave heights and periods have been derived from some experimental data and can be used to get insight into the expected range of wave characteristics.

Different formulas are available from experiments and models to calculate the wave heights, amplitude and period. Most of the formulas describe the first waves and the maximum waves. In figure 9 an example of a possible wave height record is shown. The formulas are given in appendix B.
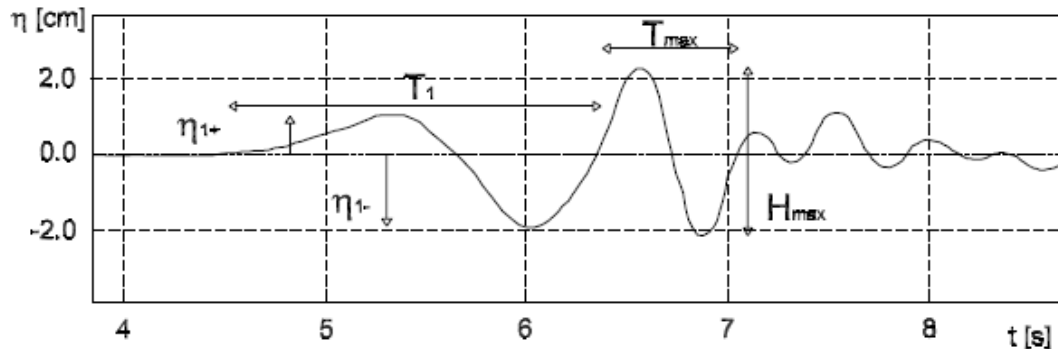
Figure 9: Example of measured wave height (Panizzo et al., 2005)

With these formulas an estimate can be made of the wave height and period of the experiment with the planned parameters of the first two sets. These estimates are used to get an impression of the wave height and period that can be expected in the experiments before the experiments are carried out.

Table 10: Predicted wave height and period

	H_{max} (m)	T_{max} (s)
Watts	0.0002	-
Panizzo	0.02 - 0.04	0.34– 0.5
Kamphuis & Bowering	$0.01272 - 0.02748$ (H_c)	-
Fritz et al.	$0.00052 - 0.00244$ (η^+)	-
Huber & Hager	$0.04 - 0.1187$	-
Walder et al.	$0.00432 - 0.00848$	-

With most of the formulas a wave height in the order of 10 mm is calculated. However, it should be noted that most formulas are not directly suitable to make an estimate of the wave height in the Delft UT experiment since they are deduced for two-dimensional problems.

7.   Experimental results

7.1.   Observations

Four different sets of experimental configurations have been tested in the wave basin. Two parameters were varied, namely the initial position of the landslide and the landslide velocity. In two sets the initial position of the landslide was sub-aerial and the landslide velocities were varied. In the remaining two sets the landslide motion was initiated at different initial positions and the landslide was pulled at a limited number of landslide velocities.

In this section, a qualitative overview will be given of the results of the four test series. Therefore, some tests will be highlighted and when available, photographs of the wave pattern will be used to clarify the observations.

From the sets with a sub-aerial initial position, the tests with landslide velocities of 0.7 m/s and 1.3 m/s are chosen. Tests with a lower landslide velocity than 0.7 m/s are not suitable for this purpose, as the wave pattern is less visible in these cases. Tests with higher landslide velocities than 1.3 m/s were not conducted.

For the sub-aerial tests it can be seen that when the landslide moves into the water, it pushes away the fluid generating a first positive crest. The first crest amplitude increases initially, peaks and when the landslide model gradually enters into deeper water, it decreases. At the same time, its wavelength increases when the wave enters deeper water.
The accelerating fluid and turbulent wake above and behind the landslide create a region of low pressure, which results in a water surface depression. As the first crest, this first trough increases initially, peaks and gradually decreases. The trough is forced to propagate at the same speed as the landslide until the landslide enters deeper water and the influence of the landslide on the water surface declines.
At the trailing edge of the landslide, a set of small amplitude waves with short wave lengths is generated. These waves are dispersive.
Not only waves propagating downstream are generated. The landslide also generates waves in an upstream direction, which eventually cause run-up and run-down at the coast. These upstream propagating waves are generated at the trailing edge of the landslide.
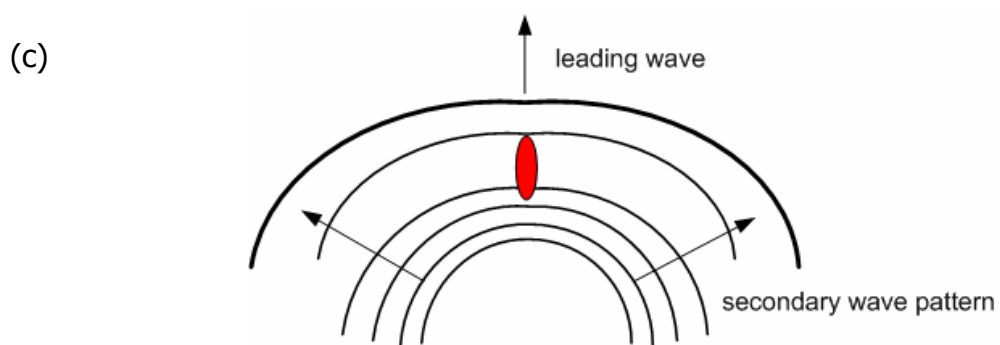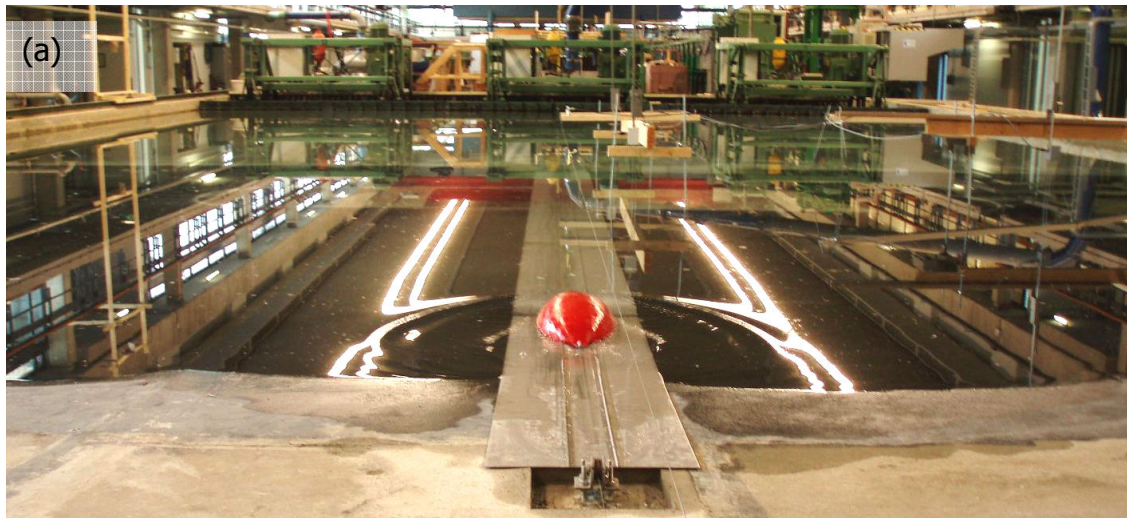
(a)

(b)

(c)

Figure 10a,b,c: Tsunami generation landslide velocity 0.7 m/s, Froude < 1, a: the landslide is pulled into the water, b: the landslide is fully submerged, c: a schematization of the wave pattern which is observed.
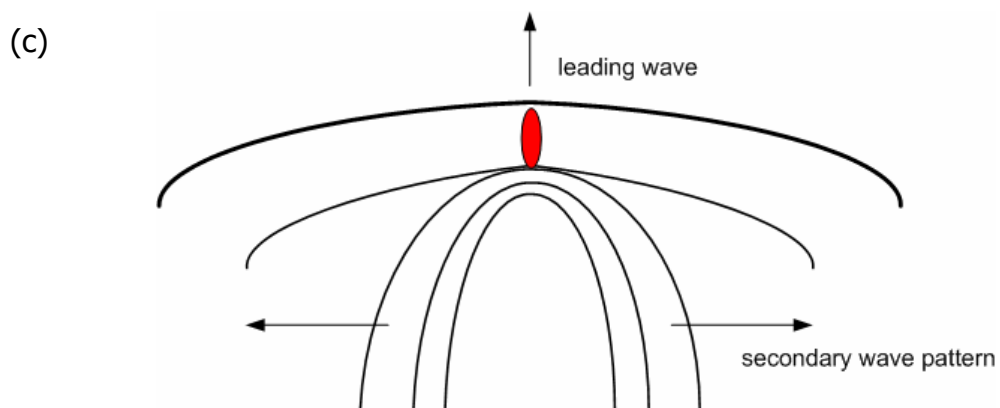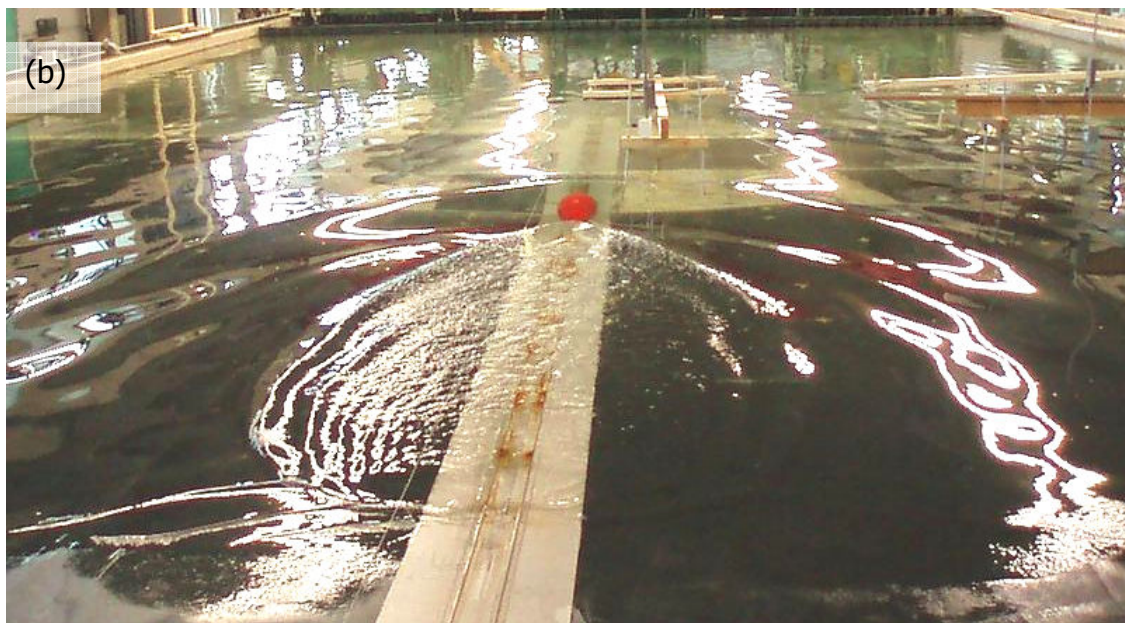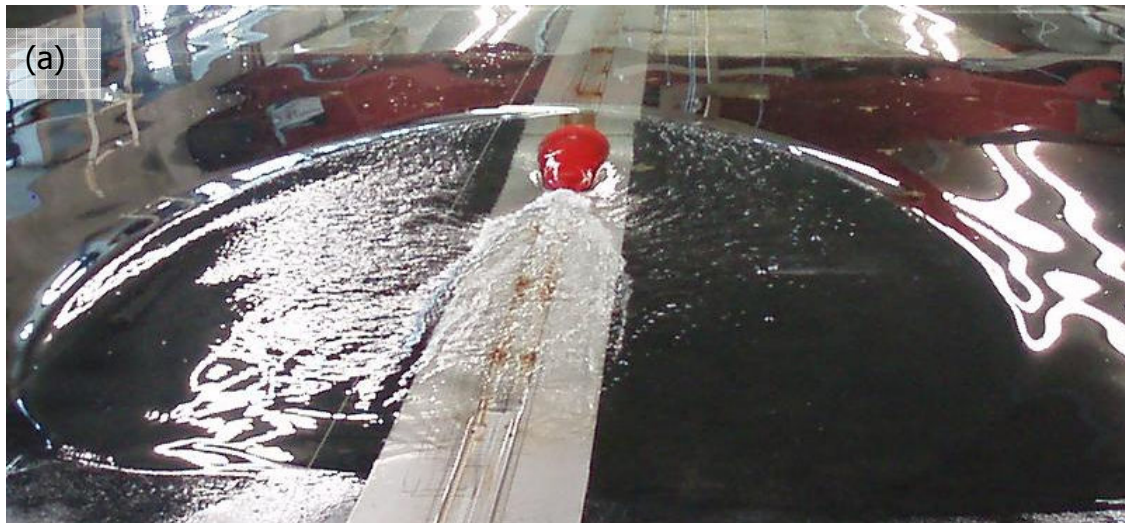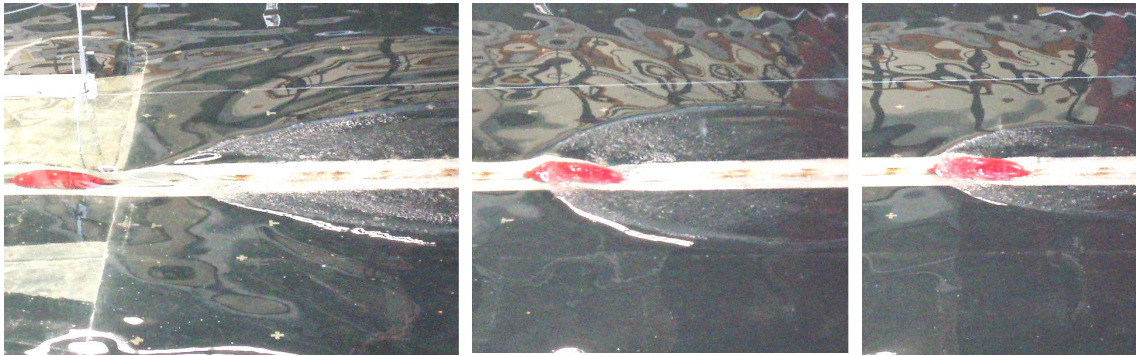
(a)

(b)

(c)

leading wave

secondary wave pattern

Figure 11a,b,c: Tsunami generation landslide velocity 1.3 m/s, Froude > 1, a: the landslide is partly submerged, b: the landslide is fully submerged, c: a schematization of the wave pattern which is observed.

Figure 12: Time series tsunami generation landslide velocity 1.3 m/s from right to left.

A difference in wave pattern is observed between tests of the low landslide velocities and the higher landslide velocities, see figures 10a,b,c, 11a,b,c and 13 and 14. In figure 13, one clear first crest and first peak can be observed for a landslide velocity of 1.3 m/s, whereas for a landslide velocity 0.7 m/s several local peaks can be observed between the first two up crossings. This can be explained by the difference in landslide velocity. For the 0.7 m/s test, the landslide velocity is slower than the wave celerity. This means that the waves can propagate away from the landslide model and pass the wake above the landslide, which is bound to the landslide velocity. For the 1.3 m/s test, the landslide velocity approaches the wave celerity and the waves cannot propagate away from the landslide. Therefore only one single wave peak in front of the landslide can be noticed. Moreover, this wave peak is much higher than the wave peak in the 0.7 m/s test as more energy can be transferred from the landslide.

When regarding figure 14, the radiation of the waves in another direction, outside the axis of motion, can be observed for the two tests. The wave pattern behind the landslide model is focused sideward in the case of 1.3 m/s. Therefore a strong excitation of the water can be observed for wave meter G11 which differs from the signal found for wave meter G26. For the case of 0.7 m/s no large differences could be seen in the signals of the two wave meters.
In the figures 10c and 11c a schematization of the main features of the wave pattern for the case of 0.7 m/s and the case of 1.3 m/s are given.
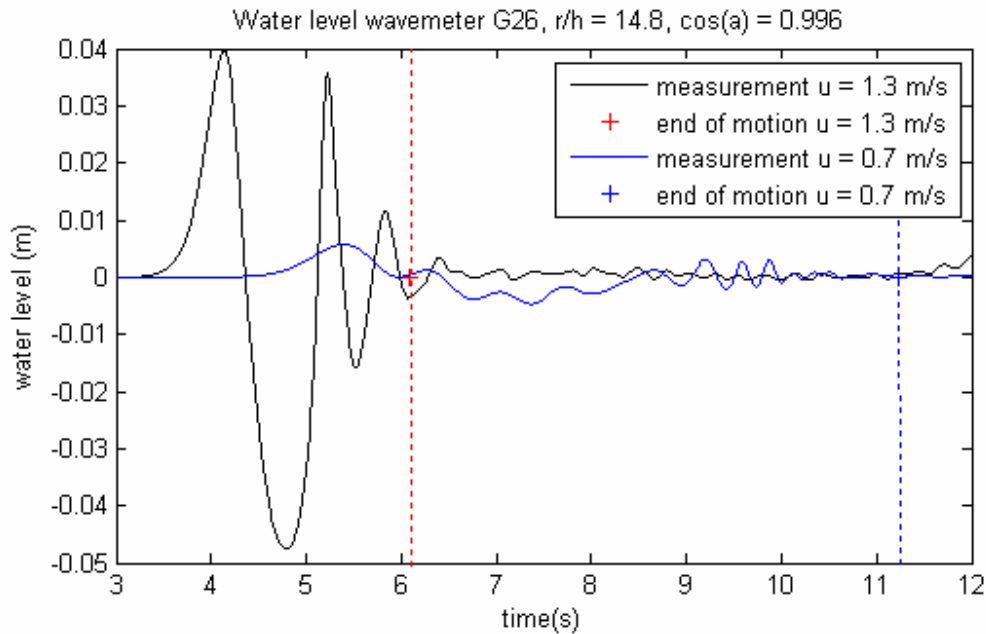
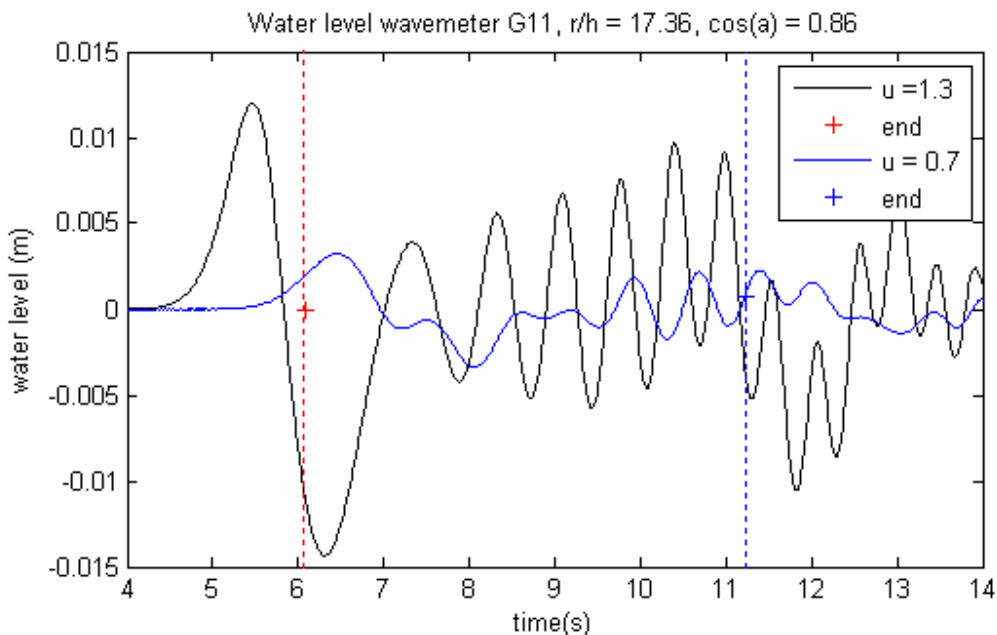Figure 13: Water level measured at wave meter G26 for the case of 1.3 m/s and the case of 0.7 m/s

Figure 14: Water level measured at wave meter G11 for the case of 1.3 m/s and the case of 0.7 m/s

From the sets with a submerged initial position, three tests with different initial positions are chosen for a qualitative analysis. The test with the shallowest initial position, r = 3 m, the test with an initial position of r = 4 m and the test with an initial position of r = 5 m are chosen. The test with an initial position of r = 3 m is not fully submerged.

In general, the generation process is the same as for the sub-aerial slides. When landslide motion is initiated, the landslide pushes away the fluid generating a first positive crest. A wave trough is formed above the landslide.
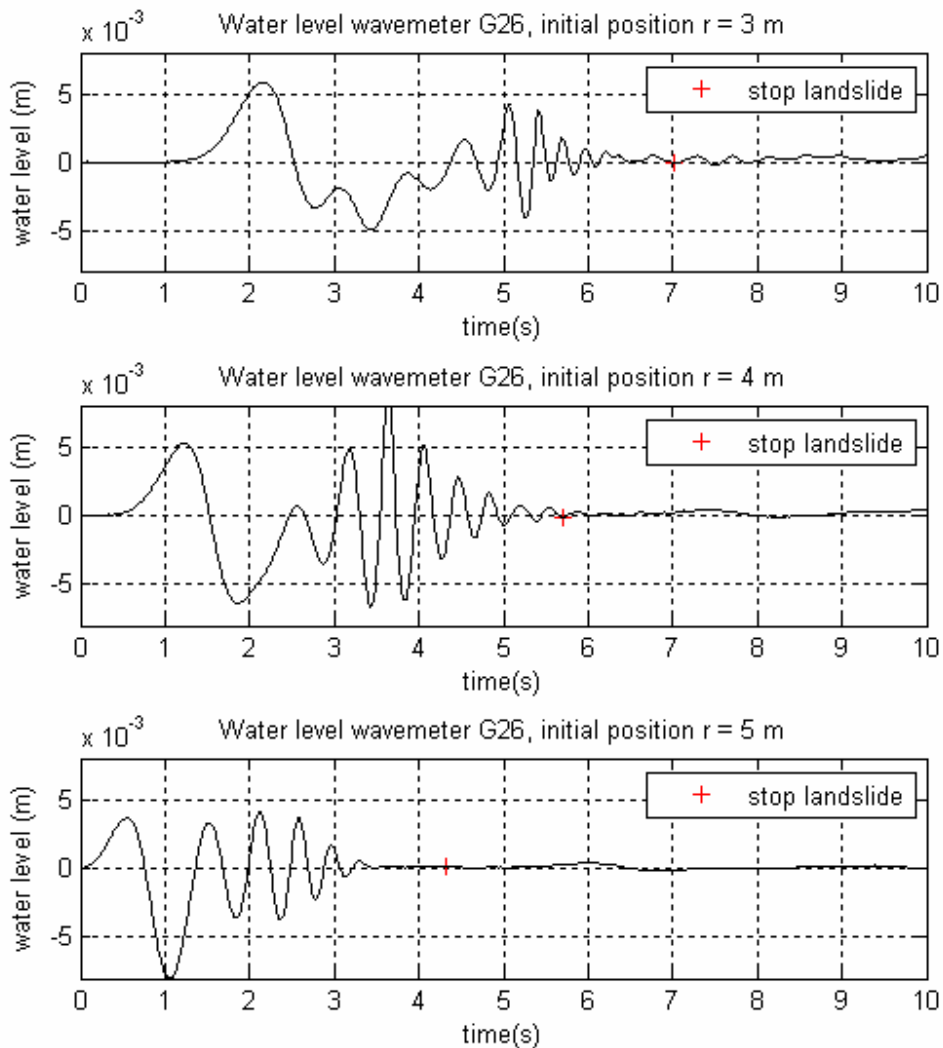
Figure 15: Tests with different initial positions: r = 3 m, r = 4 m and r = 5 m for wave meter G26. The landslide velocity is 0.7 m/s.

In figure 15, not only the effect of different initial positions can be seen, but also the influence of the distance between the generation area of the waves and the wave meter. As the submergence of the initial position increases, the distance between the wave generation area and the wave meter G26 decreases.

It can be seen that as the submergence of the initial position increases, the wave amplitude of the first crest decreases. However, because of the smaller distance to the wave meter for more submerged landslides, a relation between the submergence and the first crest cannot be determined without taking the distance into account.

For the first trough, the distance from the generation area to the wave meter is of more influence than the effect of submergence as can be seen in figure 15.

7.2. Data processing

In this section some aspects of the measured data and the data processing methods will be analyzed in more detail. Important for the reliability of the experiment are the accuracy and the repeatability of the measurements. Furthermore, some comment will be given on the processing methods that were used: how the relevant time interval is chosen from the raw data signals and how the signal will be denoised. After that the method to find the peaks, troughs and zero-crossings is explained. This information can be used to analyze the signals further. Finally, the wave pattern analysis that is carried out on the signal is commented.

7.2.1. Accuracy of the raw signals

The absolute and relative errors of the measurements need to be defined, to see how reliable the comparison of the measurements with the numerical results is. The absolute error depends on the accuracy of the measuring device. The maximum relative error occurs at the lowest values of the measured parameters. Table 11 summarizes the relative errors of the various measured parameters.

Table 11: Reliability of the measurements

Measure	Instrument	Absolute error	Average low value	Relative error
Surface elevation	Wave gauge	0.1 mm	1 mm [1]	10 %
			4 mm [2]	2.5 %
			24 mm [3]	0.4 %
	Acoustic wave gauge	0.3 mm	1 mm [1]	30 %
			4 mm [2]	7.5 %
			24 mm [3]	1.25 %
	Video imaging			
Time	Stop watch	0.1 sec.	5 sec.	2 %
Distance	Meter	50 mm	1000 mm	5 %
	Line/markings	5 mm	100 mm	5 %
Still water level	Meter line	0.5 mm	40 mm	1.3 %
Slope length	Meter line	5 mm	1200 mm	0.4 %
Slope height	Meter line	1 mm	60 mm	1.7 %
Landslide length	Meter line	0.5 mm	70 mm	0.7 %
Landslide width	Meter line	0.5 mm	25 mm	2 %
Landslide thickness	Meter line	0.5 mm	10 mm	5 %
Landslide weight	Scales	0.01 kg	25.92	0.04 %

[1] Average value of the surface elevation for the first peak measured in set 1, test 5 (0.5 m/s).
[2] Average value of the surface elevation for the first peak measured in set 1, test 7 (0.7 m/s).
[3] Average value of the surface elevation for the first peak measured in set 3, test 7 (1.3 m/s).

The relative errors of the landslide velocity, wave celerity, Froude number and the slope can be derived from the errors in the measured variables. It is assumed that the variables have a normal

distribution with a standard deviation equal to the absolute error. The absolute error of a function *f(x,y)* with measured parameters *x* and *y* is calculated as follows:

$$\Delta f^2 = \Delta x^2 \left(\frac{\delta f}{\delta x} \right)^2 + \Delta y^2 \left(\frac{\delta f}{\delta y} \right)^2$$ according to Gauss, see Handleiding Experiment Materiaalkunde

Table 12: Reliability of the calculations

		Relative error	
Velocity	u	$r_u^2 = r_x^2 + r_t^2$	5.4 %
Wave celerity	c	$r_c^2 = r_h^2$	1.3 %
Froude	Fr	$r_{Fr}^2 = r_x^2 + r_t^2 + r_h^2$	5.5 %
Slope	α	$r_\alpha^2 = r_L^2 + r_D^2$	1.7 %

From table 11, it can be concluded that the accuracy of the surface elevation measurement is highly dependent on the height of the first peak/ trough. For low landslide velocities the relative error becomes unacceptably high. For landslide velocities of 0.7 m/s and higher the error becomes acceptable and therefore the measurements with landslide velocities of 0.7 m/s should be preferred.
Another relatively large error is made by measuring the landslide velocity. For a landslide velocity of 0.7 m/s, the landslide velocity could be 0.04 m/s lower or higher. This error is acceptable, but attention should be paid, when comparing the numerical result with the experimental result, that this error exists.
Furthermore, the errors in the slope, the landslide dimensions and the still water level could cause small discrepancies between the numerical and the experimental model. These errors are relatively small, but also in this case attention should be paid, when comparing the numerical result with the experimental result, that this error exists.

7.2.2. Repeatability

Figure 16 illustrates the repeatability of one of the water level measurements. In this figure, the same test was performed three times. The water surface time history of the nearest wave meter was plotted for the first 20 seconds after release of the landslide model.
The repeatability of the first peak and first trough is very good. However, small discrepancies can be seen, especially after 12 seconds. These discrepancies can be explained by the fact that the initial water surface was never completely still. Furthermore, the time when the landslide motion was stopped, varied. This time is important, because a wave crest is created by the abrupt deceleration.
Not all the measurements have a good repeatability. The repeatability depends amongst other things on the repeatability of the velocity profile and the accuracy of the measurements. The accuracy depends on the instrument accuracy and the size of the measured values. In general, the repeatability of the experiments with higher landslide velocities and of the more accurate wave meters (resistance type of wave meters instead of the acoustic wave meters) is better. These measurements are therefore more suitable for a comparison with the numerical model results. In the case that less accurate measurements are used, the results are averaged.
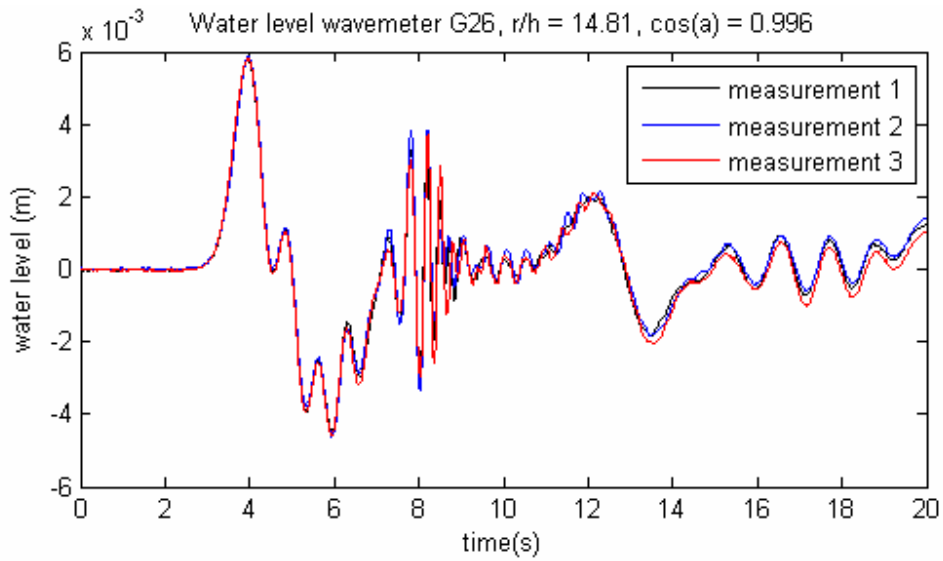
Figure 16: Repeatability of the configuration with landslide velocity 0.7 m/s at wave meter G26.

7.2.3. Denoising the data

The signal obtained from the wave meters, especially the acoustic wave meters, contains an amount of noise, see figure 17. This noise disturbs the clarity of the signal. With the Wavelet Toolbox in Matlab the signal can be decomposed and reconstructed without the noise. For this, several local thresholds have to be chosen, which define how much of the signal is admitted. The signals of the acoustic wave meters are denoised before they are further analyzed.
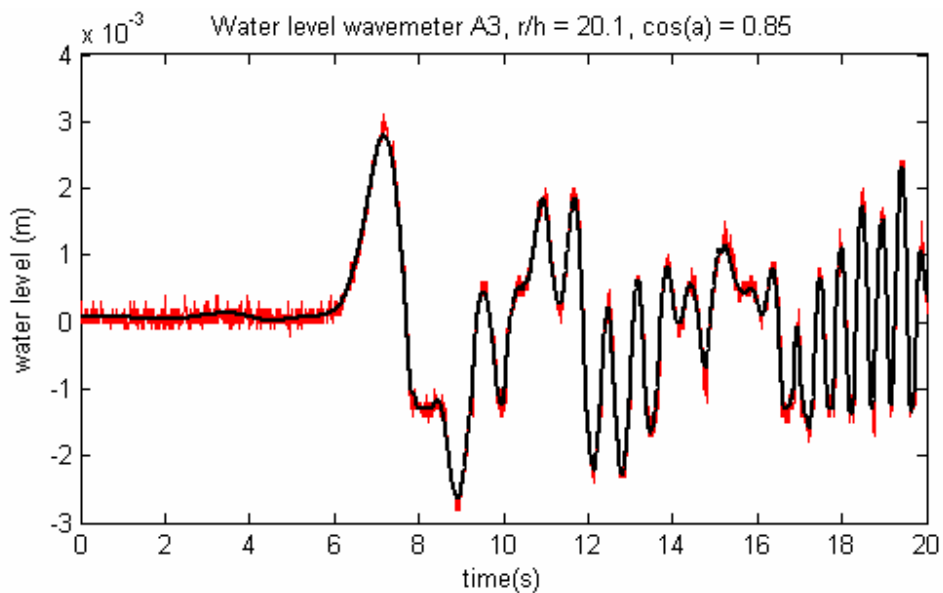
Figure 17: Signal of wave meter A3, black line is the denoised signal, red line is the noisy signal

7.2.4. Slide motion

For the analysis of the measurements the times when the landslide starts moving, t_{start}, and when the landslide stops moving, t_{end}, are clocked. With these timings the interval of interest can be found in the signals. The interval of interest is the period between t_{start} and 20 seconds later. Somewhere in this period, t_{end} can be found. In figure 18 the start and the end of the landslide motion are marked. It is interesting to see whether the abrupt stop of the landslide at t_{end} is visible in the signal.

In the area of interest the first peak and the first trough are sought. The first peak and the first trough are defined as the maximum, respectively the minimum elevation between two zero crossings. The time between the zero crossings is respectively T_{peak} and T_{min}. T_{tot} is the period of the first wave, the sum of T_{peak} and T_{min}. In some cases there are several possibilities to define the zero crossings between the peak or trough, because of several local maxima or minima. In those cases the local maxima or minima, which come from higher frequencies, are filtered from the signal.

The mean celerity at which the first peak respectively the first trough travels towards a wave meter can be calculated from the distance r (m) to the specific wave meter and the time between t_{start} and the time of the first peak for a specific wave meter. The mean celerity of the first peak respectively the first trough can be compared with the landslide velocity.
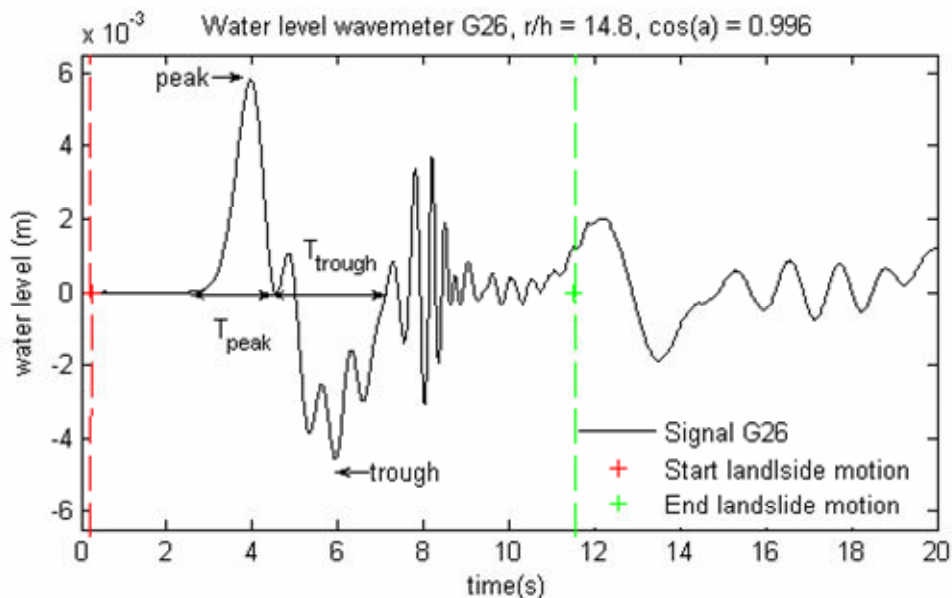

Figure 18: Start and end time landslide motion

7.2.5. Wave pattern analysis

In coastal and ocean engineering the Fourier analysis is often used. This technique provides information about the frequency domain of a signal. However, this technique is only applicable when studying periodic and stationary phenomena. Landslide generated waves are non-stationary phenomena. Therefore, a Fast Fourier Transform cannot be used. Continuous Wavelet Transform (CWT) is applicable to non-periodic and non-stationary signals and will therefore be used to analyze the wave pattern. Wavelet transform is similar to Fourier transform, but instead

of studying the spectral density of a signal, the projection of the signal on to functions called wavelets is studied.

Instead of studying the frequency content of the signal, wavelet theory concerns the relationship between the scale parameter a and the location (shift) parameter b. The continuous Wavelet transform is a function of (a,b) and is defined as follows:

$$T(a,b) = \frac{1}{\sqrt{a}} \int_{-\infty}^{\infty} f(t)\ \psi^* \left(\frac{t-b}{a} \right) dt$$

$\psi(t)$ is a basic wavelet function. A family of wavelet functions is obtained by scaling and shifting the basic function. In this analysis the Morlet wavelet is used.

The magnitude of $T(a,b)$ is called the Scaleogram and is analogous to the spectral density. It is helpful in identifying signal characteristics at different points a and b. The Energy function is defined as the square of the magnitude of the Wavelet transform:

$$E(a,b) = |T(a,b)|^2$$

On basis of the Scaleogram continuities and discontinuities in the signal can be detected. It can be seen for example whether seiches were already present in the basin and it can be seen when the wave is reflected at the walls of the basin.

The signal of the test, which will be compared with the numerical model, will be investigated with this technique. The same will be done with the signal of the numerical run and with the results a better comparison can be made between the measurement and the numerical result.

7.2.6. Reflections

Reflections at the basins walls influence the signal and therefore it should be known when the reflections could occur in the signals of the different wave meters. With a simple calculation an estimate is made of the times when reflections should be expected. For this calculation a wave celerity of 1.3 m/s was taken. An estimate was made of the distance which the first crest travels from the landslide model to the walls and back to the wave meters. The results of table 13 agree with the observation of different waves in the signals around these times.

Table 13: Time of reflections

Wave meter	r/h	$cos(\alpha)$	Estimated distance (m)	Estimated time (sec.)
G26	14.8	0.996	16	12-13
G27	22.4	0.998	18	13-14
G11	17.4	0.86	13	10
A1	18.3	1	17	13
A2	20.8	1	18	14
A3	20.1	0.85	13	10

It can be seen that the time before reflections occur is long enough that the measurements of the first wave are not influenced by reflections.

Continuous wavelet transform will be used in case the time at which reflection occur must be determined exactly.
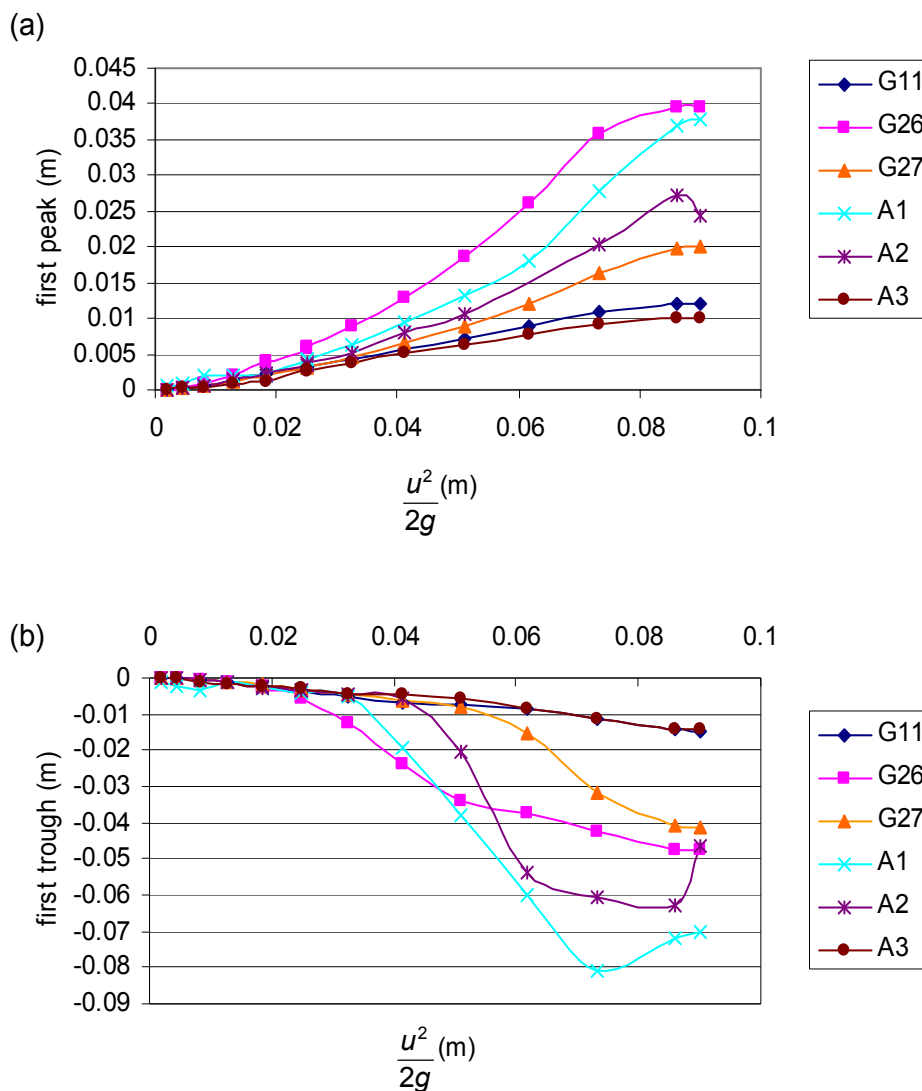
7.3.   Analysis

In the previous section, the methods that have been used to process the raw data signals have been elaborated. In this section an analysis of the measured data will be given. Relations between the varied parameters and the wave amplitudes and wave period will be sought. With the data sets several relationships can be examined:

- The relationship between the landslide velocity and the height of the first wave crest and first wave trough for a sub-aerial and for a submerged initial position.
- $\Rightarrow$ It is expected that the wave amplitude increases when the landslide velocity increases. More energy can be transferred from the landslide to the waves when the difference between the landslide velocity and the wave celerity becomes smaller. This should result in a higher first wave amplitude.

- The relationship between the landslide velocity and the wave period.
- $\Rightarrow$ It is expected that the wave period decreases when the landslide velocity increases. For larger landslide velocities the difference between the landslide velocity and the wave celerity becomes smaller. Therefore the waves become more bound to the landslide and thus the wave period decreases.

- The relationship between the initial position of the landslide and the height of the first wave crest and first wave trough.
- $\Rightarrow$ It is expected that the wave amplitude decreases when the initial position of the landslide is more submerged. A landslide has more influence on the surface elevation in shallow water. The Froude number in shallow water is higher and more energy can be transferred to the first wave. Therefore this wave can become higher when is initiated in shallower water. Moreover, the energy flux from the landslide to the water is the same for all initial positions. However, as the wave group celerity increases for deeper initial positions, the wave amplitude should decrease according to linear wave theory.

- The influence of the position of the wave meter and the first wave crest and first wave trough.
- $\Rightarrow$ It is expected that the wave amplitude decreases when the wave meter is further away from the generation area. The waves loose energy when they propagate from the generation area due to radiation and friction.

- The influence of the position of the wave meter and the wave period.
- $\Rightarrow$ It is expected that the wave period remains constant when the wave meter is located further away from the generation area. This expectation is based on linear wave theory.

In the following sub-sections the relations will be elaborated and the hypotheses about the relations between the parameters will be tested. This will be the primary part of the section results. In the secondary part the propagation of the first wave crest and wave trough will be examined. Furthermore, a Continuous Wavelet Transform will be carried out on some measurements.

7.3.1. Landslide velocity versus wave amplitude

During the test programs of set 1 and 3, the landslide velocity was varied. For set 1 the landslide velocity was varied from 0.2 m/s to 0.7 m/s, which resulted in peak heights varying from 0 to 0.006 m and trough heights varying from 0 to -0.006 m. With the larger landslide velocities in set 3, from 0.6 to 1.3 m/s, larger amplitudes where obtained varying from 0.001 m to 0.04 m for the peak heights and -0.003 m to -0.08 m for the trough heights. In figure 19a and b the landslide velocity is plotted versus the peak height respectively the trough height, at the various wave meters. In the graph, the landslide velocity has been divided by two times the gravitational acceleration; the velocity head. This results in straight lines for both the first peak and the first trough till a velocity head of approximately 0.05 m. For a velocity head becomes larger than 0.05 no linear line can be seen.

(a)

(b)

Figure 19a,b: Velocity head versus a: first peak height and b: first trough height at different wave meters for an initial position of r = 0 m.

From the figures 18a and b it can be seen that the wave amplitude increases when the landslide velocity increases. The maximum amplitude for a landslide velocity range of 0.2 – 1.33 m/s can be observed in most cases for a landslide velocity of 1.3 or 1.33 m/s. It appears that round this velocity the wave amplitude increase stagnates which could indicate that a landslide velocity of roughly 1.3 m/s forms the transition between the sub-critical and super-critical Froude domain. Unfortunately, it is unknown whether this stagnation indicates an absolute maximum or minimum amplitude around this landslide velocity, as wave amplitudes for higher landslide velocities were not measured.

In the submerged cases of set 2 and 4, the landslide velocity has also been varied. This means that the relation can be investigated of the relation between the landslide velocity and the first crest and trough height in case of a submerged initial position. For a submerged initial position of r = 4 m, six tests with different landslide velocities were carried ranging from a landslide velocity of 0.2 m/s to a velocity of 1.3 m/s. First wave crests heights were measured varying from 0 to 0.015 m and first wave troughs were measured varying from 0 to -0.035 m. From the figure 20 it can be seen that the wave amplitude increases when the landslide velocity increases.
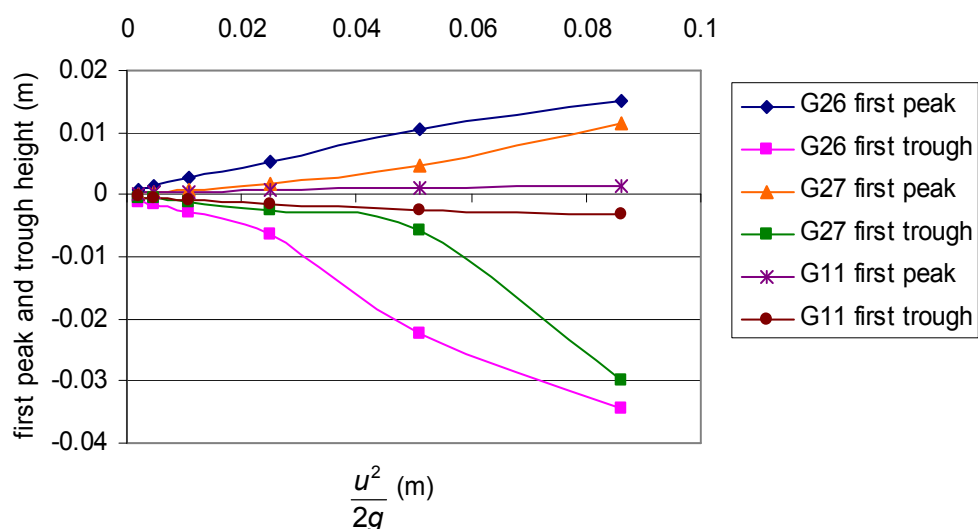

Figure 20: First peak/first trough height versus the velocity head for an initial landslide position of r = 4 m and α = 0°.

However, the measured wave amplitudes for the submerged case are smaller than the measured wave amplitudes for the sub-aerial case. This difference will be investigated further in the sub-section Initial position versus wave amplitude.

For the higher velocities in the submerged case attention has to be paid because the wave amplitudes could be influenced by the decelerating landslide. For larger submergences, the distance from the initial position of the landslide to the end of the slope becomes shorter. Therefore, the time of landslide motions decreases and this means that the stop of the landslide is in some cases already observed in the first wave trough. In figure 20 a higher trough height can be seen for wave meters G26 and G27 at a landslide velocity of 1.3 m/s.

In conclusion it can be said that when the landslide velocity increases, the wave amplitude increases for the experimental landslide velocity range. For a landslide velocity of roughly 1.3 m/s stagnation in increase can be noticed. Therefore it is not clear whether the wave amplitude increases further for landslide velocities higher than 1.3 m/s.

7.3.2. Landslide velocity versus wave period

The expectation was that when the landslide velocity increases, the wave period decreases. In figure 21 the relation between the wave period and the landslide length divided by the landslide velocity is investigated. As it is expected that the wave period is depending on the landslide length, the landslide length divided by the landslide velocity could be a measure for the wave period.

The small variations in this trend, for example for a landslide velocity of 0.7 m/s, are probably due to difficulties in defining the trough period, when also local peaks are present like in figure 18.

It can be concluded that the larger the ratio $\frac{b}{u}$ becomes, the larger the wave period becomes.

Thus it can be said that when the landslide velocity increases, the wave period decreases.
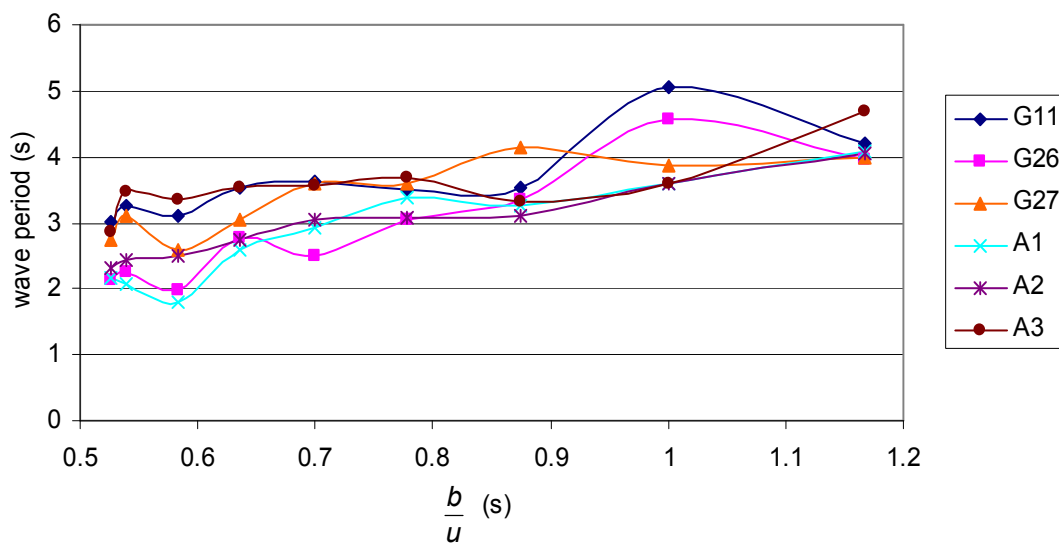
Figure 21: Landslide length divided by the landslide velocity versus wave period for an initial landslide position of $r = 0$ m and $\alpha = 0°$.

7.3.3. Initial position versus wave amplitude

In the tests of set 2 and set 4 the landslide motion has been started from different initial positions along the axis $\alpha = 0°$. With sub-aerial initial positions of set 1 and 3 figures 22 and 23 can be made for a landslide velocity of 0.7 m/s. If it is assumed that the energy flux remains constant, the wave amplitude decreases when the initial position becomes more submerged. Therefore, $\sqrt{gd_i}\eta^2 / u$ is presented versus the depth, d_i, at the initial position.

From these graphs it can be concluded that $\sqrt{gd_i}\eta^2 / u$ is not in all cases constant for different depths. In figure 23 it can be noticed that the signal of wave meter G26 is influenced by the

distance from the initial position to the landslide when the landslide initial position becomes larger than r = 3 m.

The resulting wave meters show a constant line after a certain depth. However, the expectation can be confirmed that as the wave amplitude decreases when the submergence increases.
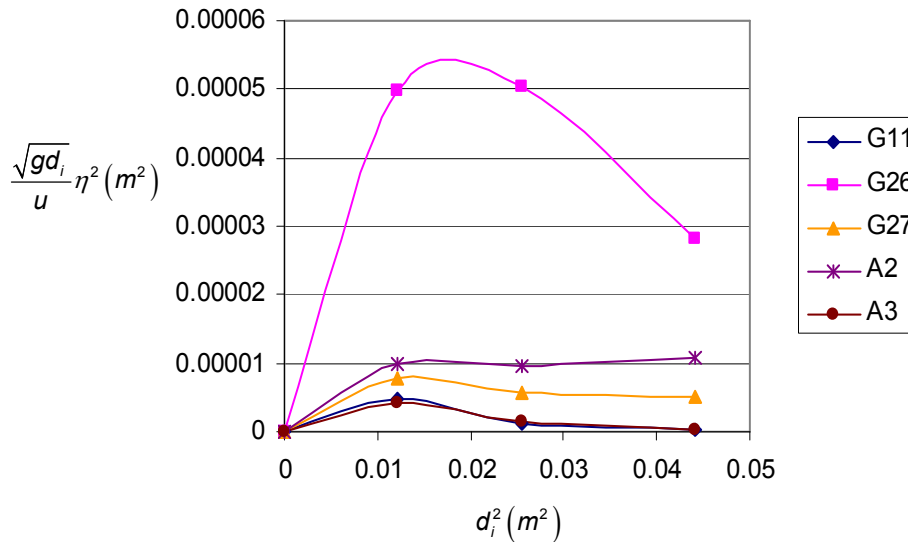

Figure 22: Depth at the initial position of the landslide versus first wave peak for a landslide velocity of 0.7 m/s.
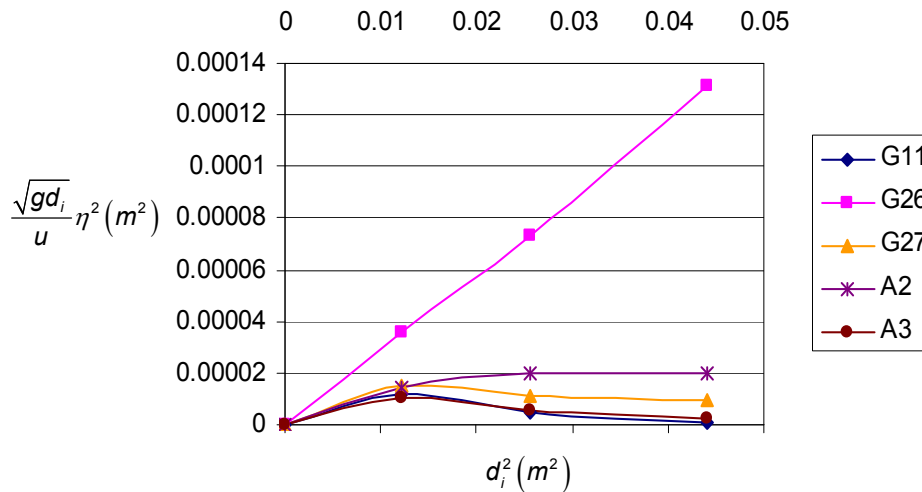

Figure 23: Depth at the initial position of the landslide versus first wave trough for a landslide velocity of 0.7 m/s.

7.3.4. Distance versus wave amplitude

The number of wave meters on one direction of wave propagation α, for example the axis of landslide motion α = 0°, has not been larger than two wave meters. Therefore, it is not possible to establish an adequate relation between the increase or decrease in peak/trough height and the distance that the first peak or trough has travelled for one direction of wave propagation. However, by using r/h, the location of the wave meter divided by the local water depth, some relations can be discovered.

In figure 24, the wave amplitude versus r/h has been lined out. A difference can be observed between the wave meters along or in the neighbourhood of the axis of landslide motion and the other two wave meters. Therefore these two groups will be examined separately. For the first wave peak a clear increase in wave amplitude can be noticed for both groups when r/h increases. This means that when the location of the wave meter is further from the initial position of the landslide and in deeper water, the first peak height becomes smaller. In principle, the same relation can be seen for the first wave trough. However, for the wave trough it is more important whether the wave meters are located on the axis of motion. A difference can be seen between wave meters A1 and A2, which are located on the axis of motion and wave meters G26 and G27, which are situated near this axis of motion.

It can be concluded that the wave amplitude decreases when the distance to the generation area increases.
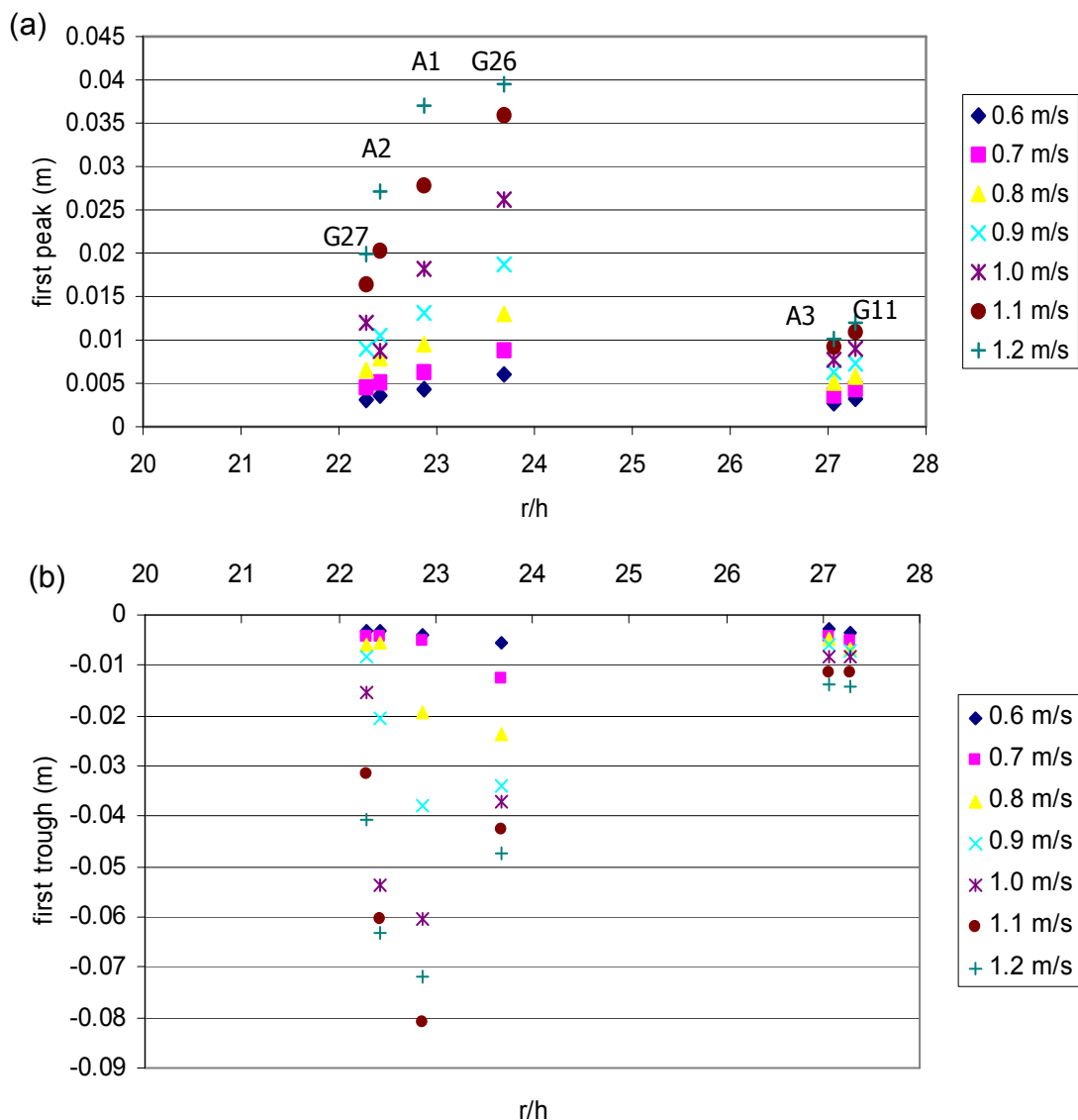

Figure 24: Wave meter location, defined as r/h, versus first wave peak (a) and trough (b) for various landslide velocities and for all measurements an initial position of the landslide of $r = 0$ m and $\alpha = 0°$.

7.3.5. Distance versus wave period

In figure 25 the wave period versus r/h is shown. It was expected that the wave period stays constant when the first wave moves into deeper water. When examining figure 25 it is hard to define a relationship which meets all the trends seen for different velocities. It must be concluded that with these parameters and with this set of measurements it is not possible to set up a relationship between the wave period and r/h. However, a difference in wave period per location can be noticed.
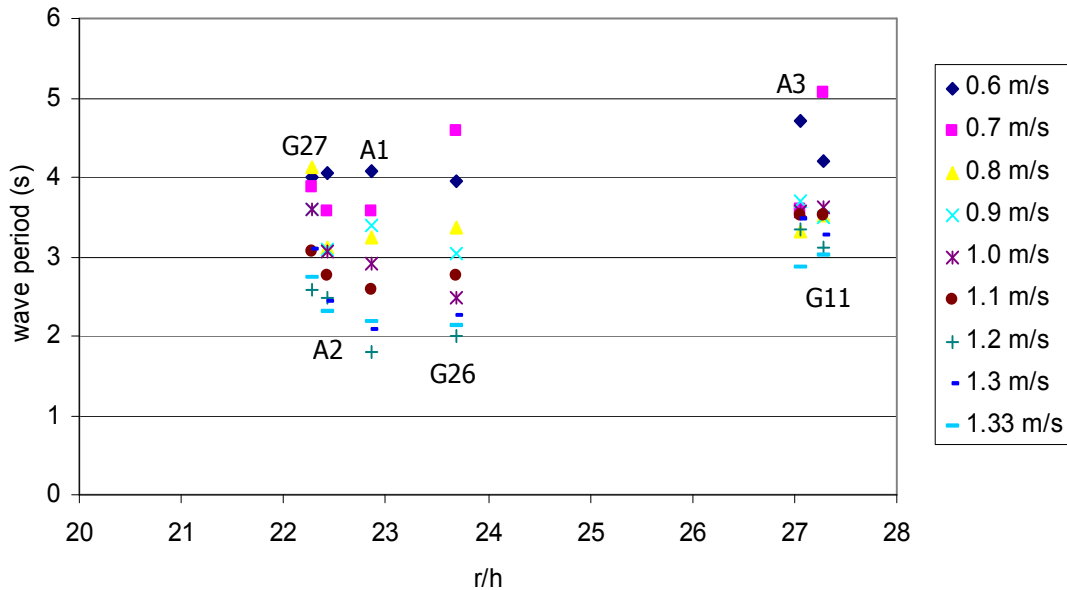
Figure 25: Wave meter locations, defined as r/h, versus wave period for various landslide velocities and for all measurements an initial position of the landslide of $r = 0$ m and $\alpha = 0°$.

7.3.6. Propagation

The mean celerity of the first peak respectively first trough at which the wave propagates towards a wave meter has been calculated for the different wave meters. As has been found in literature, the first peak propagates freely away from the moving landslide in the sub-critical domain. The first trough is bound to the moving landslide till a certain depth and has therefore a smaller mean celerity.

In figure 26a and b the mean peak celerity and the mean trough celerity to different wave meters are shown. In 26a the celerity is plotted for a landslide velocity of 0.7 m/s and in b for a landslide velocity of 1.3 m/s. Furthermore, the wave celerity is calculated with linear wave theory.

Linear wave theory: $\quad c = \sqrt{\dfrac{g\lambda}{2\pi} \tanh\left(\dfrac{2\pi h}{\lambda}\right)}$

In this calculation a constant wave length of 3.5 m is assumed. This is an estimate that has been done with the help of the numerical model. This wave length is an approximation of the wave length, but is not always a correct estimate as the wave length increases for increasing depth. Moreover, as the first trough is bound to landslide velocity and the first peak is not in the sub-critical domain, the first peak propagates faster and thus the length of the first wave probably increases in time.

(a) Mean wave celerity for the different wave meters
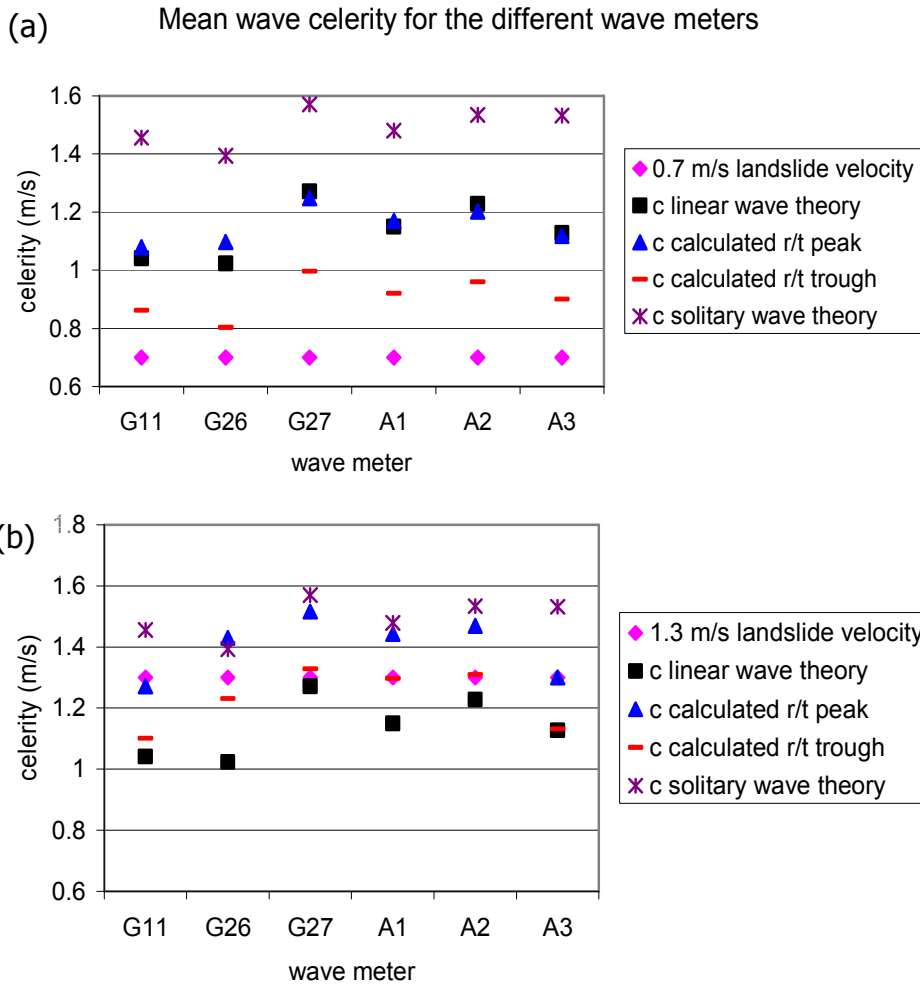

(b)

Figure 26a,b: Mean wave celerity to different wave meters for a landslide velocity of a: 0.7 m/s and b: 1.3 m/s

From figure 26a it can be seen that the linear wave theory gives a relatively good approximation for the mean wave celerity of the first wave crest.

As the trough velocity is bound to the landslide velocity for a certain time, it can be seen that this velocity is lower. However, it is not equal to the landslide velocity and therefore it can be concluded that at a certain depth the landslide looses the grip on the wave trough and the wave trough propagates freely too. In figure 26b the landslide moves faster and it can be seen that the trough velocity is equal to the landslide velocity at the wave meters which are located along or near the axis of landslide motion (G26, G27, A1 and A2). The difference in velocity between the peak and trough has decreased in figure 26b in comparison to 26a. The crest velocity does not behave according to linear theory anymore. A schematization with the solitary wave velocity comes closer to the crest velocity when the landslide velocity is 1.3 m/s.

Solitary wave theory: $c = \sqrt{g(h+H)}$)

H is the wave height of the first wave. In the calculation of the solitary wave celerity a wave height of 0.1 m was assumed, based on the first peak and first trough heights of the experiment.

7.3.7. Wavelet spectra

The continuous wavelet transform analysis is applied to study the signal of the test with r = 4 m and a landslide velocity of 0.7 m/s. In the following figures the wavelet spectra from the different signals at the wave meters are shown.
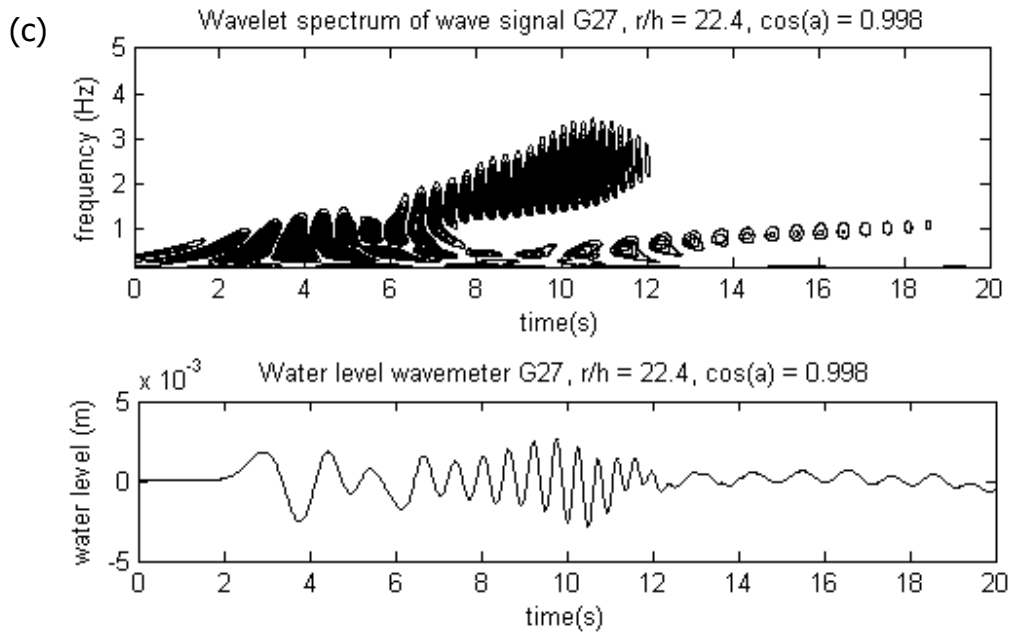
(a)

(b)

(c)
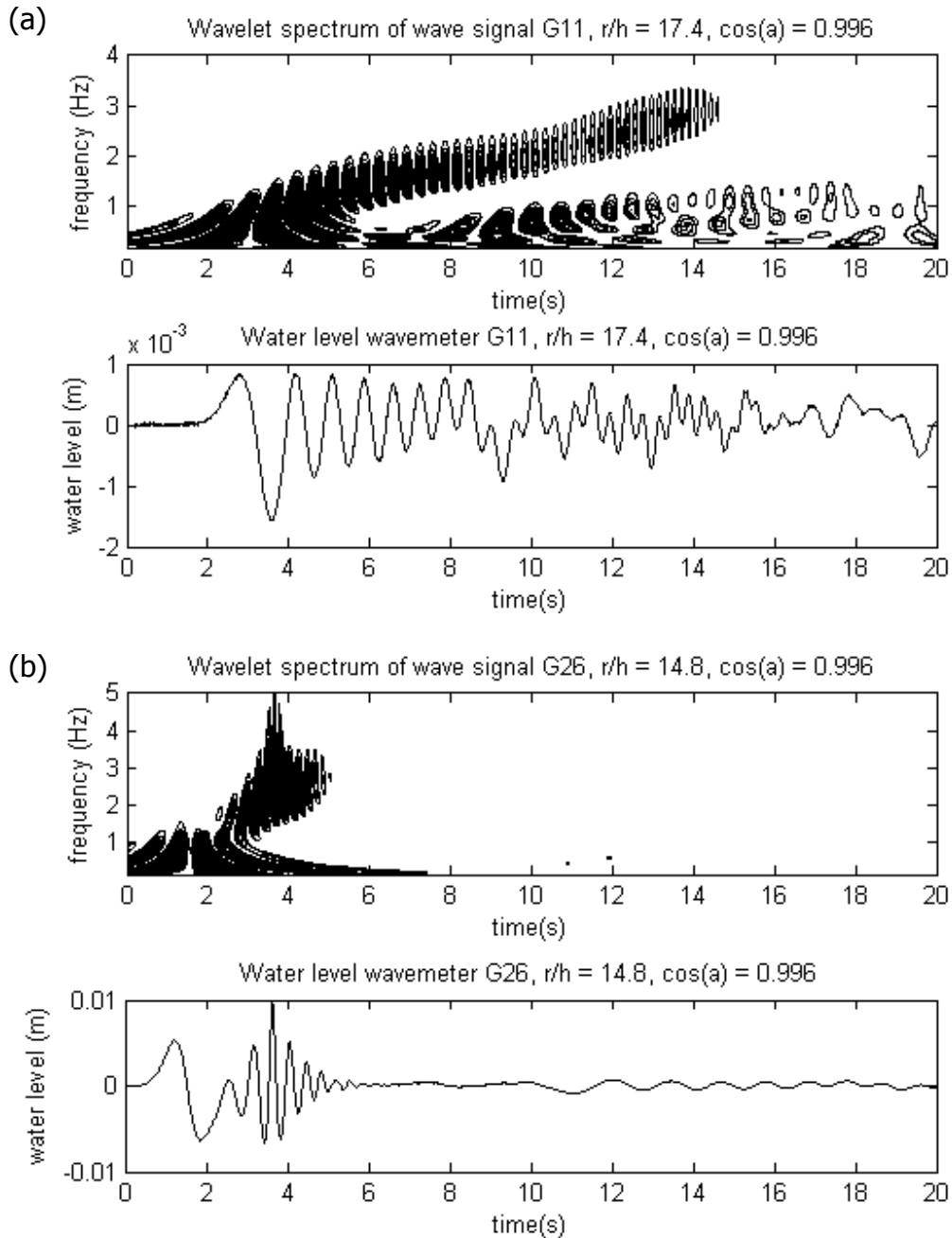
Figure 27a, b, c: Continuous wavelet transform for the wave meters a: G11, b: G26 and c: G27.

In the wavelet spectra the leading wave followed by higher frequency waves at the trailing end of the landslide can be observed. If the wavelet spectrum of figure 27b is compared with the wavelet spectrum of figure 27c a spreading of the spectrum can be seen. This spreading of the higher frequencies starts when the first trough and the waves behind this trough start to propagate freely.

Furthermore reflections can be noticed in the spectra. The energy of the impact wave is shifted by an amount of time which is the time the wave energy has to travel between the wave meter and the wall. In figure 27a and 27c the reflected energy can be seen after approximately 8 seconds.

7.4.   Discussion

In the discussion subjects will be discussed which are related to the objective of the study. In sub-section 7.4.1 the secondary objective of the experimental study will be regarded and the experimental results will be compared with results from similar experiments and formulas of landslide generation. In sub-section 7.4.2 the objective of the experimental study to provide results, with which the numerical model of the landslide wave generation can be verified, will be discussed.
Finally, in sub-section 7.4.3 a first attempt will be made to say something about the wave generation in the La Palma case with help of the experimental measurements.

7.4.1.   Important parameters for landslide wave generation

In section 7.3 several relationships between various parameters have been examined. Most of the relations meet their expectations. It can be said that the wave amplitude is dependent on the landslide velocity, the initial landslide position, the distance from the generation area and also on the location, along the axis of motion or somewhere off this line. The wave period is in any event dependent on the landslide velocity. No clear relation between the wave period and the distance divided by the water depth could be found.

As discussed in the previous chapter, there have been several experiments in the past, which have similar experimental parameters. The main difference of this experiment with other experiments is the slope angle. Most experiments used steeper slopes in their settings. As it is stated in literature that the slope has influence on the wave height, it is interesting to compare the experiments of this thesis with some experiments done in the past.
For the sub-aerial part of this experiment, there is an experiment of Panizzo et al. 2005. Furthermore, there are some formulas to calculate the wave height. These formulas have been described in the previous chapter and can be found in appendix C. The formula of Panizzo will be used for the sub-aerial cases and the formula of Watts will be used for the submerged cases.

Panizzo
From Panizzo et al. two results have been chosen for a comparison with some results of the DUT experiment. In figure 30 a case is shown. The parameters used in these experiments are explained below the graph.
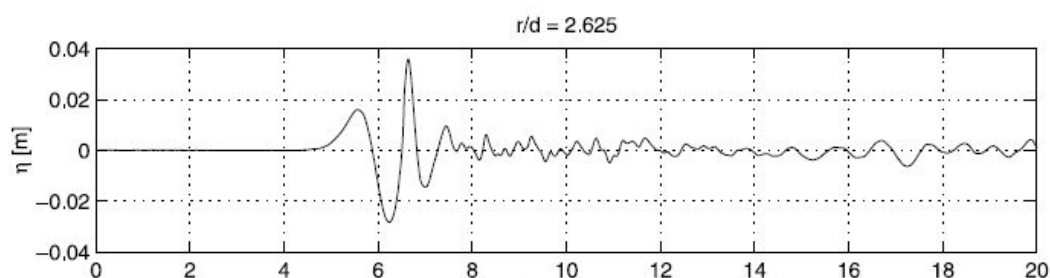

Figure 28: Experiment Panizzo et al. 2005, a landslide with a length of 0.41 m, a width of 0.3 meter, a height of 0.18 meter is released into a basin on a 16 degrees slope with an impact velocity of 3.7 m/s. The water depth is 0.4 m.

In the DUT experiment less parameters have been varied, the landslide velocity has been constant and the slope was very gentle. However, there are some similarities noticeable for the signals that are measured at the same depth in the axis of motion. The main difference is the height of the first wave, which is smaller in the Panizzo experiment than in the DUT experiment.

This is interesting, because the landslide velocity is much larger in the Panizzo experiment, but only during impact. The difference could be explained with the difference in slope angle and with the faster landslide stop in the Panizzo experiment.
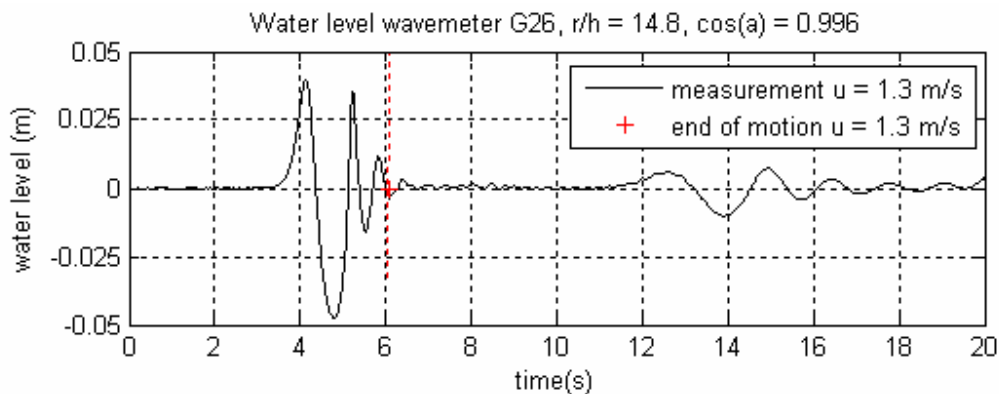

Figure 29: Signal of wave meter G26 at a depth of 0.25 m and a landslide velocity of 1.3 m/s

When using the formula, produced by Panizzo, for the parameters used in the DUT experiment and with a landslide velocity of 1.3 m/s or a time of landslide underwater motion of 6 seconds, a maximum wave height of 0.02 m is calculated with a wave period of 0.77 seconds. The maximum wave height for this experiment is defined as the wave height of the second wave. The formula gives a value that is low compared with the wave height from figure 31, which is roughly 0.08 meter.

From this example and some other tests with the parameters of the DUT experiment it can be concluded that the formula of Panizzo does not provide a correct answer when a slope of 3 degrees is used.

Watts

In the formula of Watts, which can also calculate the three dimensional wave amplitudes, see appendix C, the experimental parameters for the submerged case, $r = 4$ m and submergence is 0.16 m are used. A tsunami amplitude of 0.00016 m is obtained from the Watts formula. This result is not coupled to a landslide velocity or to a distance. For a constant landslide velocity of 0.3 m/s the wave amplitude is similar to the calculated wave amplitude. However, it is quite difficult to make predictions of the wave amplitude with such a formula.

7.4.2.   Selection of the verification case

One of the reasons the submergence tests is to provide a dataset, which can be used to verify the results of the numerical model. The test with an initial position of r = 5 m, which corresponds with a depth of 0.21 m and therefore a submergence 0.11 m, will be used for comparison. For this initial position, submergence tests have been carried out with landslide velocities of 0.46, 0.7, 1.0 and 1.3 m/s.
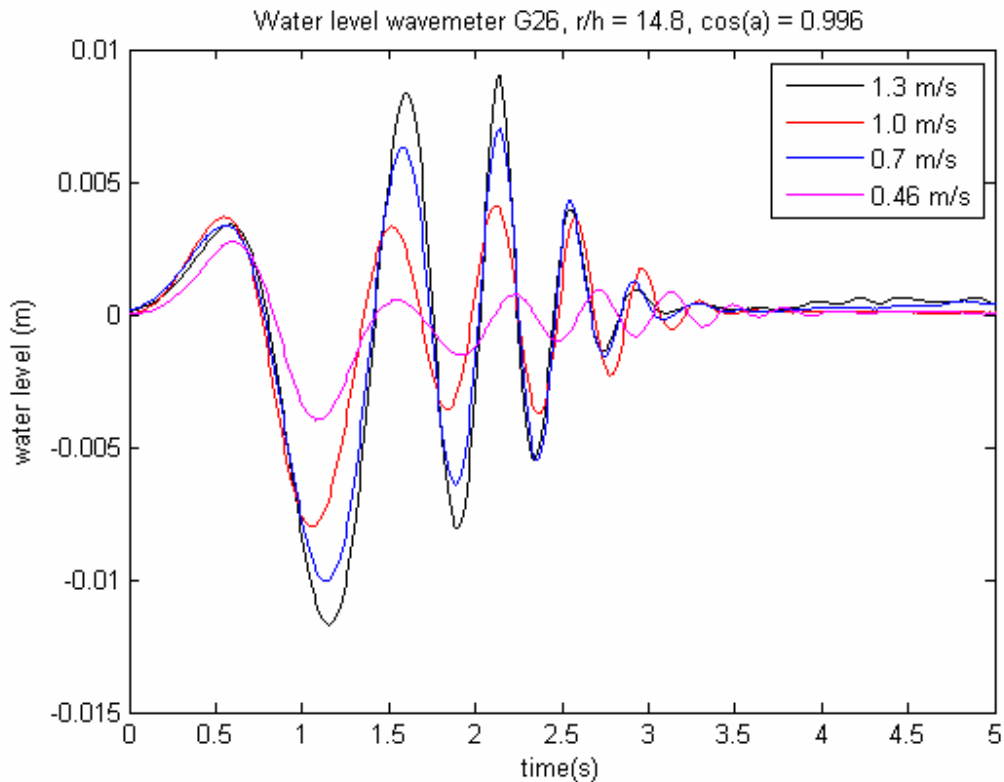
Figure 30: Water level time histories for a initial landslide position of r = 5 m and α = 0° and wave meter G26.

For the landslide velocities of 1.3 m/s it can be seen that the second wave is higher at wave meters G26 and G27. This is due to the abrupt stop of the landslide when the landslide arrives at r = 8 m. With higher landslide velocities, the time of landslide motion is shorter and therefore the influence of the abrupt stop can already be seen in the second wave. For lower landslide velocities a higher peak can be seen further back in the signals of the wave meters.

The dataset that will be used for a comparison with the numerical results should have a sufficient accuracy. Therefore the wave height should be as high as possible. On the other hand, the abrupt stop of the landslide should not influence the first wave. Therefore the test with an initial position of 4 meter and a landslide velocity of 0.7 m/s will be compared with the numerical model results. This comparison can be found in Part VI.

7.4.3.   La Palma

One part of the objective of this study is to quantify the generation of waves of a landslide induced tsunami in La Palma. No numerical computations with bathymetry information have yet been carried out for this case. However, some statements can be made already on basis of the laboratory experiments.

It must be noted with these preliminary judgments on basis on the experiments, that the whole problem is highly schematized in the experiments. The bottom profile and the velocity profile have been simplified and will be adapted to more realistic values in the numerical model.

For the La Palma case it has been stated by Nieuwenhuis (2005) that the upper boundary for a landslide velocity is 30 m/s (100 km/h). With the scaling analysis for a laboratory scale this corresponds with a landslide velocity of 0.3 m/s.

With the results of the sub-aerial tests that have been done for a landslide velocity of 0.3 m/s, the wave height at certain distances from the coast of La Palma can be calculated. These locations correspond with the wave meter location multiplied with a scale of 1:8500. At a distance of roughly 40 km from the coast, a tsunami wave height of roughly 5 meters is left for a landslide velocity of 30 m/s, see figure 28.
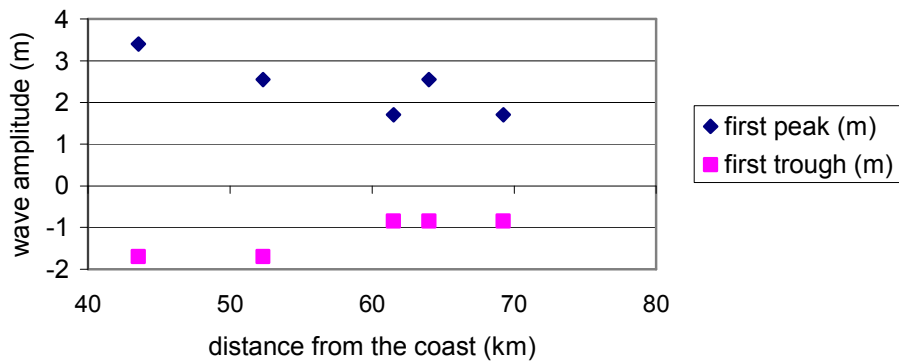
First wave in the La Palma case

Figure 31: First wave when scaling to La Palma dimensions

7.5. Conclusions and Recommendations

7.5.1. Conclusions

From the experiments some results were obtained which make it possible to understand the tsunami generation process better. In the experiments, the initial position and landslide velocity were varied. Furthermore, the water surface elevation was measured at different locations in space.

Landslide velocity
A clear relation between landslide velocity and wave amplitude is observed. Until a certain landslide velocity the wave amplitude increases. After this point the increase stagnates and in some cases a decrease can be noticed. The wave period decreases when the landslide velocity increases.

Initial position
The depth at the initial position of the landslide has influence on the waves which are generated. When the depth at the initial position is deeper, lower waves are generated. The energy flux from the landslide to the water is in most cases constant. With exception of the energy flux at very shallow depths.

Distance
When the distance from the wave generation area increases, the wave amplitude decreases. On the axis of landslide motion a strong influence from the landslide model can be noticed. Along this axis the wave amplitude is higher than wave amplitudes besides this axis. No clear relation could be found between the distance to the wave generation area and the wave period.

Wave celerity
The wave celerity of the generated trough which propagates along the axis of motion is influenced by the landslide motion and is the same as the landslide velocity till a certain depth. The wave crest propagates freely according to linear wave theory for low Froude numbers. For landslide velocities larger than 1 m/s the linear wave theory cannot be used anymore and the theory for solitary waves gives better results.

Accuracy of the experiment
Attention has to be paid regarding the following issues. The measurement errors made when measuring waves for low landslide velocities, are relatively high. For low landslide velocities the absolute error of the surface elevation measurement is 10 % or higher. For landslide velocities of 0.7 m/s and higher, the absolute error becomes lower than 10 % and thus acceptable. Furthermore, the time when the landslide model was stopped, can be seen in most signals as an increase in wave amplitude. Especially for the higher landslide velocities, when the time of landslide motion becomes shorter, the stop can influence the first trough amplitude.

Empirical formulas
The formulas for landslide tsunami generation, which were found in literature, have limitations. Some formulas produce answers close to the measured surface elevation. However it can be seen that the parameter range of this experiment is, for some parameters, far from the parameter range that was used to derive the formulas. In particular the slope angle of this experiment was completely different to the slope angles used in former experiments.

7.5.2.   Recommendations

<u>Variation of parameters</u>
In this experiment the number of parameters that could be varied, was limited. The slope angle for example could not be varied and it was noticed that the small slope angle was the main reason why the formulas, which were found in literature, failed to predict a correct wave amplitude.
Furthermore, because the slope angle was so different as compared to other experiments, it was hard to compare experiments from the past with this experiment. Therefore, it would be interesting to do some experiments with a larger set of variables to get a better view on the processes of landslide tsunami generation.

<u>Accuracy wave meters</u>
Another recommendation should be done regarding the measurements. In this experiment six wave meters were used to measure the wave heights. Three of them were acoustic wave meters, which could not provide the same accuracy as the resistance wave meters, but they could be placed above the axis of landslide motion, which was not possible with the resistance wave meters. For experiments in the future with the same landslide velocity range it should be recommended to use resistance wave meters, or wave meters with the same accuracy, instead of acoustic wave meters.

<u>Three-dimensional information</u>
Furthermore, when doing three-dimensional tests in future it is recommended to use more wave meters or put more time into the video imaging. Especially along the axis of motion it is suggested to locate more wave meters in order to get more precise information about the celerity of the first wave and the influence of the distance to the wave generation area.

PART IV: Numerical model

8. Introduction

The numerical model Finlab has been used to model the generation of tsunami waves due to a mass failure. In the following chapters, the numerical model has been extended step by step. In order to finally simulate in chapter 12 the landslide generated tsunami for the case of La Palma. Initially, a basic 2-dimensional numerical model is made and described in chapter 9. The model is verified with the experimental results of Sue (2007). After this verification the influence of different parameters is examined. For the landslide velocity it was already known from the physical model experiments that it influences the wave amplitude and the wave period. However, in this case also the landslide length, landslide height and the slope are varied.
In the following step, described in chapter 10, the basic 2-dimensional model is extended to a basic 3-dimensional model. The experimental results are used to verify this 3-dimensional model. Finally in chapter 11, the 3-dimensional basic numerical model is extended with bathymetry information from the Canary Islands. With this model the water elevations in the La Palma case are computed.

9. 2DV-numerical model

9.1. Verification using measurements by Sue (2007)

9.1.1. Introduction

Sue (2007) has done several 2-dimensional laboratory experiments aimed at producing generation data of underwater landslide-induced tsunamis. In these experiments, the landslide density and initial submergence were varied and information of wave heights, length, propagation speeds and shore run-up was measured.

As Sue (2007) generated an extensive dataset of experimental data, this dataset can be used to calibrate the 2DV-numerical model in Finlab. For this validation the dataset with the smallest initial submergence and a landslide density similar to the landslide model density of the experiments described in chapter 6 is chosen. Table 1 produces some further details on the experiment.

Table 1: Details experiment Sue 2007

Landslide length b	0.5 m
Landslide width w	0.25 m
Landslide thickness T	0.026 m
Basin length L	14 m
Water depth h	0.435 m
Slope angle θ	15°
Initial submergence d_i	0.1 m (case IS4)
Specific gravity γ	2.23 (case SG2)

9.1.2. Model set-up

Model domain

For the numerical model domain, the same dimensions are taken as the dimensions of the flume in the experiments of Sue. Figure 1 shows the set-up of the numerical model. The basic dimensions can be found in appendix B.
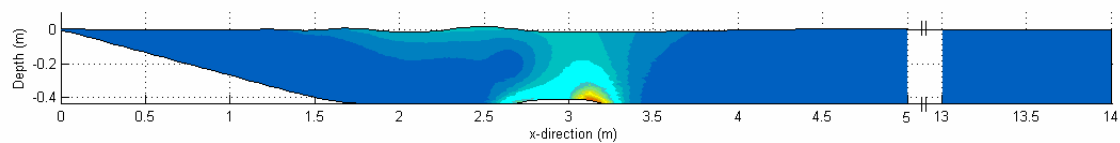

Figure 1: Model domain

The depth profile of the model can be described with the following function.

For: $0.03 \text{ m} \leq x$ h(x)=0.009 m

For the slope:
$0.03 \text{ m} \leq x \leq 1.297 \text{ m}$ h(x)=x $\cdot \tan(15^\circ)$

For the transition between the slope and the horizontal:

$1.297 \text{ m} \leq x \leq 1.807 \text{ m}$ $h(x) = -0.19(x-1.297)^3 - 0.1024(x-1.297)^2 + 0.2728(x-1.297) + 0.3475$

For: $1.807 \text{ m} \leq x$ $h(x) = 0.435 \text{ m}$

In figure 2 the start position of the landslide is displayed. In this figure the slope and the transition between the slope and the horizontal are visible.
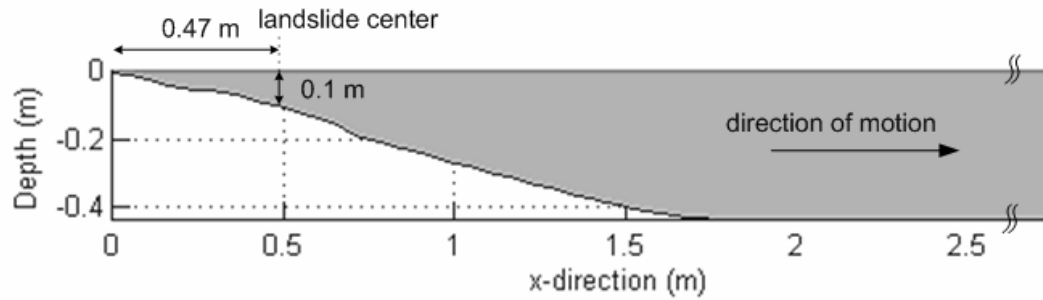

Figure 2: Start position landslide in the model

Near $x = 0$ m, the slope becomes horizontal with a depth of 0.009 m. This was the minimum value for the model.

Choice of spatial and temporal calculation steps
The size of a spatial mesh size is usually determined by the spatial resolution required to investigate the problem. In this case the problem is the landslide with dimensions of 0.5 m in length and 0.026 m in height. It is decided that a spatial resolution of 0.04 m in x-direction is sufficient to analyze the problem. This means that the landslide is represented by 12 mesh points. In y-direction (vertically) the number of mesh points is 34, which means that the spatial resolution is minimal 0.013 m at a depth of 0.435 m and in shallower areas the spatial resolution is higher.

The temporal step size is related to the time scale of the process being examined. However demands for numerical stability and accuracy are usually more stringent. To calculate the necessary time step, the Courant number is used. For this computation a Courant number of less than one is desirable for the accuracy, see equation 1.

$$c\frac{\Delta t}{\Delta x} < 1 \qquad \text{so} \quad \Delta t < \frac{\Delta x}{c} \qquad\qquad \text{Eq. 1}$$

For the Courant condition either the landslide velocity or the wave propagation velocity can determine the time step. The maximum landslide velocity is 1.2 m/s, the maximum propagation velocity on the contrary is approximately 1.98 m/s and is therefore the determining condition. A time step of 0.01 seconds is chosen.

Simulation period
The simulation period is determined by the experimental settings. The longest simulation period in the experimental simulation was 7 seconds and therefore a simulation period of 7 seconds was chosen.

Initial and boundary conditions

To be able to model the problem, some conditions are required. The boundary at $x = 0$ m and the boundary at $x = 14$ m have been modelled as a wall. Waves reflect against these walls. This condition resembles reality, as the wave flume in the experiments has wall boundaries too.

9.1.3. Velocity profile

To obtain a landslide velocity profile for the numerical model, the landslide velocity time history and the acceleration time history of the experiment have been schematized into three different stages. Figure 3 shows the profiles of the experiment and the schematizations.
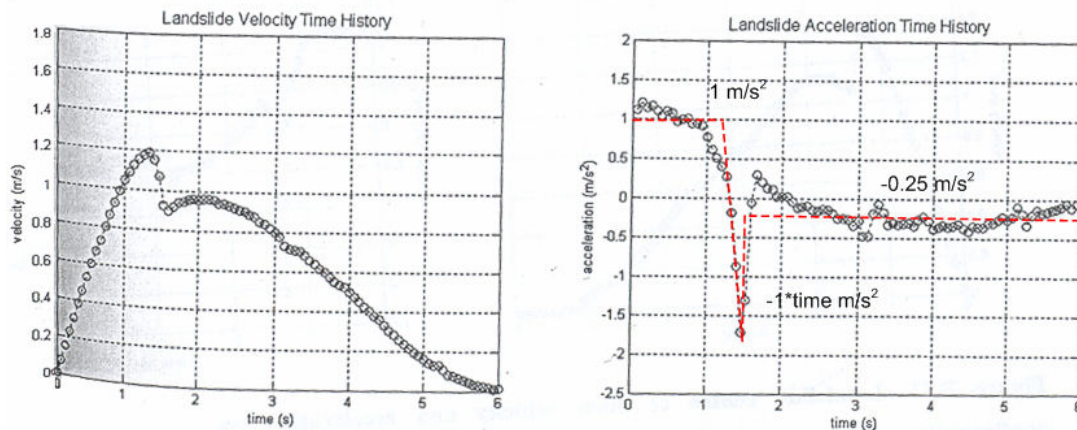
Figure 3: Landslide velocity and acceleration time histories (Sue, 2007)

During the first stage, the landslide starts moving and has an acceleration of approximately 1 m/s^2. The acceleration of the landslide lasts until the slide reaches the end of the slope at 1.2 seconds after the start of the motion. Then, in the second stage, the landslide undergoes a rapid variable deceleration of 0.1 second. At a time of 1.3 seconds, the slide reaches the last stage, and moves at a constant deceleration of 0.25 m/s^2 till zero velocity is reached. The following formulas are used to describe the velocity profile.

Stage 1
Place where the slide reaches the end of the slope

$$x_1 = x_0 + u_0 \cdot (t_1 - t_0) + \frac{1}{2} a_1 \cdot (t_1 - t_0)^2$$

Stage 2
Fast variable deceleration

$$x_2 = x_1 + u_1 \cdot (t_2 - t_1) + \frac{1}{6} a_2 \cdot (t_2 - t_1)^3$$

$$u_1 = a_1 \cdot (t_1 - t_0)$$

Stage 3
Run out time

$$x_3 = x_2 + u_2 \cdot (t_3 - t_2) + \frac{1}{2} a_3 \cdot (t_3 - t_2)^2$$

$$u_2 = u_1 + \frac{1}{2} a_2 \cdot (t_2 - t_1)^2$$

$$t_3 = \frac{u_2}{a_3}$$

9.1.4. Landslide model shape

In his experiments Sue (2007) has used a semi-elliptical shape for the landslide model, see figure 4. To convert this shape into a two-dimensional shape, which can be described in a numerical model, he investigated the water surface response of different shapes.

Figure 4: Landslide model (Sue, 2007)

He came to the conclusion that the solution is relatively insensitive to the slide shape. A quartic shape was chosen for his semi-analytical and numerical simulation, as this shape has a steep, but not infinite slope at the ends and a zero slope at its centre.
The basic function for the quartic shape is:

$$f(x) = 0.982 \cdot (1 - x^2) \qquad \text{for } -1 \leq x \leq 1$$

$$\frac{df}{dx} = -3.928 \cdot x^3 \qquad \text{for } -1 \leq x \leq 1$$

For the Finlab simulation, the quartic shape has been used too. In figure 5 an image of the quartic shape and its dimensions is given.
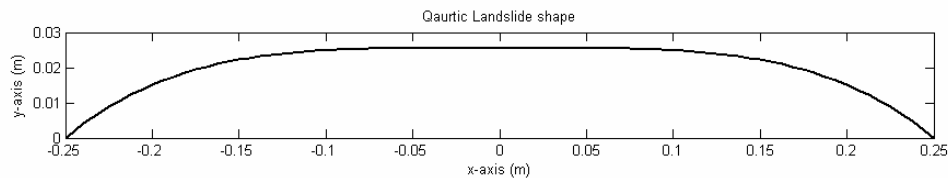

Figure 5: Quartic landslide shape

9.1.5. Numerical model settings

To obtain the final results of the case with Sue's results, some parameters/ settings where varied in the model to get the most resembling results, see table 3.

Table 2: Settings

	Variation	Final setting
Numerical method	Backward Euler or Fractional step method	Fractional step method
Viscosity	1E-3 to 1E-10 m^2/s	1E-3 m^2/s
H-error and maximum iterations	1E-4 to 1E-10 Max. iterations: 100 - 10000	Error: 1E-4 Max. iterations: 100
v-error and maximum iterations	1E-4 to 1E-10 Max. iterations: 100 - 10000	Error: 1E-4 Max. iterations: 100
Velocity profile	Different settings during the three stages	See velocity profile

The numerical method is important for the correct reproduction of the wave elevations. The backward Euler method produced smaller wave elevations than the Fractional step method. Moreover, the wave heights decrease faster in time with the backward Euler method, see figure 6. Compared to the experiment results, the Fractional step method represented the measured wave elevations better.
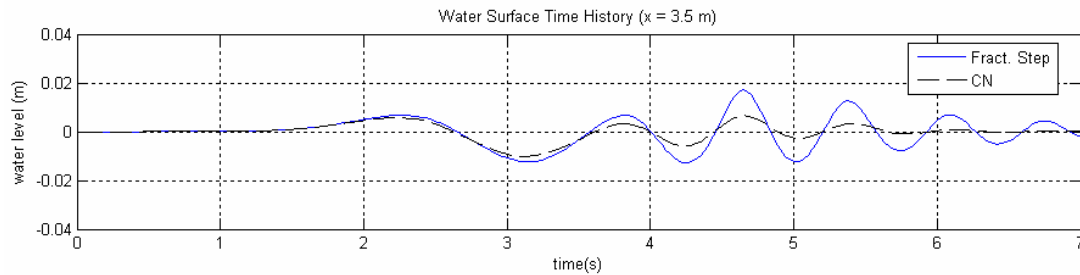

Figure 6: Comparison between the numerical methods

The viscosity was reduced for both numerical methods. This was done mainly because the numerical results had more damping than was observed with the experiment results. The possibility exists that with a reduced viscosity, the backward Euler method would get better results. However the effect of the viscosity is not enough to represent the experiment results better than the Fractional step method with a viscosity of 1E-3 kg/ms.

In addition to this the surface elevation error, the velocity error and the maximum iteration steps were varied. The effect of a lower error and more iteration steps could have resulted in a better resemblance between the experimental and numerical results. On the other hand, the computation time increases with such a measure. Since the improvement in the results was very small, it was chosen to use the largest error in the range and the smallest maximum iteration steps for the computations.

The last variation factor was the velocity profile. The exact timing of the acceleration and deceleration stage is crucial to reproduce the experimental results. As the exact velocity profile could not be reproduced in the model, runs with different velocity profile schematizations were done. The final velocity profile is already presented in section 9.1.3. However, this velocity profile is only a schematization of the real velocity profile and therefore some discrepancies between the elevations in the numerical model and the experimental results could be explained by this incorrect reproduction.

9.2. Results

In this section some results of the numerical model are presented. When experimental graphs are available, the numerical results are compared to the experimental results.

9.2.1. Water surface time history and profile

Sue presented the water surface times history at several locations in the wave flume. With the numerical model output for the same locations can be computed. Small discrepancies can be observed between the results, especially at x = 2.5 m and x = 3.5 m.
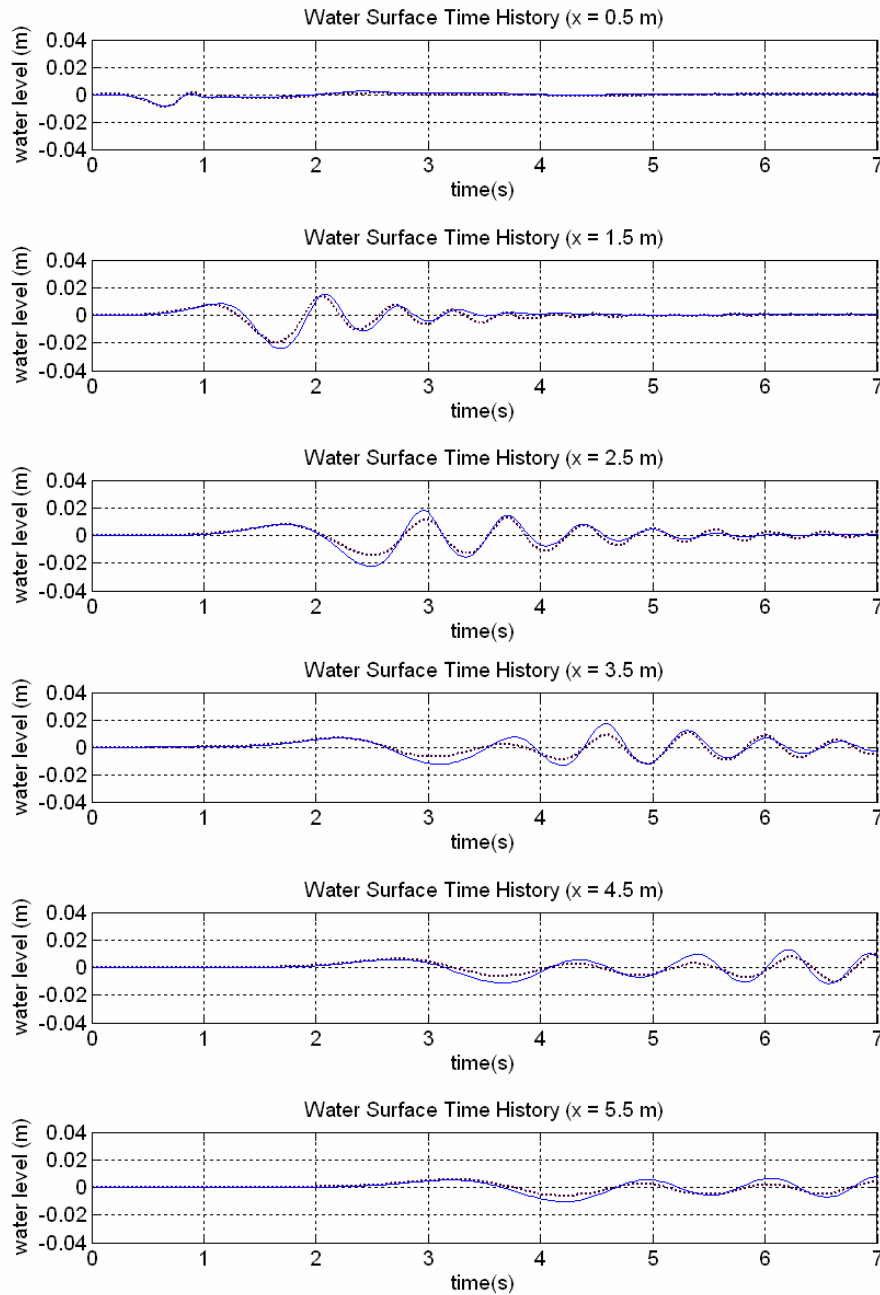

Figure 7: Water times surface time histories for various locations
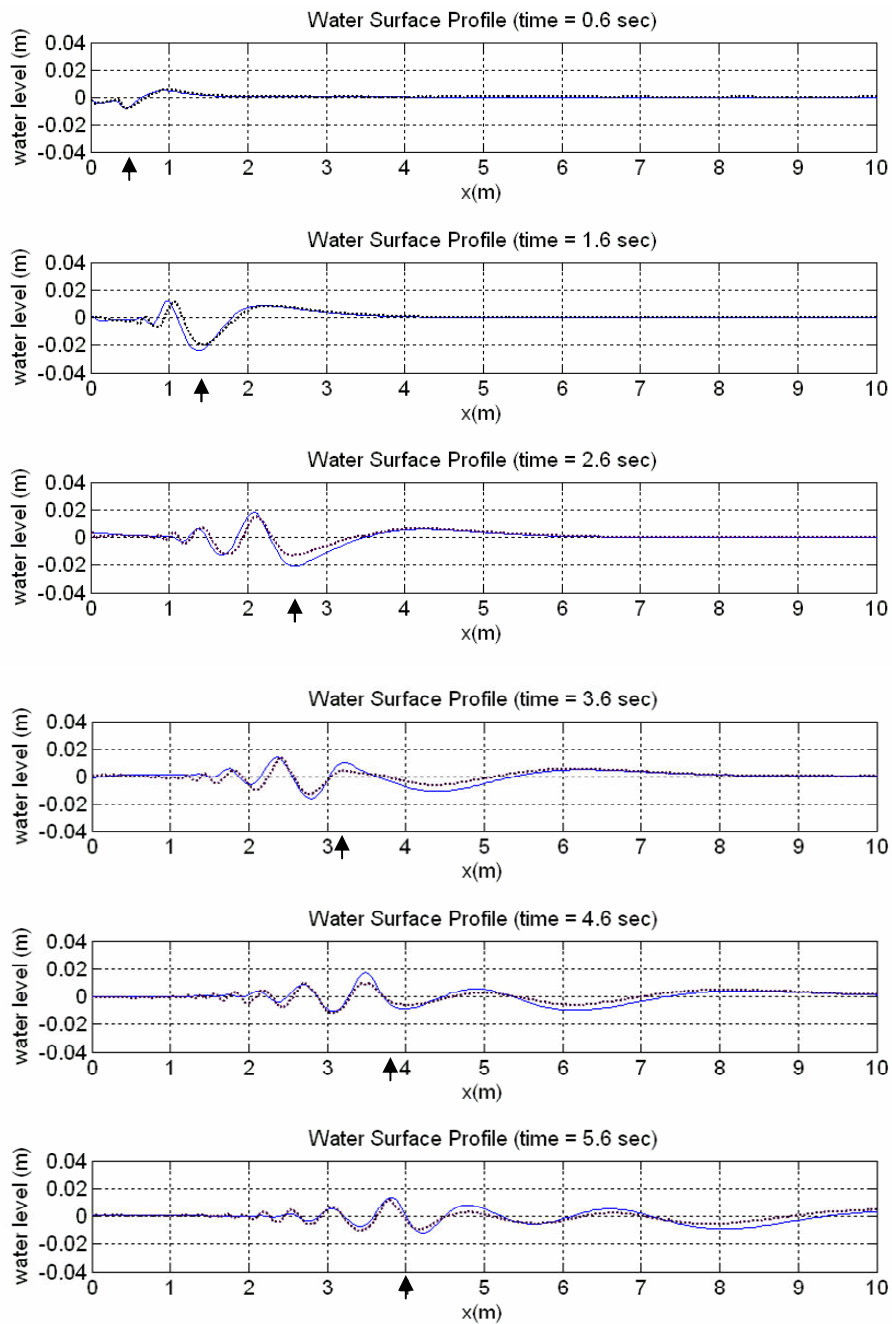Blue line: numerical result, Black dotted line: experimental result Sue 2007

Figure 8: Water surface profiles for various times
Blue line: numerical result, Black dotted line: experimental result Sue 2007

In figure 8 the water surface can be seen for the length of the flume at different times. In this figures the motion of the landslide can be noticed, see the black arrows. After 2.6 seconds, the landslide velocity decreases and the wave trough can propagate freely. The numerical results are similar to Sue's results. It is interesting to note that the largest difference between the results can be observed near the landslide.

9.2.2.   Maximum and minimum water level envelope and time history

To obtain a maximum and minimum water level envelope, the maximum and minimum water level in time were sought and presented over the length of the wave flume. The largest surface elevation can be observed for a x-location of approximately 1.9 m in Sue's case and 2.4 m in the numerical case. The envelope is clearly larger in the numerical case.
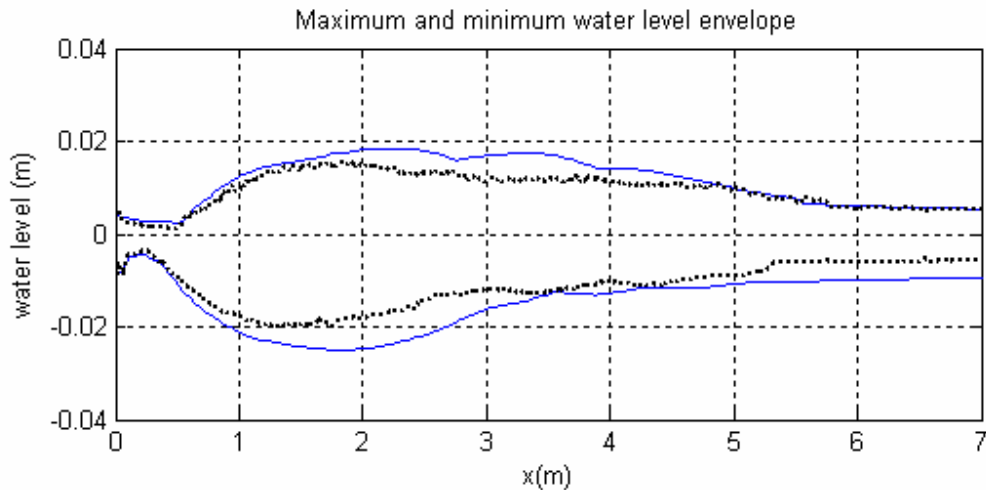

Figure 9: Maximum and minimum water level envelope
Blue line: numerical result, Black dotted line: experimental result Sue 2007

The maximum and minimum water level time history is obtained by taking the maximum and minimum water level over the flume for various times. In this graph it is can be seen that the timing of the time history is different for the numerical results. In addition, the numerical model gives larger results than Sue's experimental results.
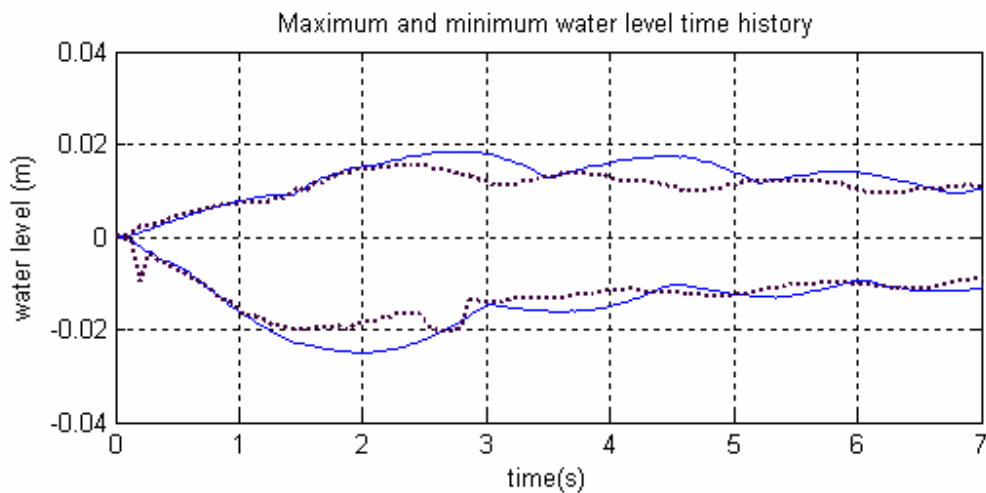

Figure 10: Maximum and minimum water level time history
Blue line: numerical result, Black dotted line: experimental result Sue 2007

9.2.3. Sub-surface velocity distribution

The sub-surface velocity of the first crest is positive according to the numerical model at x = 3m. On the contrary the velocity of the first trough is directed in negative direction and near the bottom an increase in velocity can be observed. No results of Sue were available for a comparison.
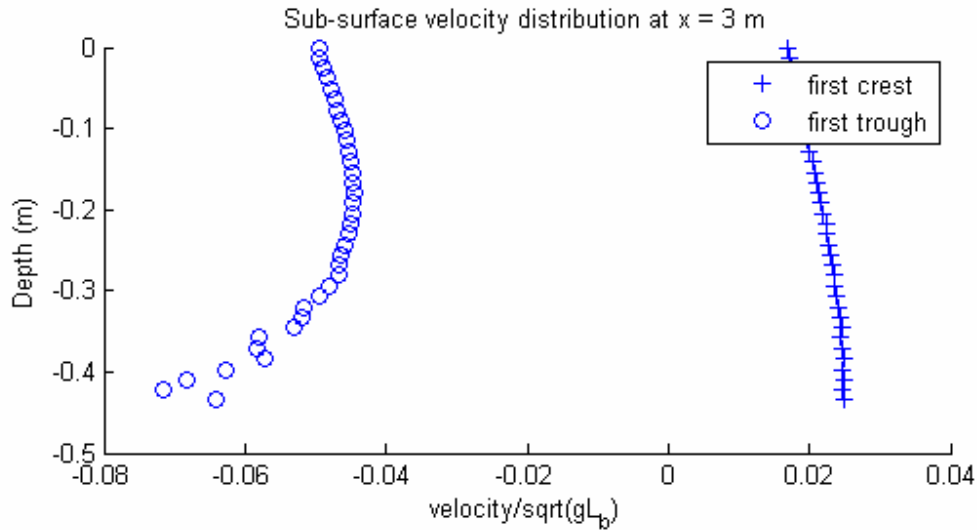

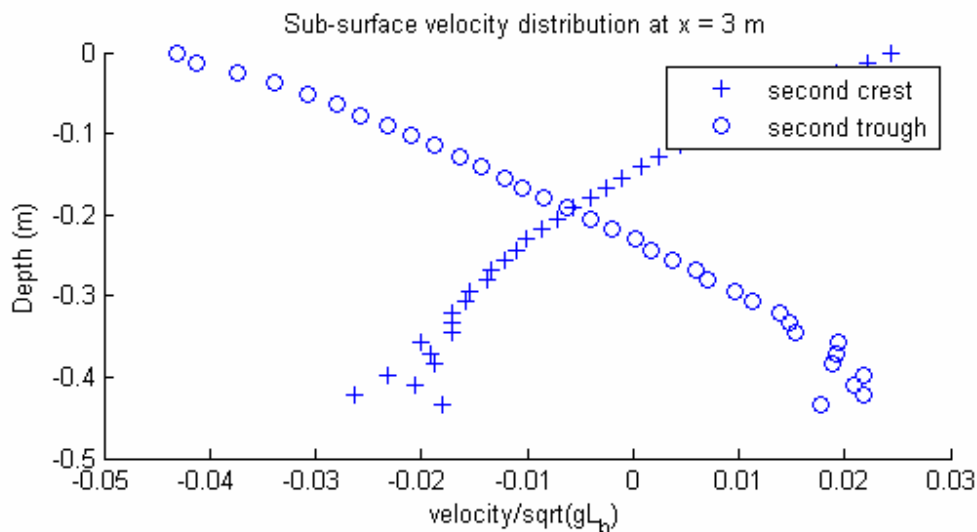Figure 11: Sub-surface velocity distribution first crest and first trough at x = 3 m numerical model

Figure 12: Sub-surface velocity distribution second crest and second trough at x = 3 m numerical model

The velocities of the second crest and the second trough are presented in figure 12. The second crest has a negative velocity near the bottom and a positive velocity near the water surface, whereas the velocity distribution of the second trough is reversed to the velocity distribution of the second crest.

9.2.4. Crest and trough amplitude and half-wave length time history

As has been concluded earlier, the wave amplitude of the first wave is larger for the numerical results, see figures 13 and 14.
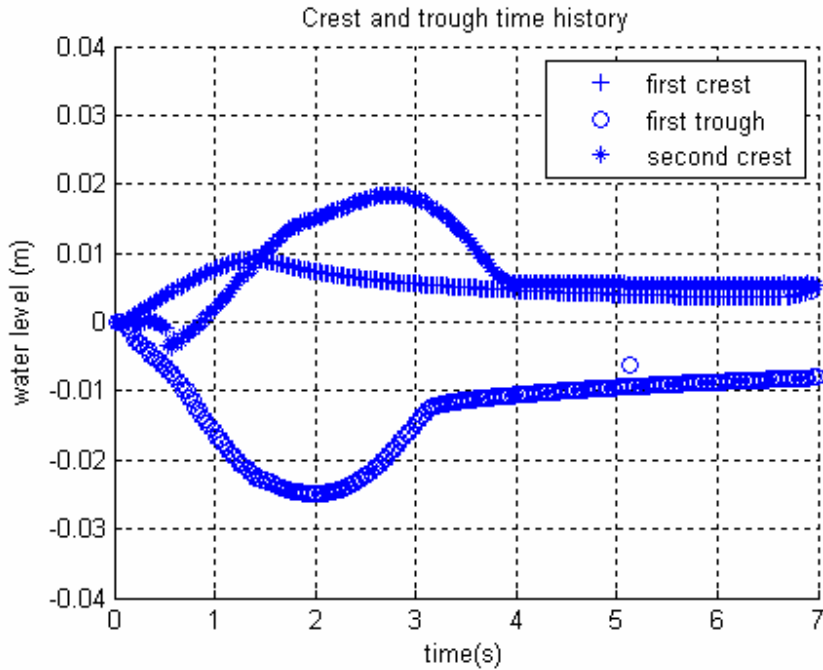

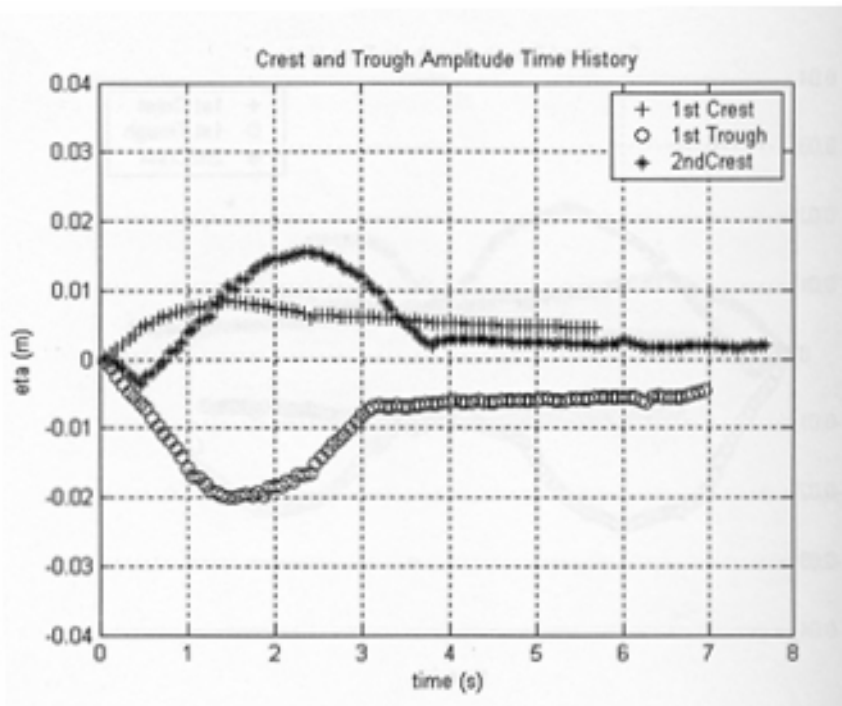Figure 13: Crest and trough time history computed with the numerical model

Figure 14: Crest and trough time history experimental result Sue 2007

The half-wave length of the first trough and the second crest are reasonably well computed by the numerical model, see figures 15 and 16.
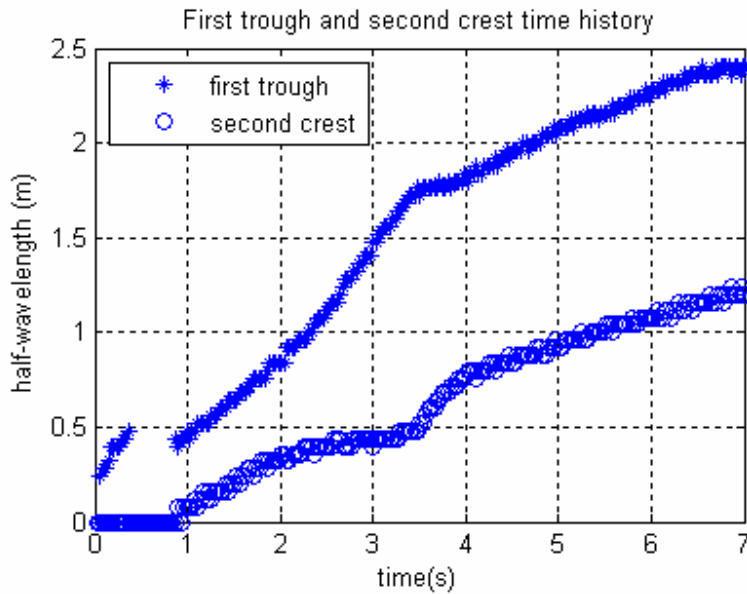

Figure 15: Crest and trough length time history computed with the numerical model
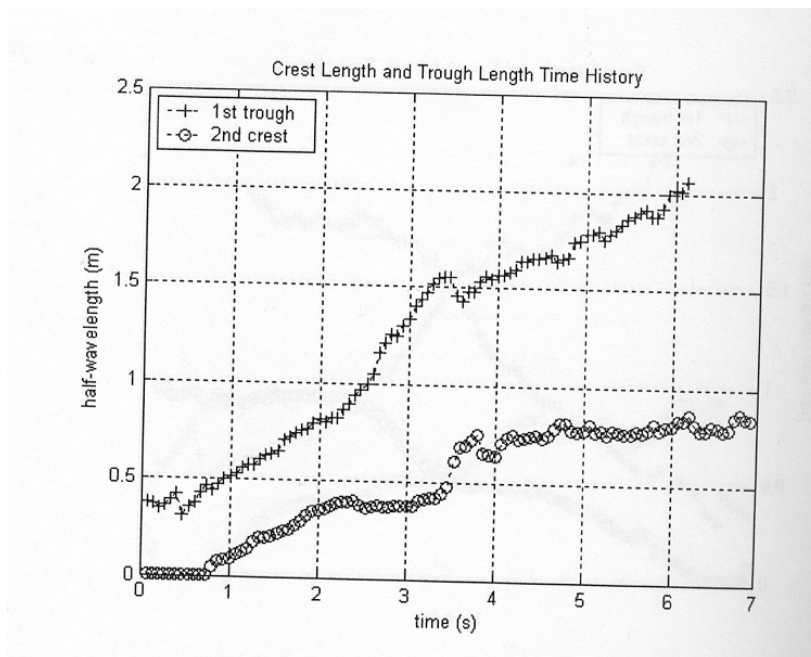
Figure 16: Crest and trough length time history experimental results Sue 2007

9.2.5. Characteristic curve

In figures 17 and 18 the generation of waves in time and in space has been displayed for respectively the numerical model and for Sue's experimental results. In figure 17 the landslide motion has been indicated with the blue line. It can be clearly seen that the first trough is bounded to the landslide motion for 2.5 seconds.

Figure 17: Characteristic curve computed with numerical model

Figure 18: Characteristic curve experimental results Sue 2007

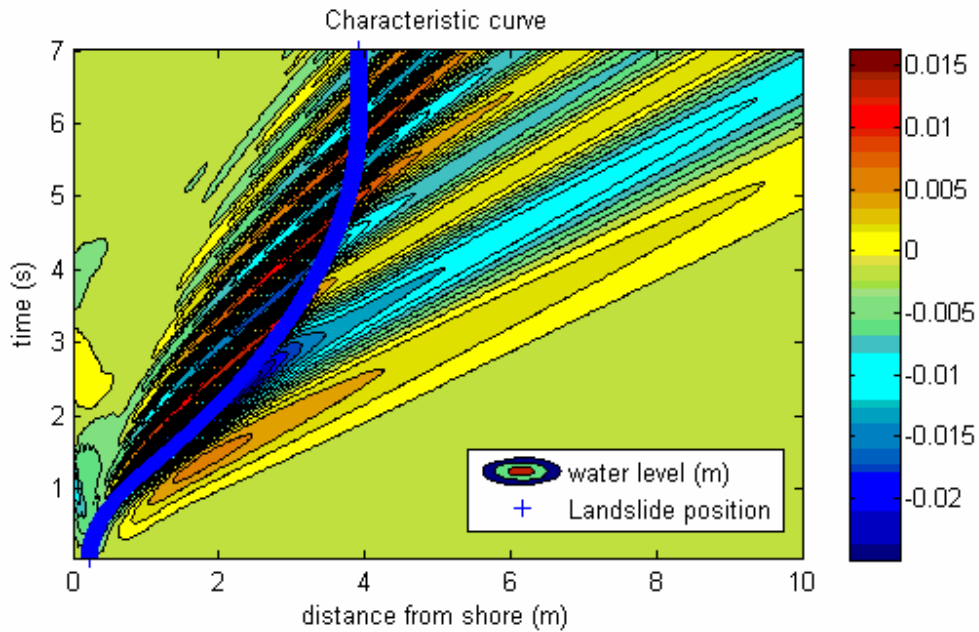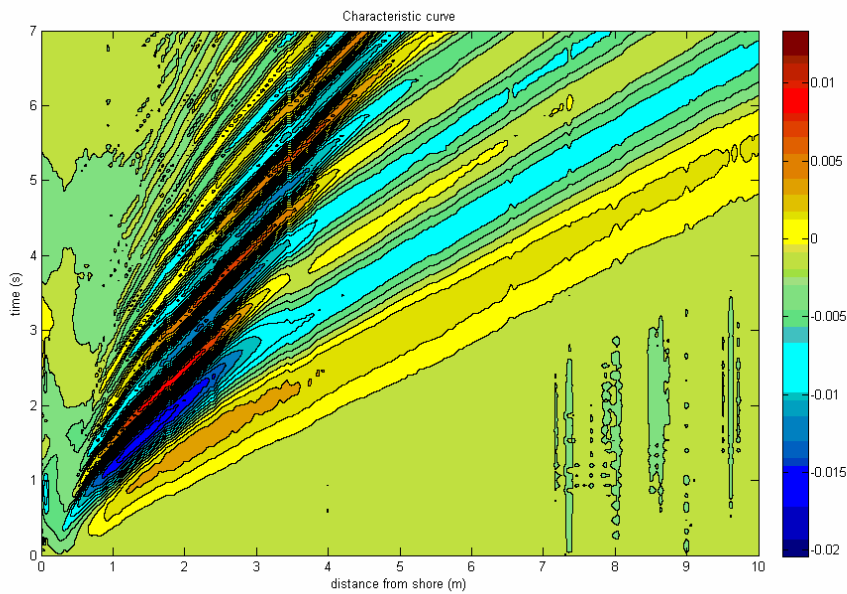### 9.2.6. Differences between the numerical model and Sue

The results of the numerical model correspond relatively well to the experiment results of Sue. The periods of the wave are nearly the same and the wave amplitudes match almost. Generally, the numerical model computes slightly larger waves which can be seen in the maximum and minimum water level envelope and the time histories in figures 9 and 10.

Some small differences in the settings of the two models can be distinguished. For example, the numerical model has no rigid landslide, whereas in Sue's experiments a rigid slide model was used. Furthermore, the velocity profile of the landslide in the numerical model was not exactly the same as the velocity profile during the experiments. This could explain some small differences in wave heights when the timing of decelerations was not exactly the same. Finally, one part of the slope was open in the experiment, which enables a flow in the direction of the slope.

It can be seen that the velocity profile of a test is relatively important for the timing of the waves. Therefore, it can be concluded that a constant velocity in an experimental test is favourable, if this test is done to verify numerical models.

9.3. Parameter variation

9.3.1. Introduction

In this case the influence of various parameters is investigated for a two-dimensional domain. Consecutively, the slope, the length of the landslide, the thickness of the landslide and the landslide velocity will be varied. To make a comparison possible a reference case is set up. The values of the parameters of the reference case can be found in table 4. For the landslide shape the quartic function was used, which was explained in section 9.1.4.

Table 3: Details parameter variation

	Reference case	Variation
Slope angle θ	16°	3°, 8°, 25°
Landslide length b	0.5 m	+/- 0.25 m
Landslide thickness T	0.05 m	+/- 0.025 m
Landslide velocity u	0.5 m/s	+/- 0.3 m/s

9.3.2. Model set-up

Model domain

For the numerical model domain, the same set-up was used as the set-up for the experiments carried out for this Master's thesis. The flume has a length of 28 meters of which 24 meters is filled with water till a height of 0.4 meters.

For this test case, two various slopes were used. The slope of 3 degrees is present in the flume of the DUT laboratory, the slope of 15 degrees is frequently used in experiments done in the past, see for example case Sue in section 9.1.

In the figures 19 and 20, the model domains of two cases with different slopes are presented. In both cases the first two meters of the inundated flume have been left out of the computations. This is done because the numerical model has difficulties with simulations were the bottom is higher than the surface elevation. 0.1 meters height are needed to ensure that the landslide can move into the model domain. Therefore the length of the model domain becomes 22 meters, see figures.
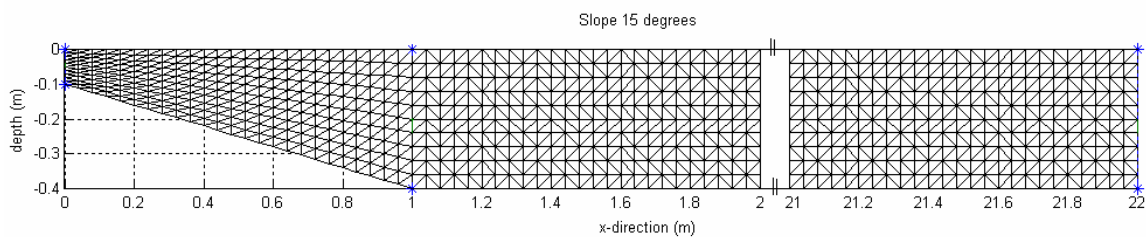

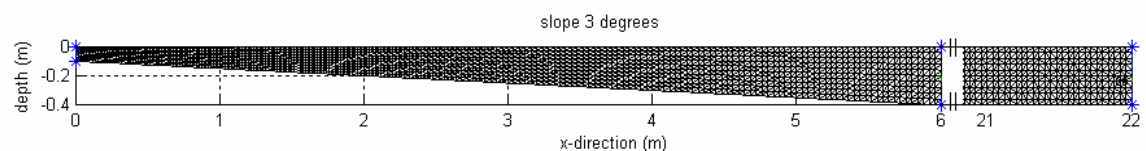Figure 19: Model domain slope 16°

Figure 20: Model domain slope 3°

Choice of spatial and temporal calculation steps

For this case, the size of the spatial calculation step is determined like in the previous section with the case Sue. A spatial resolution of 0.04 m in x-direction and a spatial resolution between 0.01 and 0.04 m, depending on the depth, in y-direction are chosen for this problem. This means that the landslide is represented by 17 mesh points in x-direction and a 1 to 7 mesh points in y-direction.

With the courant condition the temporal step size is determined. In this case again either the landslide velocity or the wave propagation velocity can determine the time step. The landslide velocity is 0.5 m/s (or 0.2, 0.8 m/s), the maximum propagation velocity on the contrary is approximately 1.98 m/s and is therefore the determining condition. A time step of 0.01 seconds is chosen for this problem.

Simulation period

The simulation period is determined by the time that the landslide with a velocity of 0.5 m/s needs to reach the end of the 3° slope. The simulation period is therefore 12 seconds.

Initial and boundary conditions

To be able to model the problem, some conditions are required. For the boundary at $x = 0$ m the Riemann condition has been applied. The boundary at $x = 22$ m has been modelled as a wall. Waves reflect against these walls. This condition resembles reality, as the wave flume in the experiments has wall boundaries too.

Settings

As the settings of the numerical model were optimized in the previous section, the same settings were used for the simulations in this case. Table 5 shows the most important settings.

Table 4: Settings model

	Setting
Numerical method	Fractional step method
Viscosity	1E-3 kg/ms
H-error and maximum iterations	Error: 1E-4 Max. iterations: 100
v-error and maximum iterations	Error: 1E-4 Max. iterations: 100

9.3.3. Results parameter variation

Variation slope

In figure 21 the influence of different slopes can be noticed. The wave generation was computed for very gentle slopes (3°) as well as very steep slopes (25°). For $x = 0.5$ m the differences in first wave crest are small. On the contrary a large difference in wave trough can already be noticed. When the waves propagate further in space, a delay can be observed for the first peaks of the more gentle slopes. Furthermore, after a few meters the more gentle slopes (especially 3°) generate a larger wave crest than the steep slopes.

These differences can be explained with conservation of energy flux. When considering one x-location, the depth of the more gentle slopes is smaller than the depth of the steeper slopes. Therefore the wave group celerity at this location is smaller for the more gentle slopes.

This explains the delay of the wave peak. When keeping the conservation of energy flux in mind, the wave amplitude should be higher for the more gentle slopes.
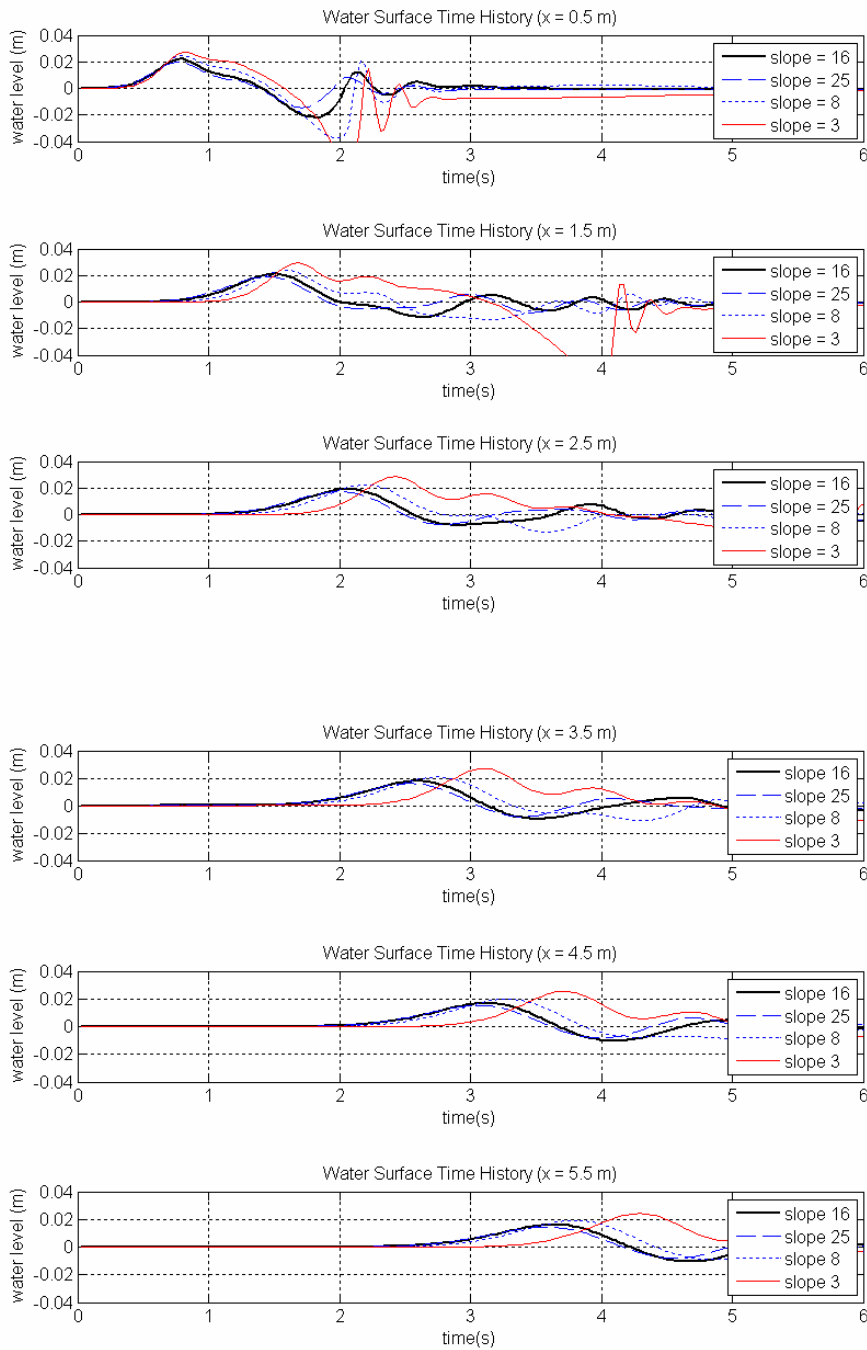
Figure 21: Water surface time history, various slopes, for a velocity of 0.5 m/s

Variation landslide length

In figures 22 and 23, respectively the water surface times histories and the water surface profiles have been displayed for different landslide lengths. It can be seen that the landslide length has only a small influence on the wave amplitude, but a large influence on the length of the wave trough. In figure 23 it can be noticed that the first wave length increases for larger landslide lengths.

Figure 22: Water surface time histories, various landslide lengths, for a velocity of 0.5 m/s
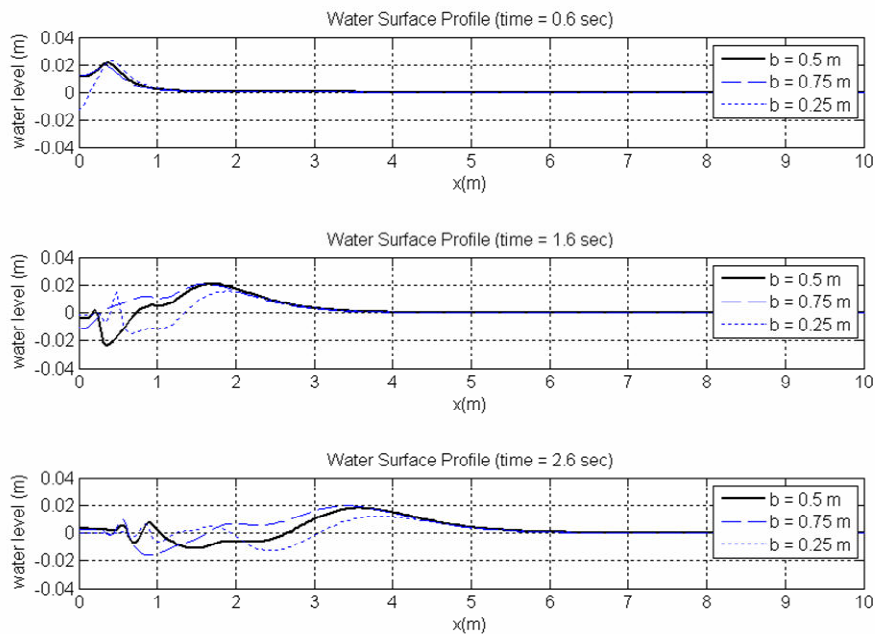
Figure 23: Water surface profiles, various landslide lengths, for a velocity of 0.5 m/s

Variation landslide height

In figure 24 the results can be seen of various runs with different landslide heights. The influence of the landslide height can be seen for the first crest height as well as the first trough height. It can be concluded that when the landslide height becomes higher, the first wave becomes higher. Furthermore, a small delay of the first trough can be observed when the landslide height increases.
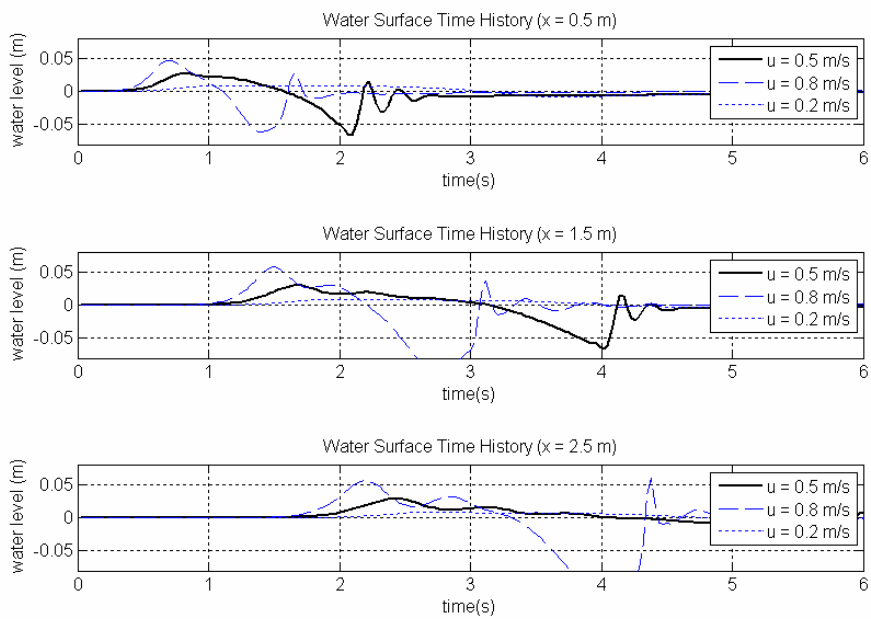
Variation landslide velocity

Figure 25 shows the influence of the landslide velocity, which has already been investigated in chapter 8. It can be clearly seen that the first wave amplitude increases for higher landslide velocities. Furthermore, a decrease in wave period can be noticed when the landslide velocity increases.
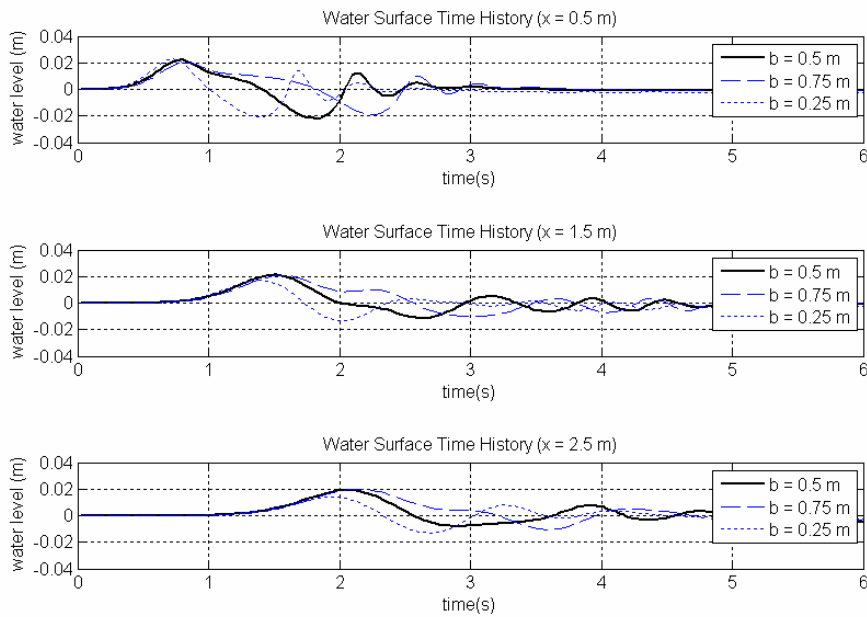

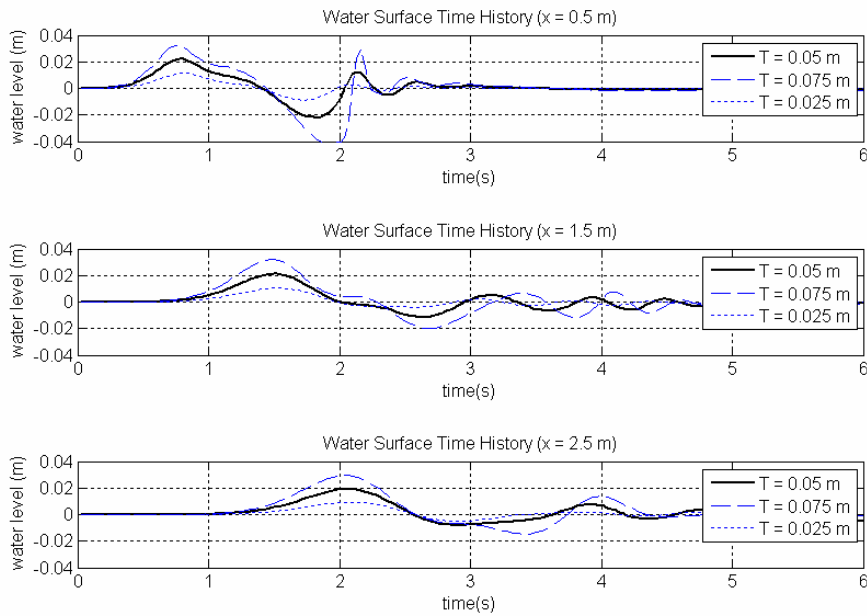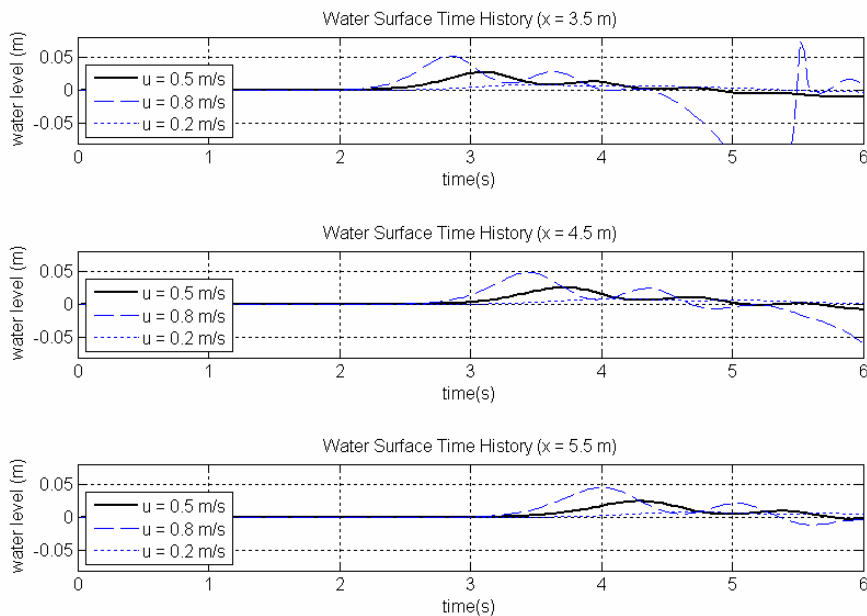Figure 24: Water surface time histories, various landslide heights, for a velocity of 0.5 m/s

Figure 25: Water surface time histories for various landslide velocities, for a slope of 3 degrees.

9.4.   Conclusions

9.4.1.   Verification 2DV-model

The two-dimensional numerical model was compared to the experimental result of Sue (2007). The results of the numerical model correspond relatively well to the experiment results of Sue. The periods of the wave are nearly the same and the wave amplitudes match almost. Therefore it can be concluded that Finlab can compute a two-dimensional case of a landslide induced tsunami correctly.

9.4.2.   Parameter variation

Slope

From the cases with the variable slope it can be concluded that waves generated on a gentle slope are higher than waves generated on a steep slope. This could be explained with the fact that when the slope is gentle the landslide has a longer course on the slope, thus shallow water, and can produce more and higher waves.

Landslide length

A varying landslide length results not directly in a difference in wave amplitudes, see figures 22 and 23. However, it can be seen that the landslide length has influence on the wave length. Longer waves are being generated when the landslide length is longer.

Landslide height

The landslide thickness, on the contrary has a strong influence on the wave amplitude as can be seen in figure 24. In particular the first wave trough is much higher when the landslide is thicker.

Landslide velocity

Finally the landslide velocity has clearly influence on the wave amplitude. When the landslide velocity increases, an increase is noticed in the first wave amplitude and a decrease in the wave period.

It should be noted that these comparisons were made for two-dimensional situations. In a three-dimensional domain the wave amplitudes could be different, but it is expected that the relations between the parameters are not entirely different. Because of the two-dimensionality, the landslide width could not be varied.

10. 3D-numerical model

10.1. Model

10.1.1. Introduction 3D-numerical model

The physical scale model of this study has been carried out to provide a data set to verify the three-dimensional numerical model. In order to make a good comparison possible, the numerical model should use the similar model parameters as have been used in the physical scale model. In chapter 8 a data set was chosen for the comparison. This is the data set with an initial position at r = 5 meter and a landslide velocity of 0.7 m/s. The initial position coordinate of the physical scale model should be converted for the numerical model, as the waterline in the experiment lies at r = 0.8 m. Thus, an initial position of x = 4.2 m will be used for the numerical model. In table 5 a summary of the experiment details is shown.

Table 5: Details of the experiment

Landslide length b	0.7 m
Landslide width w	0.3 m
Landslide thickness T	0.1 m
Landslide shape	Quartic
Slope angle θ	3°
Velocity u	0.7 m/s
Initial position d_i	4.2 m (r = 5 m)
Length model L	21 m
Width model W	15 m
Depth model h	0.4 m

10.1.2. Model set-up

Model domain

The model domain differs from the dimensions of the physical scale model. The model domain is taken smaller than the dimensions of the physical scale model. This is done to save computation time.

As the wave generation is symmetrical around the axis of landslide motion, only one half of the basin will be used to compute the wave generation. Furthermore, the area of interest for the wave generation lies for the most part at the slope and near the axis of landslide motion. However it is important that the model domain includes the locations of the wave meters. Therefore, the whole area on the slope and some area near the axis of motion in the deeper part is included in the model domain, see figure 26.
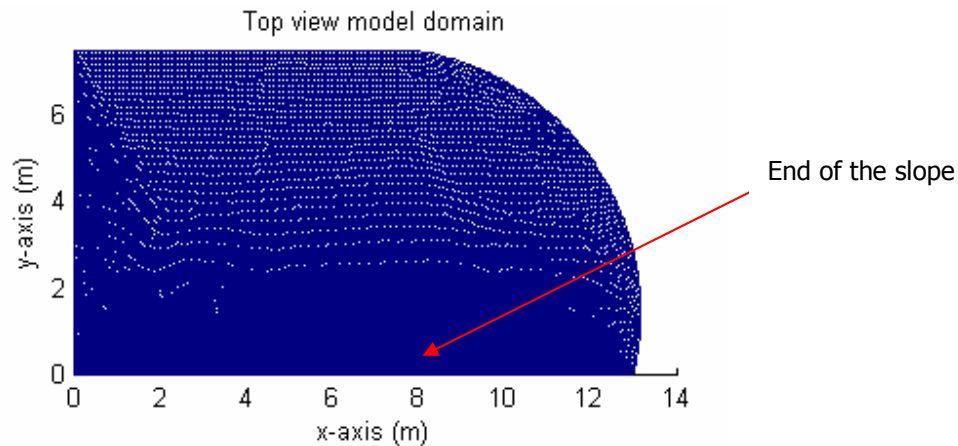
Figure 26: Top view of the model domain

A 3° slope is used, but for the area near $x = 0$ m a minimum depth of 0.02 m is taken. This was necessary, as the numerical model cannot handle a slope which approaches $z = 0$ m.
Figure 27 shows the three-dimensional model domain and its symmetrical opposite in distorted view.
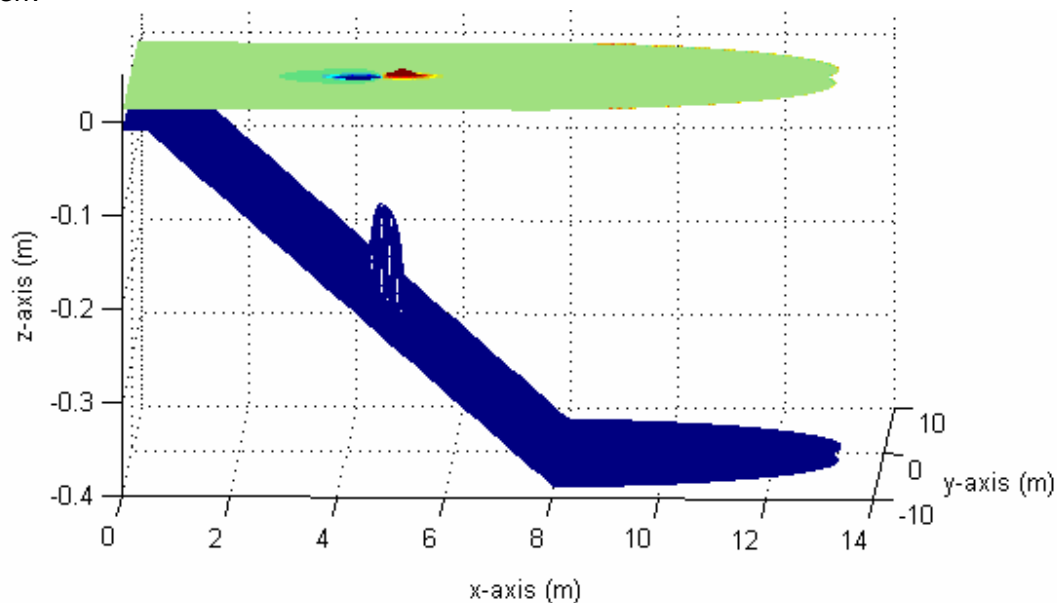
Figure 27: Model domain in distorted view

Choice of spatial and temporal calculation steps
The size of a spatial calculation step is a compromise between the minimum required mesh size with which the landslide can be reproduced accurately and the maximum number of mesh points to make the computation feasible. The landslide has a length of 0.7 m, a width of 0.15 m (half of the landslide) and a height of 0.1 m. It is decided that a spatial resolution of 0.04 m in x-direction is sufficient to analyze the problem for the area near the axis of motion. In the other area the spatial resolution could be coarser, depending on the minimal required resolution to represent the waves accurately. By choosing a resolution for the waves it should be considered that it should not differ too much from the resolution in the z-direction. In y-direction the mesh

size in the area of the moving landslide should certainly not be larger than 0.04 m and if possible in the shallow parts smaller. In z-direction the requirement is the same as in the y-direction.

The minimal required resolutions are chosen, see table 6. Depending on the results it could be considered to enhance the spatial resolution in y and z-direction in the area where the landslide passes.

Table 6: Resolution of the model

Δx	0.04-0.08 m
Δy	0.04-0.08 m
Δz	0.04 m
Δt	0.01 s

The temporal step size is related to the time scale of the process being examined. However demands for numerical stability and accuracy are usually more stringent. To calculate the necessary time step, the Courant number is used. For this computation a Courant number of less than one is desirable for the accuracy, see equation 1.
For the courant condition either the landslide velocity or the wave propagation velocity can determine the time step. The maximum landslide velocity is 1.33 m/s, the maximum propagation velocity on the contrary is approximately 1.98 m/s and is therefore the determining condition. A time step of 0.01 seconds is chosen.

Simulation period
The simulation period is determined by the requirement that the first wave should have passed the locations where the wave meters are located in the experiment. As the wave period of the first wave is approximately 5 seconds, 9 second simulation period should be on the safe site for the computation.

Boundary conditions
To be able to model the problem, some boundary conditions are required. The different boundaries in the problem are shown in figure 28.

	Boundary
B1	Symmetrical
B2	Riemann
B3	Wall
B4	Wall
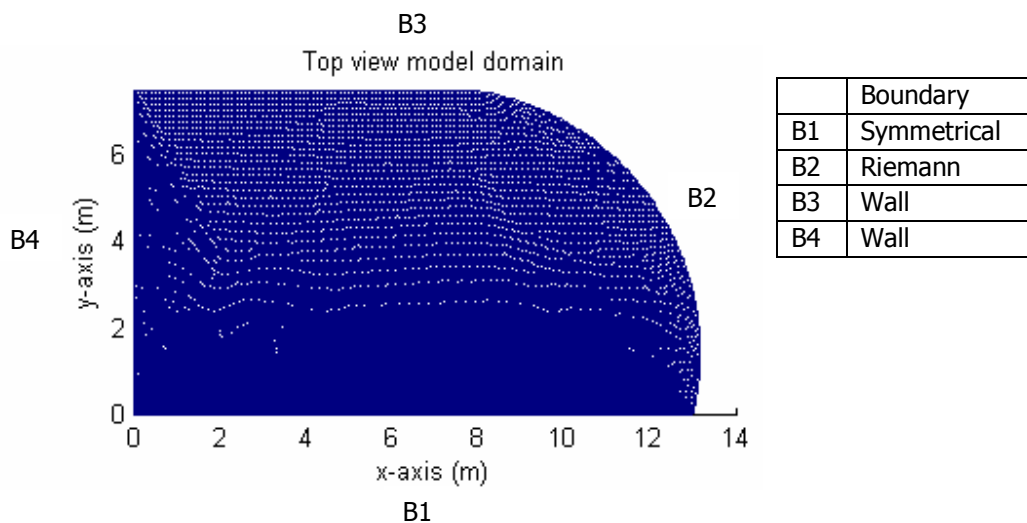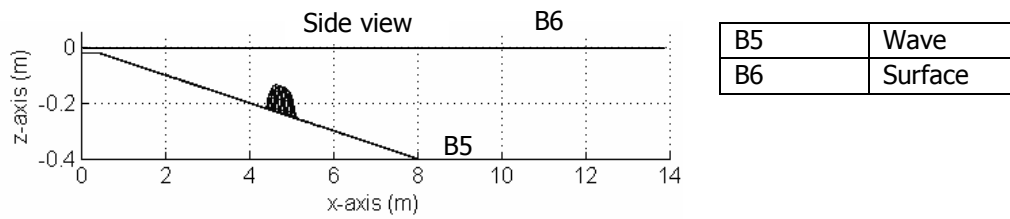
Figure 28: Boundary conditions

10.1.3. Landslide model shape

In the experiments a semi-elliptical shape was used for the landslide model, see chapter 7. To convert this shape into a three-dimensional shape, which can be described in a numerical model, the quartic two-dimensional shape from the Sue's experiments was extended to a three-dimensional semi-quartic shape.

The basic function for the three-dimensional semi-quartic shape is:

$$z = \sqrt{\left(1 - \left(\frac{x}{b}\right)^4 - \left(\frac{y}{w}\right)^2\right) \cdot T^2}$$

In figure 29 the three-dimensional landslide is shown.
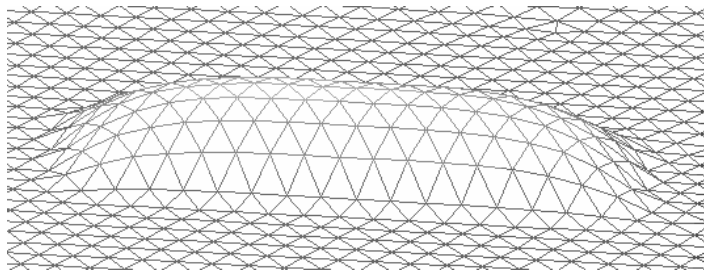
Figure 29: Semi-quartic landslide shape

10.1.4. Landslide velocity

For the numerical computation a landslide velocity was used that is the same as in the experiment. In this case a landslide velocity of 0.7 m/s was chosen for the comparison with the numerical model. Regarding the accuracy of the landslide velocity in the experiment, the landslide velocity of the experiment could deviate from the numerical landslide velocity with 5.4%.

10.2. Verification of the numerical results

10.2.1. Comparison

With the model set-up described in the previous section the numerical model has computed the landslide induced tsunami generation for a landslide velocity of 0.7 m/s and a submerged initial position. From this run water level time series are plotted for the various wave meter locations. As the same plots are available from the experimental data, the results can be compared.
In figure 34 and 35 the graphs with this comparison are shown.
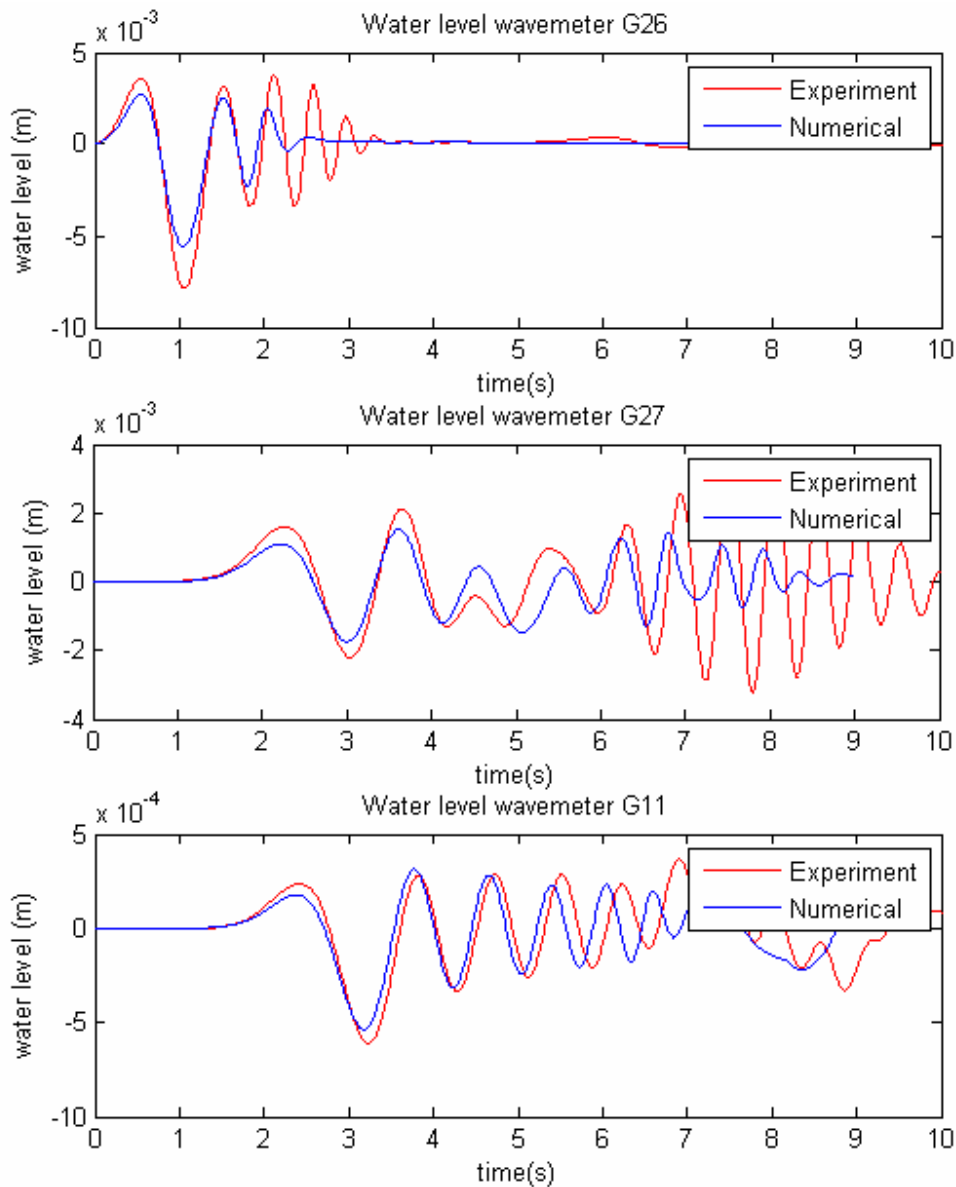
Figure 30: Water level time series for wave meter G26, G27 and G11 from the experimental data and the numerical run.
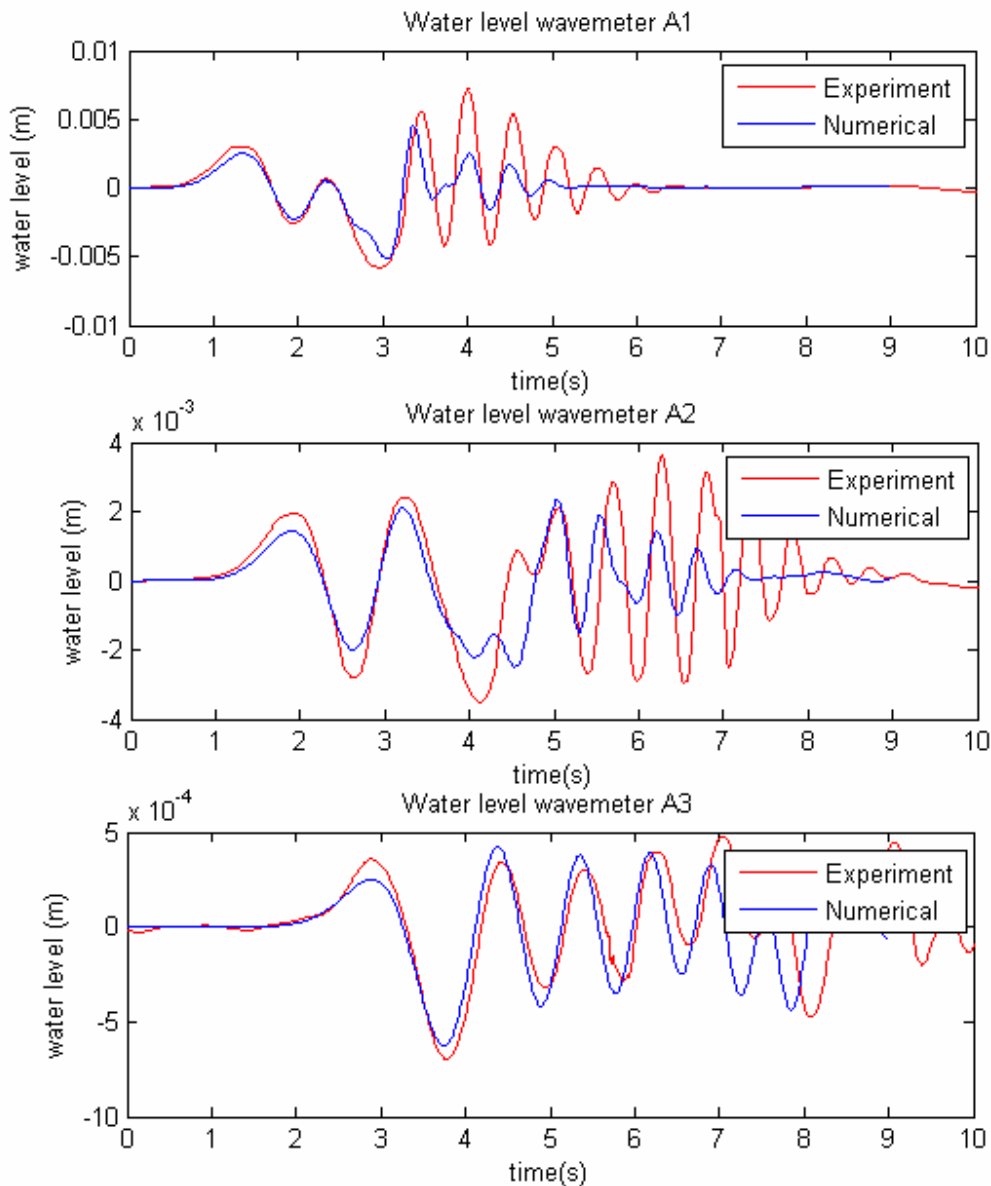
Figure 31: Water level time series for wave meter A1, A2 and A3 from the experimental data and the numerical run.

The results are reasonable. Though the first wave is for all cases lower in the numerical result, the difference between the models is not so large. Furthermore, the timing and the period of the first wave is in all cases good. The high frequency tail is computed less accurate by the numerical model.

In figure 32 the wavelet spectra of wave meters G26, G27 and G11 are shown for the numerical results and the experimental results. In general it can be seen that the correspondence between the higher frequencies of the numerical model and the experimental model is not good. This was already noticed in the time series. In the experimental model, the high frequency waves do not damp as fast as in the numerical model.

Wavelet spectrum of wave signal G26

Wavelet spectrum of wave signal G27
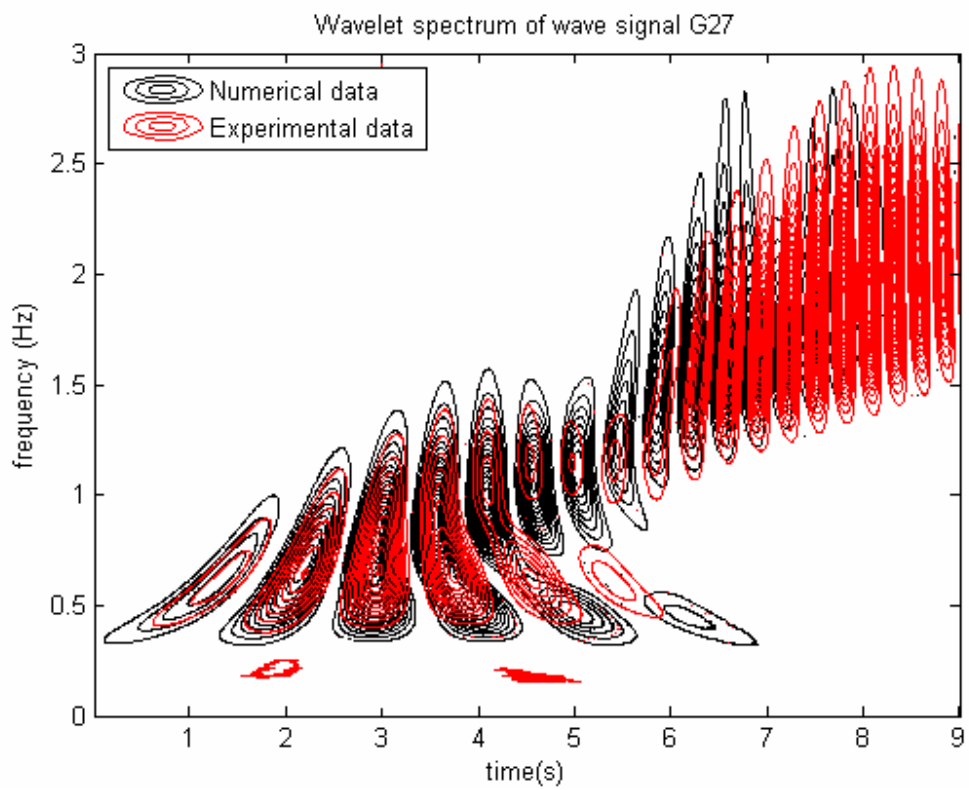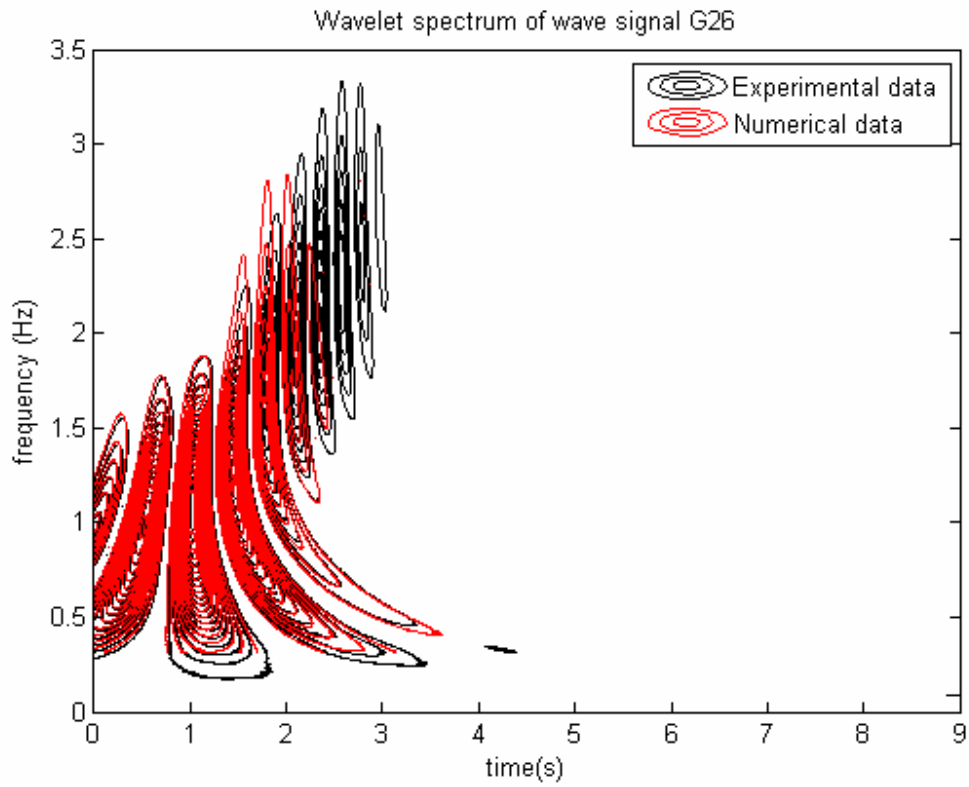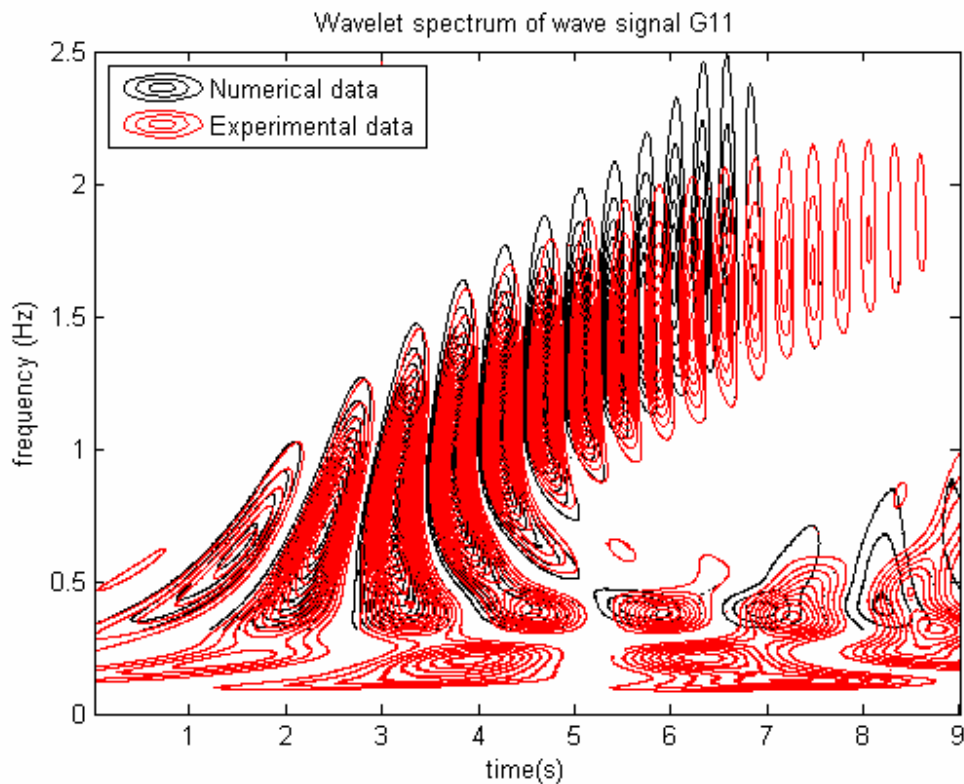
Figure 32a,b,c: Wavelet spectrum for wave meter G26, G26 and G11 for the numerical data and the experimental data

In figure 32b the stop of the landslide can be observed after 4.3 seconds in the experimental result. As the stop of the landslide was not included in the numerical model, a difference can be seen in the graph after 4.3 seconds between the experimental and the numerical spectrum. The experimental result in figure 32c shows that lower frequencies of approximately 0.2 Hz are present in the wave basin, whereas they were not computed with the numerical model.

10.2.2.   Discussion of the numerical model settings

In the previous section the experimental model results were compared with the numerical model results. Some differences were found between the model results. In this sub-section explanations for these differences are sought and in some cases improvements are proposed.

The shape of the numerical landslide in y-direction could be improved. In the runs, this shape was parabolic. However, the landslide model in the experiment had an elliptical shape and this difference could cause a difference in wave amplitude, as the surface of the elliptical shape is larger. Also the landslide height of the landslide model in the experiment should be higher than 0.1 m as the extra height of the wheels was not taken into account. However, this increase in height is smaller than 1 cm. As it was concluded that the landslide height has a large influence on the wave height and it is known from literature that the surface area in cross direction has also influence on the wave height, changes in the landslide shape could improve the result.

Moreover, a lower wave amplitude is computed for wave meters G26, G27, A1 and A2, than it was measured in the physical scale model. In chapter 10 it was concluded that the landslide width and height have a large influence on the wave amplitude. However, the spatial resolution of the mesh was low in y-direction in the current numerical model settings. In figure 33 half of the landslide width is covered by five points. It is expected that a higher resolution could improve the results, as with more mesh points the landslide shape can be presented better in the model.
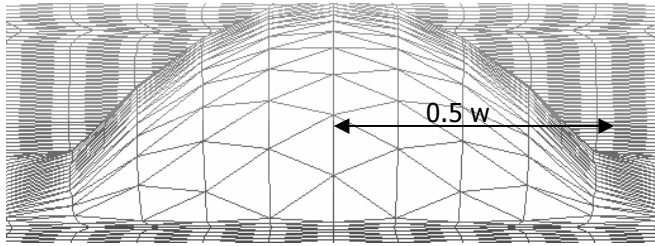
Figure 33: number of mesh points in landslide width

Furthermore, when regarding the height of the first wave, also the measurement accuracy of the first wave of the experimental results is important. For the wave meters G26, G27 and G11, the absolute error of the measurement is 0.1 mm and for wave meters A1, A2 and A3 it is 0.3 mm. In figure 34 the error range of wave meter A1 is indicated for the first wave and in figure 35 the error range of wave meter G11 is indicated.
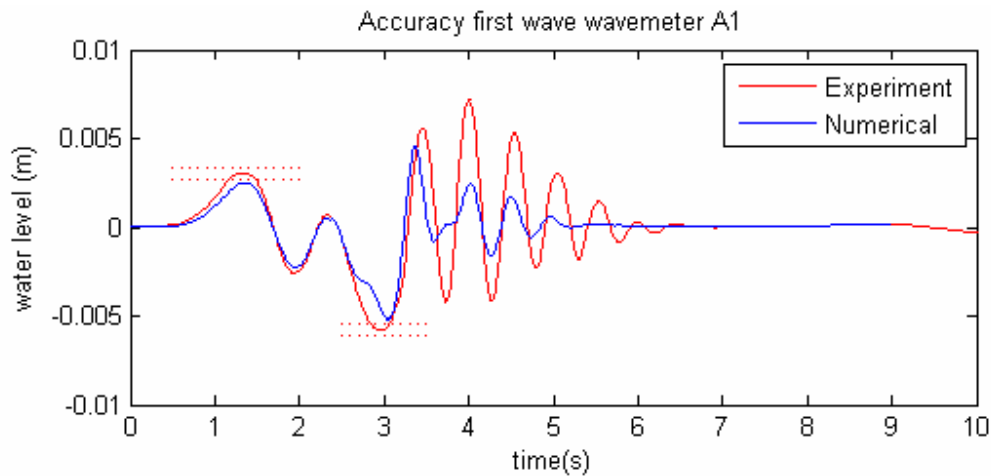
Figure 34: Error range of wave meter A1 indicated for the first wave with a dotted line.
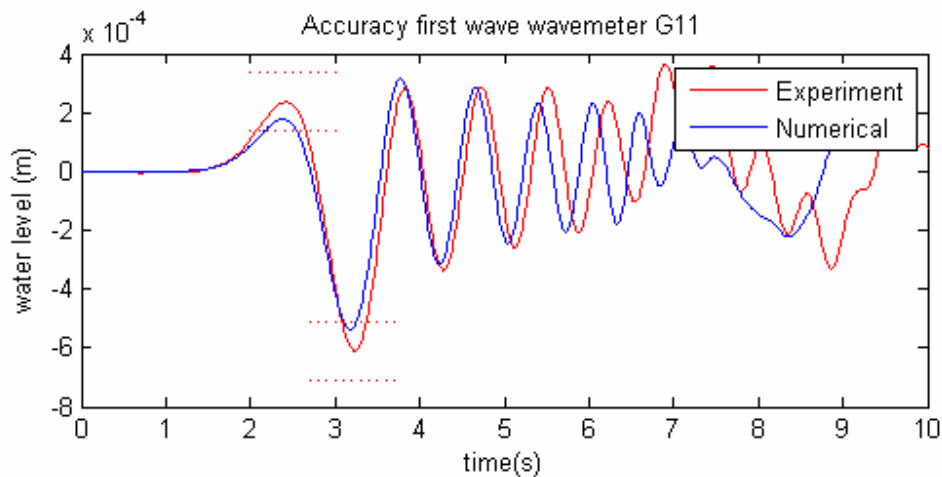
Figure 35: Error range of wave meter G11 indicated for the first wave with a dotted line.

It can be seen that the numerically computes first wave amplitude lies in the error range of the measurement for some wave meters.

Not only measurement errors have been made in the measurement of the surface elevation. Also the accuracy of the wave meter locations could play a role in the resemblance. The absolute measurement error made when measuring the coordinates of the wave meter location is 5 cm. When taking this error into account, several locations in the numerical model could give a better result. For wave meter G26 this locations that lie in the range of 5 cm from the measured location have also been plotted.
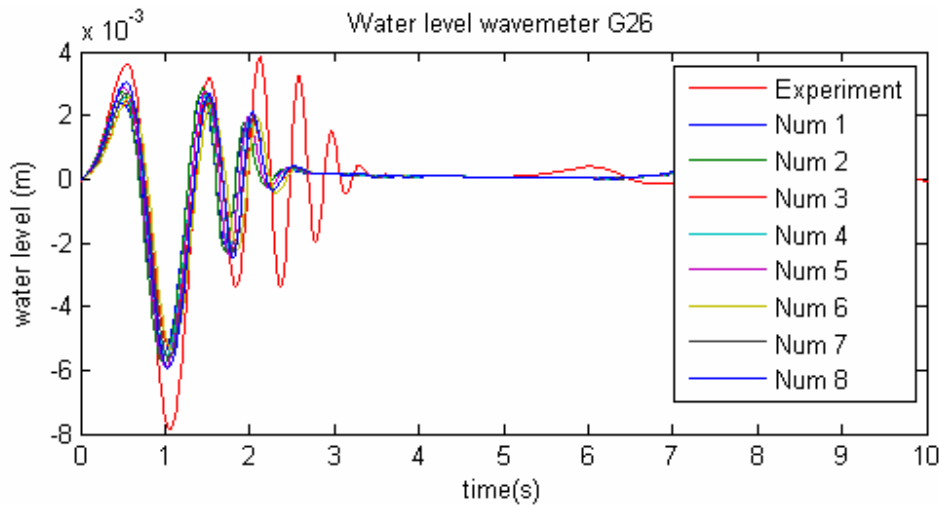
Figure 36: Water level wave meter G26 for an error range of 5 cm.

From 36 it can be seen that the exact location could make a difference in wave amplitude, which is in this case 0.7 mm.

Moreover, the accuracy of the landslide velocity measurement could play a role. The landslide velocity could differ with 0.04 m/s. As has been seen in chapter 8, the landslide velocity has a large influence on the amplitude of the first wave.

For the differences between the high frequency waves in the numerical model and the high frequency waves in the experimental model also several explanations can be found.

The number of mesh points in one wave length is important for the quality of the numerical computation of a wave in Finlab. When the number of mesh points is less than 20 in one wave length, the wave is not computed correctly. For a number of mesh points between 20 and 40 the quality is reasonable and when the number of mesh points in one wave length is larger than 40, the quality of the computed wave is good.
For the computation in the numerical model run, waves have been observed in the range of 0.1 to 5 meter. The grid size of the model is ranging from 0.04 meter along the axis of landslide motion and 0.08 meter off this axis.
It can be calculated that the wave length should be higher than 1.8 meter for a grid size of 0.04 m and higher than 3.6 meter for a grid size of 0.08. The first wave has a wave length of 2 meter or higher along the axis of landslide motion. Therefore, for the grid of 0.04 m relatively good results will be computed for the first wave. However, the high frequency waves have a wave lengths ranging from 0.1 and 2 meter. This means that the computation quality of these waves could be poor. The low spatial resolution in the higher frequency waves could therefore explain why the numerical waves damp much faster than the experimental waves.

Finally, the abrupt stop of the landslide after 4.3 seconds in the experimental model could explain some differences in wave period and amplitude at this time. In the numerical model no stop was included. For example in the surface elevation at wave meter G27 in figure 30 a clear difference in signal can be noticed after 4.3 seconds.

10.3.   Analysis

In this section some results of the numerical computations will be discussed. Though the numerical results are not exactly the same as the experimental results, they are good enough to give an impression of the spatial distribution of the waves. This could not be examined with the experimental results, because they were bounded to certain locations.
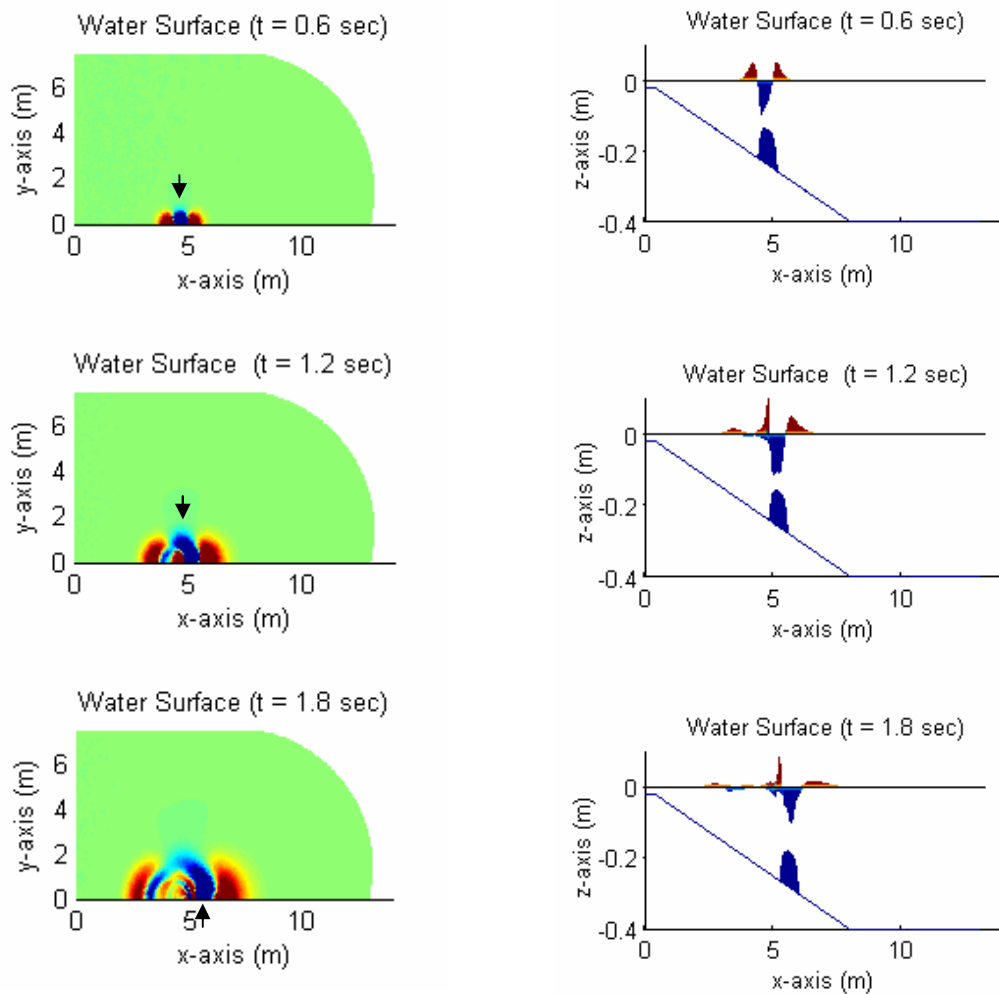
Figure 37: Top view and side view of the tsunami generation for t = 0.6, 1.2 and 1.8 seconds

In figures 37, 38 and 39, the top and side views for certain points of times are shown. In the top view the locations of the landslide is indicated with a small arrow.
In figure 37 the influence of landslide can be clearly seen. The first trough is bound to the landslide and therefore the first peak elongates. At the trailing edge high frequency waves can be noticed, which propagate towards shore.
The highest waves can be found near the landslide. At some distance from the landslide the waves have become much lower. Some radial spreading of the waves can be noticed, but most wave energy propagates along the axis of landslide motion.
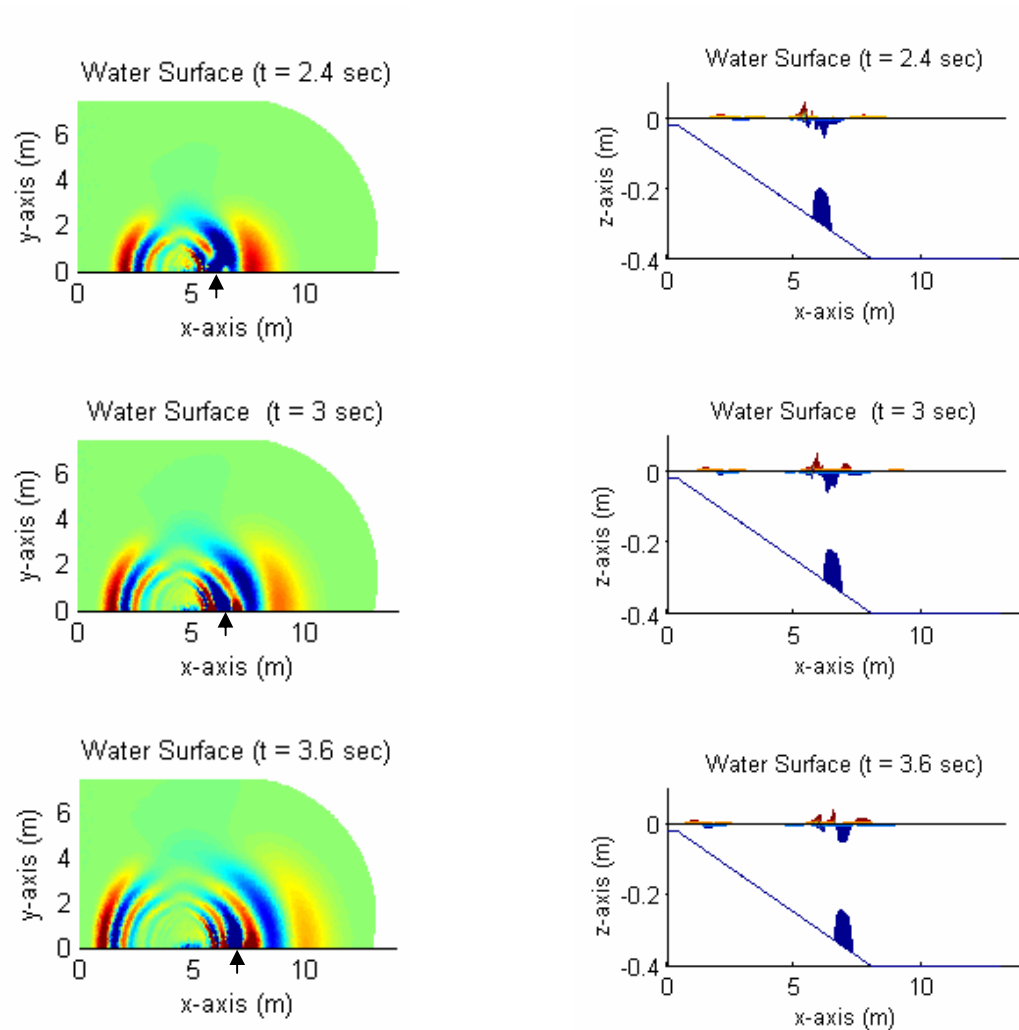
Figure 38: Top view and side view of the tsunami generation for t = 2.4, 3 and 3.6 seconds

In figure 38, in the time interval between 2.4 and 3.6 seconds, the influence of the landslide on the water surface becomes smaller. Waves which were bound to the trailing end of the landslide start to propagate over the landslide.

The first wave becomes smaller, as no energy is transferred from the landslide to the wave anymore. On the other hand, the waves that propagate towards the shore become higher as they run up the slope.
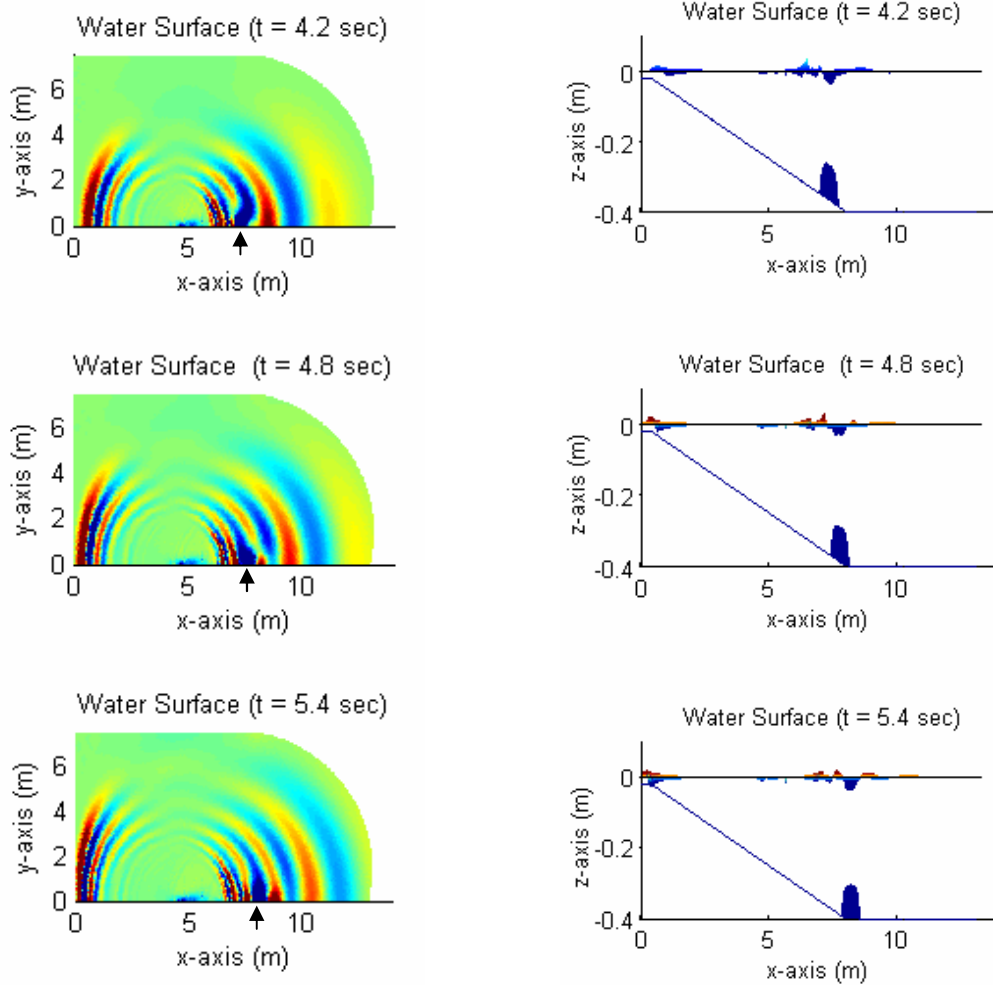
Figure 39: Top view and side view of the tsunami generation for t = 4.2, 4.8 and 5.4 seconds

In figure 39 still a small influence from the landslide mainly around the landslide can be noticed. After 5.4 seconds the landslide has reached the end of the slope and stops moving. At this moment the first peak has already propagated out of the model domain.
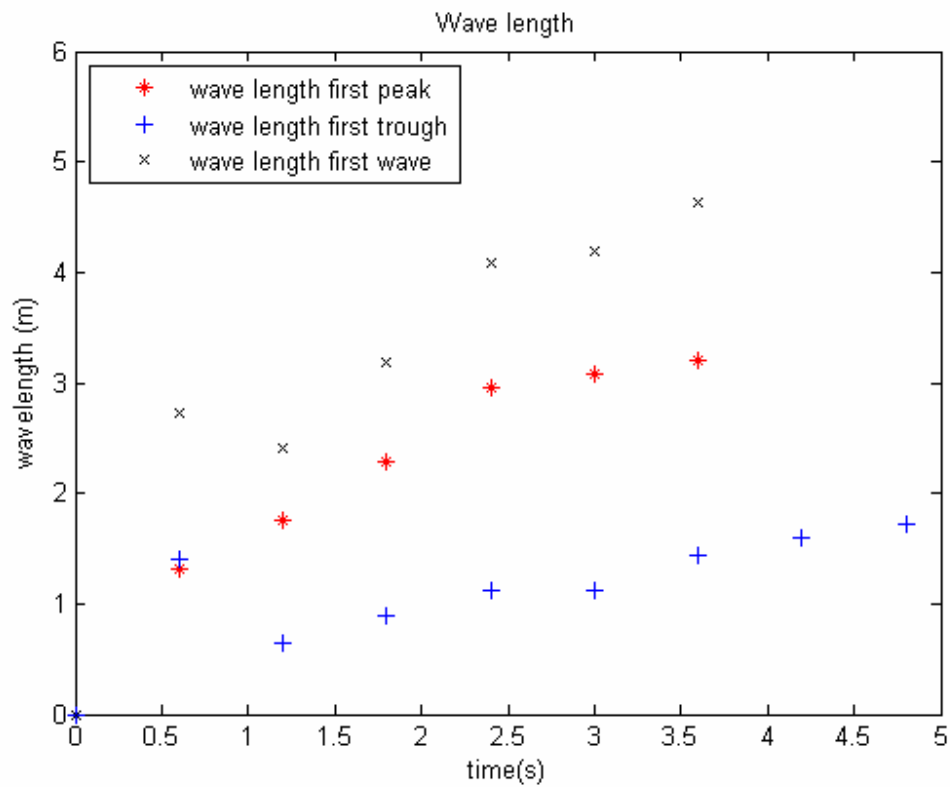
Figure 40: Wave length versus time for the first wave

According to figure 40, the wave length of the first wave increases when it propagates into deeper water. The first wave length ranges from 2 to 4.5 meter. From this wave length, the first peak length is 1 to 3 meter and the first trough length is 0.5 to 2 meter. The first trough is approximately 0.7 meter until after roughly three seconds the landslides influence becomes smaller and the first trough propagates over the landslide.
The waves which are generated at the trailing edge of the landslide have a half - wave length between 0.1 and 1 meter.

10.4.   Conclusions

The three-dimensional model was verified with the experimental model results of this study. It can be concluded that the leading waves are predicted reasonably good by the numerical model. However the high frequency waves generated at the trailing end of the landslide are predicted badly. Various improvements to the numerical model can help to make the resemblance between the results better. Preliminary tests to improve the landslide shape have shown that a significantly improvement in resemblance can be achieved. Therefore it can be concluded that with further improvements, Finlab can be used to model three-dimensional cases of landslide induced tsunamis when the initial position of the landslide is submerged.

11.   Numerical model for the La Palma case

11.1.   La Palma model

11.1.1.   Introduction

The objective of this study is to understand and quantify the generation of a landslide induced tsunami in the case of a flank collapse of the Cumbre Vieja volcano in La Palma. In the previous chapters, the tsunami generation process has been investigated experimentally as well as numerically. In addition, an indication of the wave amplitudes at some distances of the La Palma coast was given in chapter 8, based on the experiment results. However, a more accurate quantification of a landslide induced tsunami in case of a flank collapse of the Cumbre Vieja has not been presented yet.

To provide insight into the wave heights which could be expected near the coast of La Palma, the three-dimensional model from the previous chapter will be extended with the bathymetry of the La Palma island. Bathymetry of the west side of La Palma has been made available for this project by the Southampton oceanographic centre.
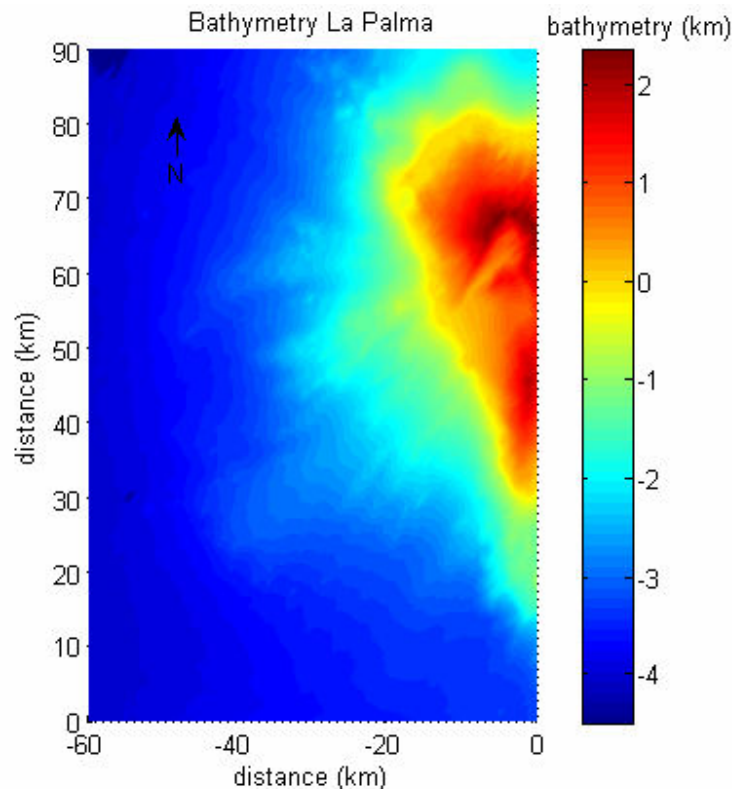
Figure 41: Bathymetry of the La Palmas west coast

Bathymetry 60 kilometres westward of the island and 90 kilometres over the length of the island is available, see figure 42.
It must be noted that the La Palma model will be still a simplified model, as not enough time is available to take into account all the different aspects of the landslide behaviour. The landslide dimensions of chapter 6 will be used for the computation. Furthermore, the maximum landslide velocity, mentioned in chapter 6, will be used for the landslide motion.

In table 7 a summary can be found with details on the La Palma case:

Table 7: Details on the La Palma case

Landslide length b	2500 m
Landslide width w	6000 m
Landslide thickness T	900 m
Landslide velocity u	30 m/s

11.1.2.   Model set-up

Model domain

The bathymetry of the west side of La Palma is used as a basis for the model domain. On the eastern side of the model domain, the coastline of La Palma was used as a boundary, see figure 43. The western side of the model domain is bounded by a circle line. This shape was chosen to use as much as possible of the available bathymetry, but on the other hand save computation time.

The northern and southern boundaries of the model domain are the same as the northern and southern boundaries in the bathymetry data.
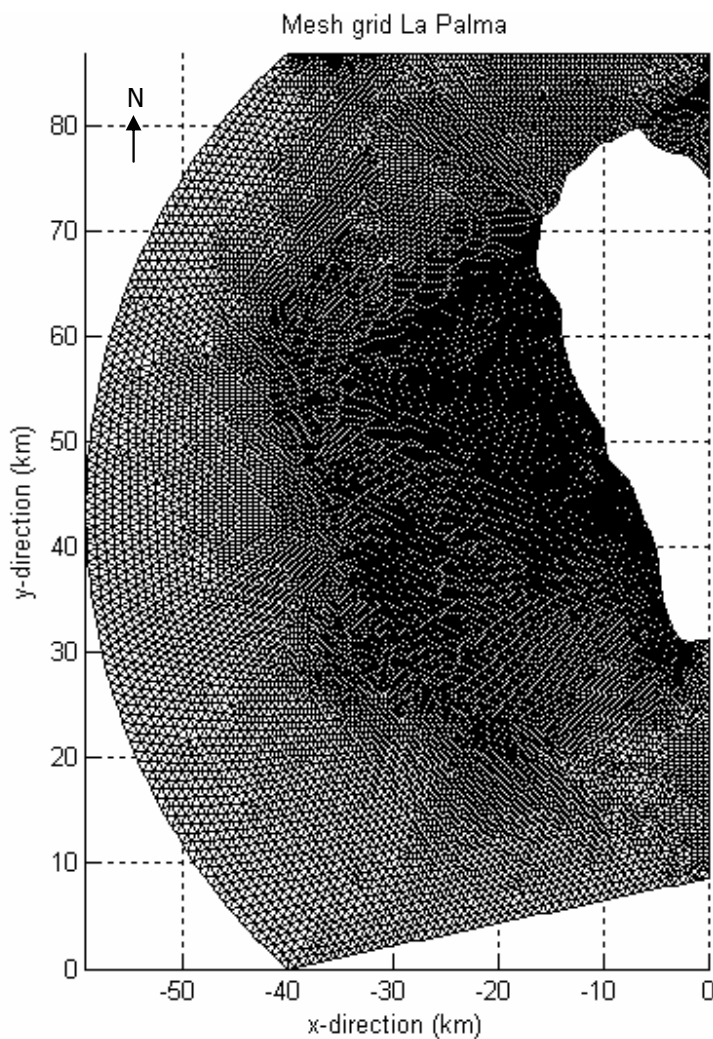
Figure 42: Model domain La Palma

Choice of spatial and temporal calculation steps
The spatial and temporal calculation steps for the La Palma case are based on the scaled spatial and temporal calculation steps of the 3D-numerical model of chapter 10. The mesh size in x-, y- and z-direction varies between 200 m and 500 m, depending on the proximity to the trajectory of the landslide. The grid can be seen in figure 43.

To check the Courant condition, either the landslide velocity or the wave celerity should be taken into account. The landslide velocity in this case is 30 m/s, whereas the wave celerity for a depth of 4000 m is 198 m/s. Therefore the wave celerity will be used. For all the spatial and temporal calculation steps a Courant condition lower than one is attained for a temporal step size of one second.

Simulation period
A simulation period of 1000 seconds is chosen. In this time the landslide slides over a distance of 30 kilometres. This simulations period was based on the scaled simulation period of the 3D-numerical model of chapter 10.

Boundary conditions
The boundary conditions for the La Palma case are similar to the boundary conditions of the 3D-numerical model. For the coastline of La Palma a wall boundary was chosen. The remaining boundaries on the northern, western and southern side of La Palma have a Riemann boundary. Finally, the bottom has a wave boundary and the water surface has a surface boundary.

11.1.3.   Landslide model shape
The simplified semi-quartic shape of the previous chapter was also used for the La Palma case. The description of this shape should be improved in future models.

11.1.4.   Initial position and landslide velocity
Unfortunately, Finlab is not able yet to handle situations where the bottom is higher than the water surface. Therefore the landslide cannot initiate at the expected initial position at a height of approximately 700 m above sea level.

For the computation of the La Palma case, a drastic simplification in the bathymetry has to be carried out. The sea bottom which is higher than -950 meters will be kept at -950 meter till the coastline of La Palma is reached. This simplification makes it possible to introduce a landslide with a height of 900 meters without the possibility that the bottom (with the landslide) is higher than the water surface.

Because of this simplification, it is expected that the waves computed by the model will be lower than when computed by a model without this simplification. Therefore the result of this case should be considered as an indication rather than a prediction of the real waves.

As mentioned before, the maximum landslide velocity of 30 m/s will be used for the La Palma case model. In future models a more realistic landslide motion should be considered.

11.2. Conclusions and Recommendations

11.2.1. Conclusions

Unfortunately, no results were obtained from the La Palma model yet. Therefore, it must be concluded that the only quantification of a tsunami wave, in case of a landslide in La Palma, can be given on the basis of the experimental results of this study, discussed in chapter 7.

11.2.2. Recommendations

La Palma model

It is recommended to improve the La Palma model to obtain a quantification of the tsunami wave. With the results of the La Palma model, several questions can be answered:

- What is the danger of a flank collapse in La Palma?
- What is the effect of the bathymetry on the wave propagation?
- Is the tsunami wave height similar to the scaled results of the experiment in this study? In other words, how good is the prediction of the tsunami wave at this moment?

Model improvements

Further model improvements are recommended in order to make a better prediction of a tsunami wave:

- It is recommended to pay more attention to the interface between Earth Sciences and Environmental Fluid mechanics. The description of the landslide shape and behaviour could be implemented more realistically into the numerical model.
- It is recommended to extend the numerical model in a way that it can handle sub-aerial landslides.

PART V: Conclusions and Recommendations

12. Conclusions and Recommendations

The objective of this study was to understand and quantify the generation of a landslide induced tsunami in the case of a flank collapse of the Cumbre Vieja volcano in La Palma with help of the finite element model Finlab. This objective is evaluated in this chapter.

Conclusions on the understanding of the tsunami generation process can be found in section 12.1. Conclusions on the quantification of the tsunami generation in case of a flank collapse in La Palma are commented in section 12.2. Finally, recommendations for landslide tsunami modeling are discussed in section 12.3. Conclusions and recommendations on individual parts of this study, which are not directly related to the objective, can be found at the end of the related chapters.

12.1. Conclusions

12.1.1. Understanding landslide induced tsunamis

The tsunami generation has been investigated with experimental and the numerical models. Due to these models the complex interaction between the landslide and the water are understood better. All models were set up with a simplified bottom profile. The shape of the landslide was semi-elliptical for the experiment and semi-quartic for the numerical model. In all models a constant landslide velocity was used. These simplifications made the generation process more transparent and thus better understandable.

For the experiment a scale of 1:8500 was used. With this scaling, scale effects were introduced that were found to be acceptable. The accuracy of the experiment was good enough for landslide velocities of 0.7 m/s and higher.

From the experimental model, more understanding was obtained in the influence of the landslide velocity and the initial position of the landslide on the wave generation. Furthermore, it could be seen that the distance to the wave generation area played an important role and some conclusions could be made on the wave celerity.

The two-dimensional numerical model was compared to the experimental result of Sue (2007) and the numerical results showed a good resemblance with Sue's results.

The three-dimensional model was verified with the experimental model results of this study. It can be concluded that the first wave is predicted reasonably well by the numerical model. The high frequency waves, which are generated at the trailing edge of the landslide, have a poor resemblance regarding the height, but they have a good resemblance regarding the period and the timing. However, the resemblance between the numerical results and the experimental results can be significantly improved by making the landslide shape in the numerical model more similar to the experimental model shape. A preliminary run has shown that optimizing the shape reduces the differences. Furthermore, taking into account the abrupt stop of the landslide in the numerical model can improve the similarity of the trailing edge waves. Finally, a finer grid could further improve the result.

From this, it can be concluded that the numerical model Finlab is suitable for the modeling of landslide induced tsunamis for two-dimensional as well a three dimensional cases when the landslide has a submerged initial position.

The two-dimensional numerical model was used to show the influence of the landslide height, the landslide length and the slope. These parameters were varied in the numerical model because they could not be varied in the experiment.

The three-dimensional numerical model was used to examine the directional spreading of the tsunami waves and to gain more information about the wave length of the tsunami wave.

An overview of the relations, found with the experimental and the numerical models, is given in table 1.

Table 1: Overview of relations between parameters

Increase ↑ of:	First crest	First trough	Wave length	Wave period	Timing
Landslide velocity	increase ↑	increase ↑	not examined	decrease ↓	crest and trough come earlier
Landslide length	no/small effect	no/small effect	increase ↑	increase ↑	trough comes later
Landslide height	increase ↑	increase ↑	no clear relation	no clear relation	no/small effect
Slope	decrease ↓	decrease ↓	not examined	decrease ↓	crest and trough come earlier
Submergence of initial position	decrease ↓	decrease ↓	not examined	not examined	not examined
Distance from generation area	decrease ↓	decrease ↓	increase ↑	no clear relation	not examined
Angle to the axis of motion	decrease ↓	decrease ↓	decrease ↓	not examined	not examined

Furthermore, the models have given insight into the landslide generation process. It was seen that the landslide velocity is not only an important parameter for the wave amplitude, but it also determines the wave pattern. The first trough is bound to the landslide motion till a certain depth, but the wave crest can propagate freely till the wave celerity is the same as the landslide velocity. Thus, when the landslide velocity is the same as, or higher than the wave celerity, the wave pattern changes. When this is the case, the first wave does not propagate according to linear wave theory, but more like a solitary wave.
The spreading of the waves is not entirely circular. More energy propagates in the direction of landslide motion and in the opposite direction of landslide motion. Therefore, the wave heights that were found on both sides of the axis of motion were much smaller than the wave heights that were found on the axis of motion.

12.1.2. La Palma case quantified

The slope-instability has been investigated at the Engineering Geology department of Delft University of Technology (van Berlo 2006) and it was concluded that it is very unlikely that the flank will collapse in the current configuration. Furthermore in the case the flank collapses, it is more probable that a landslide volume of circa 7 km^3 moves into the sea, instead of 500 km^3 which was assumed by Ward and Day (2001).
Based on the conclusions of van Berlo (2006) the landslide dimensions were determined, see table 2. An upper value for the landslide velocity was chosen on the basis of calculations by Nieuwenhuis (2005). It should be noted that these values are rough estimates of the real

situation. As a better analysis of the geological parameters is not available, these values are used as input for the numerical and experimental models.

Table 2: Landslide dimensions for a semi-elliptical landslide shape

Parameter		Landslide model	
width	w	2500	m
length	b	6000	m
thickness	T	900	m
volume (block)	V_s	$7 \cdot 10^9$	m³
Maximum landslide velocity	u	30	m/s

With the experimental model an indication of the wave height is given. The experimental model is based on the scaled landslide dimensions and La Palma bathymetry. However, the experiment has a highly schematized bottom profile and velocity profile.

A landslide velocity of 30 m/s corresponds with the scaling analysis for a laboratory scale with a landslide velocity of 0.3 m/s. With the results of the sub-aerial tests that have been done for a landslide velocity of 0.3 m/s, the wave height at certain distances from the coast of La Palma can be calculated. These locations correspond with the wave meter location multiplied with a scale of 1:8500. At a distance of roughly 40 km from the coast, a tsunami wave height of roughly 5 meters is found for a landslide velocity of 30 m/s, see figure 28.

First wave in the La Palma case
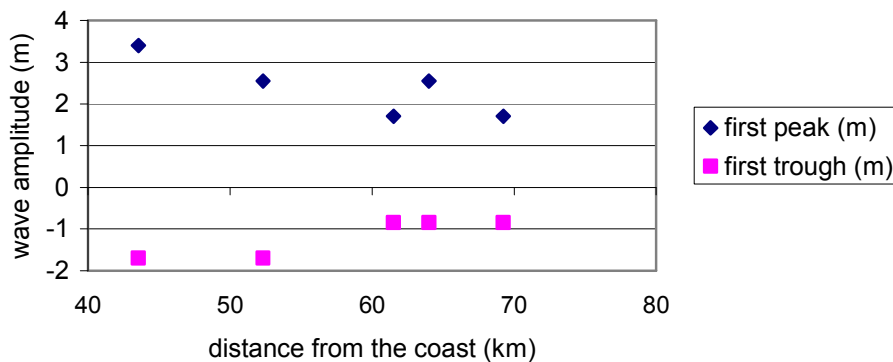
Figure 1: Leading wave when scaling experimental results to La Palma dimensions

The numerical model of the La Palma case was extended with La Palma bathymetry and reflects therefore a more realistic situation. However, it must be noted that this model is still simplified as the landslide behaviour was simplified. Unfortunately, no results were obtained from the La Palma model yet.

The experimental model and the three-dimensional numerical model of chapter 10 have given an indication of the generation of a landslide induced tsunami in the La Palma case. According to these models a 5 meter high wave can be expected at a distance of 40 kilometres from the coast, with a maximum wave length of 30 kilometres.

Several improvements should be made to the models to make more accurate predictions of the dangers of a landslide. Nevertheless, it can be stated that according to the results of the experimental model, no danger is expected for the east coast of the USA. More serious consequences of a landslide induced tsunami of the magnitude will be felt in La Palma and the surrounding Canaries.

12.2. Recommendations

12.2.1. Landslide

For future landslide induced tsunami models it is recommended to improve the knowledge of the landslide behaviour. In Earth Sciences various flank failure models for landslides are available. However, in current modelling of landslide tsunamis, the landslides are still highly schematized. Yet, the nature of the mass failure has a large influence on the tsunami potential. As has been seen in chapter 2, various types of mass failure could occur and these various types of mass failure vary in cohesiveness. Thus, some landslides have no potential to generate a tsunami of large magnitude, even if they are very voluminous.

Furthermore, it has been seen in the experiments that the landslide velocity is very important for the height of the tsunami wave. Therefore, it is important to determine the landslide motion more accurately than has been done yet. To determine the landslide motion, more has to be known about the type of mass failure, the landslide material and its properties, the landslide shape, the slope and the initial position.

Finally, the landslide dimensions have a large influence on the generation of waves. Therefore a more accurate determination of the landslide dimensions would be sensible in future.

For a better tsunami prediction the interface between Earth Sciences and Environmental Fluid Mechanics deserves more attention.

12.2.2. Tsunami generation

The numerical computation of a landslide generated tsunami is done well by the numerical model Finlab when the initial position of the landslide is submerged. However, the numerical model cannot cope yet with a sub-aerial landslide, as in this case the bottom level is higher than the water surface level. As has been seen for the La Palma case model, a simplification to the model can be made to be able to handle sub-aerial landslides. However, with such a model only an indication of the waves can be given, as the model does not represents the actual impact well enough. Therefore is should be recommended to extend the numerical model in a way that it can handle sub-aerial landslides.

12.2.3. Tsunami propagation and run-up

In this study only the generation area of the landslide induced tsunami was taken into account. However, to evaluate the danger of landslide induced tsunamis, the generation model should be extended with a propagation model to compute the propagation of the tsunami and a near-shore model to compute the run-up of the tsunami at a selection of coasts. In the La Palma case it would be for example interesting to see what the impact of the tsunami is on the surrounding Canaries. An important aspect is how to use the information of a generation model in a propagation model, because if the connection between these models cannot be made well, the usefulness of an accurate prediction of the generation model disappears.

12.2.4. Understanding of landslide generation

For the understanding of the landslide generation it would be interesting to examine the energy transfer from the landslide to the water. This could be done with experiments where stereo imaging is used or with the existing numerical model. With more knowledge of the energy transfer a more direct link can be made between the landslide parameters and the wave heights.

References

Books
Chanson, H.: The Hydraulics of open channel flow: an introduction. Elsevier second edition 2004, 253-269

Erismann, T.H., Abele, G.: Dynamics of Rockslides and Rockfalls. Springer 2001

Hughes, S.A.: Physical models and laboratory techniques in coastal engineering. World Scientific 1993

Mader, C.L.: Numerical modelling of water waves. CRC Press LLC second edition 2004

Metcalf, M., Reid, J.: Fortran 90/95 Explained. Oxford University Press 1996

Journals
Beget, E.B., Kowalik, Z., 2006 Confirmation and calibration of computer modelling of tsunamis produced by Augustine Volcano, Alaska. *Science of Tsunami Hazards* Vol. 24, No. 4 257-266

Belotti et al., 2006 Tsunami waves generated by landslides along a straight sloping coast: new three-dimensional experiments. *ICCE 2006*

Berlo, J.M.C. van, 2006 Massive flank collapse at La Palma: Numerical slope stability models of the Cumber Vieja volcano. *Master thesis UT Delft, Section for Engineering Geology*, June 2006

Bondevik, S. et al., 2005 The Storegga Slide tsunami – comparing field observations with numerical simulations. *Marine and Petroleum Geology* **22** (2005) 195-208

Carracedo, J.C., Day, S.J., Guillou, H. and Gravestock, P., 1999 The later stages of the volcanic and structural evolution of La Palma, Canary Islands. *Geol. Soc. Am. Bull.* **111** 755-768.

Enet, F., Grilli, S.T., Watts, P., 2003 Laboratory experiments for tsunamis generated by underwater landslides: Comparison with numerical modelling. *The International Society of Offshore and Polar Engineers* (2003) 372-379

Fine, I.V., 2005 The Grand Banks landslide-generated tsunami of November 18, 1929: preliminary analysis and numerical modelling. *Marine Geology* **215** (2005) 45-57

Fritz et al. 2003a Landslide generated impulse waves: Part 1. Instantaneous flow fields. *Exp. Fluids* **35**, 505-519

Gisler, G., Weaver, R., Gittings, M.L., 2006 SAGE calculations of the tsunami threat from La Palma. *Science of Tsunami Hazards*, Vol. 24, No. 4 288-301

Grilli, S.T., Watts, P., 2001 Modelling of tsunami generation by an underwater landslide in a 3D-NWT. *Proc. ISOPE 2001 Conf.* (Stavanger, Norway)

Grilli, S.T., Watts, P., 2005 Tsunami generation by submarine mass failure I: Modelling, experimental validation, and sensitivity analyses. *ASCE* November/December 2005, 283-297

Hammack, J.L., 1973 A note on tsunamis: their generation and propagation in an ocean of uniform depth. *J. Fluid Mech*. (1973), vol. 60, part4, 769-799

Harbitz, C.B. et al., 1993 Numerical simulations of large water waves due to landslides. *Journal of Hydraulic Engineering* Vol.119, No. 12, December 1993

Harbitz, C.B., Løvholt, F., Pedersen, G. & Masson, D.G., 2006 Mechanisms of tsunami generation by submarine landslides: a short review. *Norwegian Journal of Geology* Vol. 86, pp. 255-264

Huber, A., Hager, W.K., 1997 Forecasting impulse waves in reservoirs. *Rep. XIX*, pp. 993-1005, Comm. Int. des Grand Barrages, Rio de Janeiro

Kamphuis, J.W., Bowering, R.J., 1972 Impulse waves generated by landslides. Paper presented at 12th Coastal Engineering Conference, *Am. Soc. Of Civ. Eng.*, Reston, Va

Liu et al., 2005 Runup and rundown generated by three-dimensional sliding masses. *J. Fluid Mech. Vol.* **536**, 107-144

Lynett, P.J., Borrero, J.C., Liu, P.L.-F., Synolakis, C.E., 2003 Field survey and numerical simulations: A review of the 1998 Papua New Guinea tsunami. *Pure Applied Geophysics* **160** (2003) 2119-2146

Mader, C.L., 2001 Modelling the La Palma landslide tsunami. *Science of Tsunami Hazards* **19** 150-170

Mader, C.L., Gittings, M.L., 2006 Numerical model for the Krakatoa hydro-volcanic explosion and tsunami. *Science of Tsunami Hazards* Vol. 24, No. 3 174-182

Masson, D.G., Harbitz, C.B., Wynn, R.B., Pedersen, G. & Løvholt, F. 2006 Submarine landslides: processes, triggers and hazard prediction. *Phil. Trans. R. Society A* **364**, 2009-2039

Müller, D.R., 1995 Auflaufen und überschwappen von Impulswellen an Talsperren. *VAW-Mitteilung* 137, Vischer, D., ed., Versuchsanstalt für Wasserbau, Hydrologie und Glaziologie, ETH, Zürich

Nieuwenhuis, J.D., 2005 Introductory remarks on the instability of South-Western La Palma (Canary Islands). *UT Delft*

Okal, E.A., Synolakis, C.E., 2004 Source discriminants for near-field tsunamis. *Geophys. J. Int.* (2004) **158** 899-912

Panizzo A., et al., 2005 Forecasting impulse waves generated by subaerial landslides. *J. Geophys. Res.*, **110**

Perez-Torrado, F.J. et al. 2006 Tsunami deposits related to flank collapse in oceanic volcanoes: The Agaete Valley evidence, Gran Canaria, Canary Islands. *Marine Geology* **227** (2006) 135-149

Satake, K., 2002 Tsunamis. *International Handbook of Earthquake and Engineering Seismology* Volume 81A 437-451

Stefatos, A. et al., 2005 Tsunamigenic sources in an active European half-graben (Gulf of Corinth, Central Greece). *Marine Geology* **232** (2006) 35-47

Sue, P., Nokes, R.I.,, 2006 Experimental modelling of Tsunami generated by underwater landslides. *Science of Tsunami Hazards*, Vol. 24, No. 4 267-287

Sue, P., 2007 Modelling of tsunami generated by submarine landslides. *Doctor of Philosophy in Civil Engineering, University of Canterbury, Christchurch New Zealand*

Tinti, S. et al., 2004 The generating mechanisms of the August 17, 1999 Izmit bay (Turkey) tsunami: Regional (tectonic) and local instabilities causes. *Marine Geology* **225** (2006) 311-330

Tinti, S. et al., 2005 The 30 December 2002 landslide-induced tsunamis of Stromboli: sequence of the events reconstructed from eyewitness accounts. *Natural Hazards and Earth System Sciences* **5** (2005) 763-775

Walder J.S. et al., 2003 Tsunamis generated by subaerial flows. *J. Geophys. Res.* **108(B5)**, 2236

Ward, S.N., Day, S., 2001 Cumbre Vieja volcano – Potential collapse and tsunami at La Palma, Canary Islands. *Geophys. Ress. Lett.* **28** 3397-3400

Watts, P., 1997 Water waves generated by underwater landslides. *PHD thesis, California institute of Technology*, Pasadena, California

Watts, P., 1998 Wavemaker curves for tsunamis generated by underwater landslides. *Journal of Waterway, Port, Coastal and Ocean Engineering* May/June 1998 127-137

Watts, P., 2000 Tsunami features of solid block underwater landslides. *Journal of Waterway, Port, Coastal and Ocean Engineering* May/June 2000 144-152

Watts, P. et al., 2003 Landslide tsunami case studies using a Boussinesq model and a fully nonlinear tsunami generation model. *Natural Hazards and Earth System Sciences* (2003) **3** 391-402

Watts, P., Grilli, S.T., 2003 Underwater landslide shape, motion, deformation and tsunami generation. *The International Society of Offshore and Polar Engineers* (2003) 364-371

Watts, P., Grilli, S.T., 2005 Tsunami generation by submarine mass failure II: Predictive equations and case studies. *ASCE* November/December 2005, 298-310

Wiegel, R.L., 1955 Laboratory studies of gravity waves generated by the movement of a submarine body. *Trans. Am. Geophys. Union*, **36(5)** 759-774

Wynn, R.B., Masson, D.G., 2006 Canary Islands landslides and tsunami generation: Can we use turbidity deposits to interpret landslide processes? *Challenger Division, Southampton Oceanography Centre*

Zweifel, A., 2004 Impulswellen: Effekte der Rutschdichte und der Wassertiefe. *Versuchsanstalt für Wasserbau Hydrologie und Glaziologie ETH*, Zürich 2004

Web references
NOAA Tsunami portal   www.noaa.gov/tsunamis.html
NGDC Tsunami event database   www.ngdc.noaa.gov/seg/hazard/tsevsrch_idb.shtml
Google Earth
Landslides   www.knowledgenetwork.ca/slide

Data

Bathymetry information from:

- National Oceanography Centre, Southampton
- Universität Bremen, Fachbereich 5 - Geowissenschaften

Appendices

A.   Summary Master thesis Janneke van Berlo

The Master thesis project of Janneke van Berlo has assessed the contribution of various failure trigger mechanisms to enhancing instability of the Cumbre Vieja volcano, La Palma, answering the research question: Under what (boundary) conditions could the West flank of the Cumbre Vieja volcano start sliding and in what time frame would such mass movement occur?
The methodology concentrates on integrally modeling of three model attributes -geometry, material and processes- in a FEM computer model. In conclusion two mechanisms -dyke intrusion and future growth- bring the volcano dangerously close to a failure situation. However, it is important to note that this only occurs under the input of very conservative parameters and in a 2D model situation where friction of the sidewalls of the landslide mass is not taken into account. Additional mechanisms, like pore pressures occurring inside the post collapse sequence, may further enhance instability and should be investigated in further research.
Disregarding the uninvestigated mechanisms in the volcano, the results indicate that overall flank failure at least requires a combination of thoroughly weakened rock- and soilmass and steeper flanks than in the current configuration. This supplements the conclusion: To reach substantial growth over the full width of the landslide mass necessary to trigger failure, a time span in the order 10^4 years will be required.

B. Experiments

	Sue et al. (2006)	Enet et al. (2003)	Liu et al. (2005)	Walder et al.(1) (2003)	Walder et al. (2) (2003)	Belotti et al. (2007)	Panizzo (2005)
	2D	3D	3D	2D	2D	3D	3D
Water parameters							
depth at t = 0 (m)	0.435	1.8	2.44	**0.051; 0.09; 0.13**		**0.6; 0.82**	**0.4; 0.8**
Density (kg/m³)	1000	1000	1000	1000	1000	1000	1000
Wave parameters							
max. crest	7.5 - 35 mm	3 mm (for d=0.07m)	25 mm (for 475.5 kg, d=0.14)	48.6 mm	26.8 mm	15 mm	10 – 40 mm
max. trough	12.5 - 37.5 mm	5 mm (for d=0.07m)	60 mm (for 475.5 kg, d=0.14)	-	-	-	10 – 40 mm
max. run-up	1.75 - 6.75 mm	-	90 mm (for 437.6 kg, d=0), 160 mm for sub-aerial	-	-	25 mm	-
max. run-down	6 - 12.5 mm	-	90 mm (for 475.5 kg, d=0), 160 mm for sub-aerial	-	-	-	-
energy Ep-Ek	2 - 14%	-	-	-	-	-	-
energy Ep-Ep	1 - 6 %	-	-	-	-	-	-
Landslide parameters							
type	prismatic-semi-elliptical	trunc. hyp. secant	wedge (two different front faces)	block with snout	cylinder	semi-elliptical	block
width (m)	0.25	0.7	0.6525	0.15	0.05	0.4	**0.30 – 0.60**
length (m)	0.5	0.4	0.9144	**0.094 - 0.401**	**0.094 - 0.252**	0.8	0.41
thickness (m)	0.026	0.08	0.4572	**0.031; 0.051**	**0.031; 0.051**	0.05	**0.09 – 0.18**
volume (block) (m³)	2.42E-03	5.51E-03	1.36E-01	**varied**	**varied**	8.4E-3	**Varied**

	Sue et al.	Enet et al.	Liu et al. (2)	Walder et al.(1)	Walder et al. (2)	Belotti et al.	Panizzo (2005)
density (kg/m^3)	1630; 2230; 2830; 3420; 4020	2700	1400 - 3500			1830	-
	2D	3D	3D	2D	2D	3D	3D
velocity (m/s)	1.45 (for 2830 & d=0.05m)	1.849	-	1 - 3.5	1 - 3.5	0.4 – 1.4	2.8; 3.7; 4.4
acceleration (m/s^2)	1.4 (for 2830 & d=0.05m)	0.916	0.5 - 3.4	-	-	-	-
mass (kg)	3.9 - 9.7	14.86	190.96 - 475.52	-	varied	15.4	-
char. length scale (m)	10	3.558	-	-	-	-	-
char. time scale (s)	1.849	1.92	-	-	-	-	1
sub-aerial (m)	-	-	0 - 0.6	Sub-aerial	Sub-aerial	Sub-aerial	Sub-aerial
submergence (m)	0.05; 0.1; 0.15; 0.2; 0.25	0.07; 0.15; 0.22	0 - 0.55	-	-	-	-
Cd	-	0.7	-	-	-	-	-
Cm	-	1.79	-	-	-	-	-
Cn	-	-	0.1577 - 0.2746	-	-	-	-
Basin parameters							
width (m)	0.25	3.7	3.7	0.285	0.2	10.8	6
length (m)	14.7	30	104	1	6	5.4	12
depth (m)	0.505	1.8	4.6		1	0.82	0.8
slope (°)	15	15	25	11.2; 15; 19.5	30	18.43	16; 26; 36

C. Landslide induced tsunami formulas

Different empirical formulas to calculate wave heights and periods have been derived in the past from experimental data. Most of these formulas are only valid for one particular parameter range. Furthermore, the parameters that are taken into account differ significantly per formula. A main division can be made between formulas for landslides with submerged or sub-aerial initial positions. An explanatory parameter list can be found at the end of the appendix.

For submerged slides
- Watts
  The formulas of Watts are only valid for fully submerged landslides. The formula for a two-dimensional wave amplitude can be extended to a three-dimensional wave amplitude. Important parameters are the thickness of the landslide, the submergence, the slope, the landslide length and the water depth. The width of the landslide is of influence in the formula for three-dimensional cases. In this formula the landslide velocity profile has been neglected. Furthermore, the distance to the generation area is not taken into account. The wave height is calculated at the initial position of the landslide.

$$\eta_{2d} \cong 0.2139T(1 - 0.7458\sin\theta + 0.1704\sin^2\theta)\left(\frac{b\sin\theta}{d_i}\right)^{1.25}$$

$$\eta_{3d} \cong 0.2139T(1 - 0.7458\sin\theta + 0.1704\sin^2\theta)\left(\frac{b\sin\theta}{d_i}\right)^{1.25}\left(\frac{w}{w + \lambda_0}\right)$$

$$\lambda_0 \equiv t_0\sqrt{gd_i} \cong 3.87\sqrt{\frac{bd_i}{\sin\theta}}$$

For sub-aerial slides
- Panizzo et al. (2005)
  According to the formula of Panizzo, the landslide dimensions and the slope have a significant influence on the wave height. Of medium influence are the landslide velocity and the distance from the generation area. Of minor importance is the depth. In his formula, Panizzo did not take into account the submergence and the landslide length.

$$H_{max}/h = 0.07 \cdot (t_s^*/A_w^*)^{-0.45}(\sin\theta)^{-0.88}\exp(0.6\cos\alpha)(r/h)^{-0.44}$$

$$T_{max}\sqrt{g/h} = 2.50 \cdot t_s^{*-0.22}(\sin\theta)^{-0.25}(r/h)^{0.17}$$

$$H_1/h = 0.07 \cdot t_s^{*-0.3}A_w^{*0.88}(\sin\theta)^{-0.8}\exp(1.37\cos\alpha)(r/h)^{-0.81}$$

$$T_1\sqrt{g/h} = 6.96 \cdot A_w^{*0.16}\exp(0.23\cos\alpha)(r/h)^{0.18}$$

$$\eta_{1+}/h = 0.02 \cdot A_w^*(\sin\theta)^{-0.9}t_s^{*-0.27}\exp(1.6\cos\alpha)(r/h)^{-0.8}$$

$$\eta_{1-}/h = -0.11 \cdot A_w^*t_s^{*0.16}\exp(1.25\cos\alpha)(r/h)^{-0.8}$$

$$t_s^* = t_s \sqrt{\frac{g}{h}} = 0.43 \left(\frac{wT}{h^2}\right)^{-0.27} \left(\frac{u_i}{\sqrt{gh}}\right)^{-0.66} (\sin\theta)^{-1.32}$$
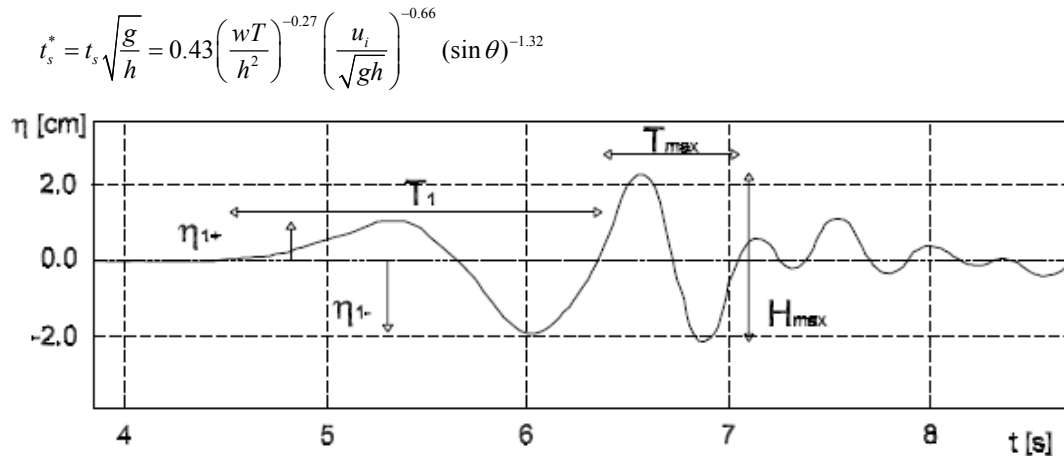

Figure 1: Waves [Panizzo et al. 2005]

- Kamphuis and Bowering (1972)

  The formula of Kamphuis and Bowering has been derived from experiments in a wave flume. According to this formula, the landslide length and thickness, the water depth and the impact velocity have influence on the wave amplitude. Also, wave amplitudes at a distance to the generation area can be calculated. Striking is that the slope has no influence on the wave amplitude. It should be noted that this formula has been derived from experiments that had the impact of a landslide in a reservoir or lake as a prototype. Therefore, it is expected that these formulas will over-estimate the impact of a landslide in an ocean.

$$H_{\max} / h = \left(\frac{u_i}{\sqrt{gh}}\right)^{0.7} \left(0.31 + 0.2\log\left(\frac{b}{h} \cdot \frac{T}{h}\right)\right)$$

$$H / h = \frac{H_c}{h} + C_3 \cdot \exp\left(-C_4 \left(x / h\right)\right)$$

$$T_1 \sqrt{\frac{g}{h}} = 11.0 + 0.255\left(\frac{x}{h}\right)$$

- Fritz et al. (2004)

  As the formula of Kamphuis and Bowering, the formula has been derived from experiments in a wave flume for landslide impacts in reservoirs. The formula resembles the formula of Kamphuis and Bowering except that the influence of the landslide length has been neglected.

$$\eta_{1-} / h = 0.25 \left(\frac{u_i}{\sqrt{gh}}\right)^{1.4} (T / h)^{0.8}$$

- Huber and Hager (1997)

  The formula of Huber and Hager resembles most the formula of Panizzo. However, the formula has been derived from a two-dimensional case.

$$H_{max} / h = 2 \cdot 0.88 \cdot \sin \theta \cdot \cos^2 \left(\frac{2\alpha}{3} \right) \left(\frac{\rho_s}{\rho_w} \right)^{0.25} M^{0.5} (r / h)^{-2/3}$$

$$M = \frac{m}{b_s h^2 \rho_s} = \frac{V_l}{b_s h^2}$$

- Walder et al. (2003)
  Walder derived formulas from an experiment in a wave flume which was based on a landslide impact into a reservoir. Again, the influence of a slope has not taken into account.

$$\eta_{1+} / h = A \cdot (t_s^* / V_w^*)^{-b} \text{ with } A = 1.32 \text{ and } b = 0.68$$

$$H_{max} / h = 0.0924 \cdot (t_s^* / A_w^*)^{-0.3136}$$

λ_0	=	Characteristic wave length (m)	η_{2d}	=	2-dimensional wave amplitude
t_0	=	Characteristic time of motion (s)	η_{3d}	=	3-dimensional wave amplitude
d	=	Submergence (m)	H_{max}	=	Maximum wave height (m), see fig. 1
T_{max}	=	Wave period of H_{max} (s), see fig. 1	H_1	=	First wave height (m)
T_1	=	Wave period of H_1 (s), see fig. 1	η_{1+}	=	First positive wave amplitude (m)
η_{1-}	=	First negative wave amplitude (m)	H	=	Wave height (m)
C_3, C_4	=	Constants			

D.   Model for center of mass motion

The landslide motion to a large extend determines what kind of wave is being generated. Not only the impact velocity, the velocity that the landslide has when it hits the water is important, but also the acceleration and deceleration of the landslide should be regarded. Therefore the landslide motion has been investigated with the first law of Newton. Coulomb friction and drag will be taken into account. The impact of the waves on the landslide will not be taken into account.

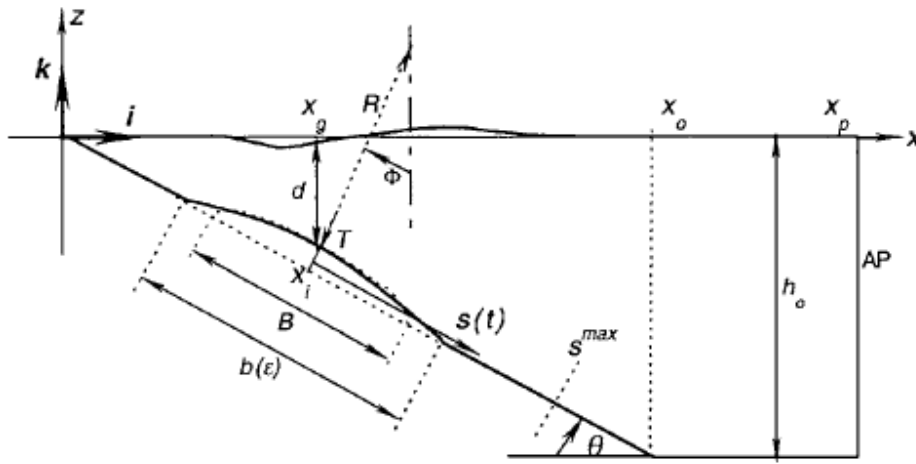### 1.1.1.   Newton's first law applied to a moving landslide

Figure 2: Landslide (source Grilli & Watts 2005)

According to Grilli & Watts (2005), the model for the center of mass motion parallel to a slope can be described with Newton's first law. The differential equation balances inertia, gravity, buoyancy, basal coulomb friction and hydrodynamic drag forces.

$$(\gamma + C_m)\ddot{S} = (\gamma - 1)(\sin\theta - C_n\cos\theta)g - C_d\frac{A_c}{2V_s}\dot{S}^2$$ Eq. 1

$C_m = \Delta M_l/(\rho_w V_l)$: hydrodynamic added mass coefficient

C_d : global hydrodynamic drag coefficient

C_n : coulomb friction

$A_c = Tw$: thickness times width, which is the main cross section perpendicular to the direction of motion

V_s : Landslide volume depending on the landslide shape

For the initial conditions and boundary conditions it is important whether the landslides initial position is sub-aerial, submerged or partially submerged. In the following sections the differential equations are solved for a submerged landslide movement and a sub-aerial landslide movement.

1.1.2.   Submerged landslide

A landslide that commences its movement underwater has a velocity profile in time where different phases can be distinguished. In the first phase, the landslide accelerates from zero velocity to a certain terminal velocity. This terminal velocity is reached when a balance between

the different forces of equation 2 is accomplished. In the second phase, the landslide moves at a constant terminal velocity until it reaches the end of the slope. In the last phase the landslide decelerates on the bottom.

The velocity profile of the first two phases can be solved with the following initial/boundary conditions: at $t=0$, $S=0$ and $\dot{S}=0$ and for $t\rightarrow\infty$, $\ddot{S}=0$.

With these initial/boundary conditions the following formulas can be derived, which describe the movement of the landslide (distance, velocity and acceleration) in time [Grilli & Watts (2005)].

$$S(t) = S_0 \ln\left(\cosh\frac{t}{t_0} \right) \qquad\qquad \text{Eq. 2}$$

$$S_0 = \frac{u_t^2}{a_0} \quad \text{and} \quad t_0 = \frac{u_t}{a_0} \qquad\qquad \text{Eq. 3 \& Eq. 4}$$

$$a_0 = g\sin\theta\left(\frac{\gamma-1}{\gamma+C_m}\right)\left(1-\frac{\tan\psi}{\tan\theta}\right) \qquad\qquad \text{Eq. 5}$$

$$u_t = \sqrt{gd}\sqrt{\frac{b\sin\theta}{d}\frac{\pi(\gamma-1)}{2C_d}\left(1-\frac{\tan\psi}{\tan\theta}\right)} \qquad\qquad \text{Eq. 6}$$

$$\dot{S} = u_t\tanh\left(\frac{t}{t_0}\right) \quad \text{and} \quad \ddot{S} = a_0\cosh^{-2}\left(\frac{t}{t_0}\right) \qquad\qquad \text{Eq. 7 \& Eq. 8}$$

Coulomb friction: $C_n = \tan\psi$

u_t is the terminal velocity, which is reached when an equilibrium between the forces is found. In the last phase, the driving force drops out and a deceleration starts. Equation 2 simplifies to:

$$(\gamma+C_m)\ddot{S} = -(\gamma-1)C_n g - C_d\frac{A_c}{2V_l}\dot{S}^2 \qquad\qquad \text{Eq. 9}$$

At $t=t_3$, $S=S_3$, $u=u_t$ and at $t=t_{end}$, $S=S_{end}$ and $u=0$ m/s.

Note, this solution is based on the assumption that u_t is reached before the end of the slope. When this is not the case, phase 2 is skipped and the end velocity of phase 1 has to be used as an initial condition for phase 3.

1.1.3. Sub-aerial landslide

When a landslide commences its movement above water, also different phases can be distinguished. In the first phase the landslide starts moving at a sub-aerial initial position and accelerates. The second phase starts when the landslide moves into the water with a velocity that is the same as the end velocity of phase 1. In phase 2, the landslide decelerates because of the extra resistance of the water. When the forces balance, a constant velocity is reached. Finally, in phase 3 the landslide reaches the end of the slope and decelerates faster until it stop moving.
The velocity of the first phase is described with a simpler equation than equation 2, as the first phase is sub-aerial. F is the factor of safety. This formulation has been taken over from

Nieuwenhuis (2005). The landslides driving force can be solely gravity, but could be also be a force, which is initiated from an erupting volcano.

$$\ddot{S}(t) = (1-F)g\sin\theta \ , \quad \dot{S}(t) = (1-F)gt\sin\theta \ , \quad S(t) = \frac{1}{2}(1-F)gt^2\sin\theta$$

At t_0, $a=a_0$ m/s^2, $u=0$ m/s, $S=0$ m
At t_1, $a=a_0$ m/s^2, $u=u_1=u_i$ m/s, $S=S_1$ m

The end velocity of the first phase will be used as initial condition in the second phase. The second phase can be described with differential equation 2. However, the solution is not the same as for the submerged case, as the initial condition differs.

At t_1, $a=a_1$ m/s^2, $u=u_1=u_i$ m/s, $S=S_2$ m
At t_2, $a=a_2$ m/s^2, $u=u_2$ m/s (maybe u_{term}), $S=S_2$ m

Solving equation 2 at $t=t_1=0$ s with $S=S_1=0$ m and $\dot{S}=u_i$ it can be derived:

$$\ddot{S} + \frac{A_c \cdot C_d}{2V_l \cdot (\gamma + C_m)}\dot{S}^2 - \frac{(\gamma-1)\cdot(\sin\theta - C_n\cos\theta)\cdot g}{(\gamma + C_m)} = 0$$

$$\ddot{S} + b\cdot\dot{S}^2 - c = 0 \qquad b = \frac{A_c \cdot C_d}{2V_l \cdot (\gamma + C_m)}, \qquad c = \frac{(\gamma-1)\cdot(\sin\theta - C_n\cos\theta)\cdot g}{(\gamma + C_m)}$$

At $\dot{S}(0) = u_i \qquad \ddot{S}(0) = c - bu_i^2 = a_i$

Solve:

$$S(t) = -\frac{1}{2b}\left(k_1 t + \ln\left(\frac{4\cdot c}{2a_i e^{k_1 t} + \dfrac{a_1^2}{k_2^2}e^{2k_1 t} + k_2^2} \right) \right) \qquad\qquad \text{Eq. 10}$$

$$k_1 = 2\sqrt{c}\sqrt{b}, \quad k_2 = (\sqrt{c} - u_i\sqrt{b})^2$$

Unfortunately, this equation is less simple than the equation for the submerged case.

Finally, the landslide meets the bottom. This deceleration phase can be described with the same formulas as for the submerged case.

At t_2, $a=a_3$ m/s^2, $u=u_2$ m/s (maybe u_{term}), $S=S_2$ m
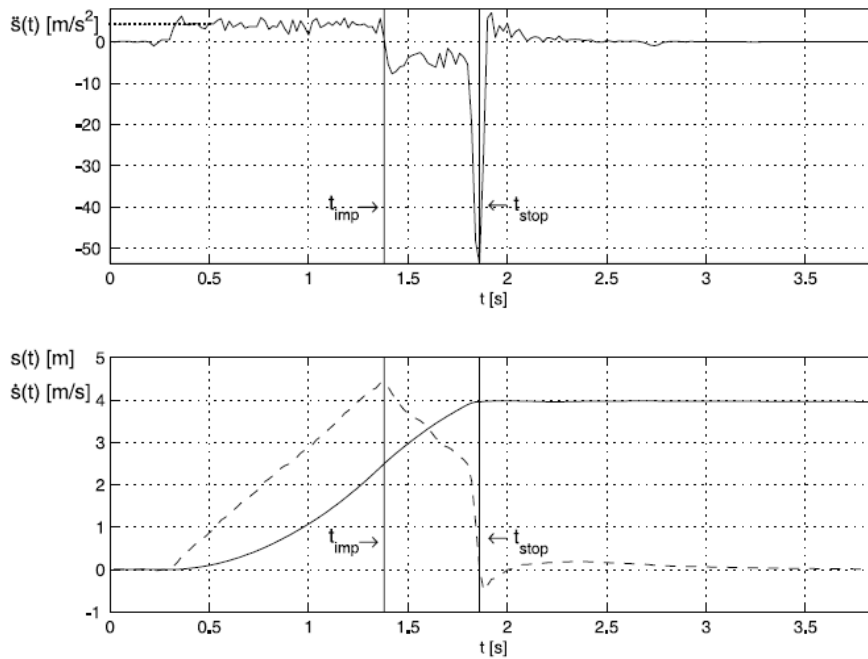At t_3, $u=0$ m/s, $S=S_3$ m

Figure 3: Landslide motion time series from test run with landslide sizes w = 0.60 m, h = 0.18 m, water depth d = 0.80 m, impact velocity u_i = 4.4 m/s, ramp inclination a = 26°. The solid line in the top panel shows the time series of the landslide acceleration, while the dashed line represents the initial landslide acceleration, equal to $g\,sin\,a$. The bottom panel shows the time series of the landslide velocity (dashed line) and motion along the ramp (solid line). Impact with water occurs at t = 1.38 s, and then the landslide stops at t = 1.86 s. The reconstructed impact velocity is u_i = 4.4098 m/s. [Panizzo et al. 2004]

In figure 9 an example is given of the landslide motion of a sub-aerial landslide in the experiments of Panizzo et al. (2004). The three different phases can be seen. In the first phase, the sub-aerial phase, the landslide experiences a constant acceleration. When the landslide enters the water, the second phase starts and the landslide is subjected to a decreasing deceleration until equilibrium is achieved between the forcing and counteracting forces. Equilibrium is not yet reached in figure 9 when the landslide motion experiences a strong deceleration as the slope merges into the horizontal bottom. This short deceleration process is the last phase.